2012-01-01

Development of a Multi-Material, Multi-Technology FDM System For Process Improvement Experimentation

David Espalin
University of Texas at El Paso, despalin@miners.utep.edu

DEVELOPMENT OF A MULTI-MATERIAL, MULTI-TECHNOLOGY FDM SYSTEM FOR PROCESS IMPROVEMENT EXPERIMENTATION

DAVID ESPALIN, JR.

Department of Mechanical Engineering

APPROVED:

Ryan Wicker, Ph.D., Chair

Norman Love, Ph.D.

Eric MacDonald, Ph.D.

Benjamin C. Flores, Ph.D.
Dean of the Graduate School

This Thesis is Dedicated To My Wife, Elissa Espalin, and Family Who Have Encouraged and Supported My Continued Education and Made Possible My Success.

DEVELOPMENT OF A MULTI-MATERIAL, MULTI-TECHNOLOGY FDM SYSTEM FOR PROCESS IMPROVEMENT EXPERIMENTATION

by

David Espalin, Jr., B.S.M.E.

THESIS

Presented to the Faculty of the Graduate School of

The University of Texas at El Paso

in Partial Fulfillment

of the Requirements

for the Degree of

MASTER OF SCIENCE

Department of Mechanical Engineering

THE UNIVERSITY OF TEXAS AT EL PASO

December 2012

Acknowledgements

I am immensely grateful to my advisor and mentor Dr. Ryan Wicker, director of the W.M. Keck Center for 3D Innovation (Keck Center), for his valuable guidance as well as his critical and constructive comments throughout my research as an undergraduate and graduate student. Mr. Frank Medina, manager of the Keck Center, has also served as a mentor to me and contributed a bounty of stimulating ideas and highly encouraged me. For that I am indebted to him. Additionally, this research would not have been possible if not for the impressive facility that Dr. Ryan Wicker and Frank Medina have constructed.

Various other people within the Keck Center deserve recognition. I would like to thank Dr. Karina Arcaute for helping in my technical writing development, Mr. David Rodriguez for aiding in the construction and machining of several components, Mr. Alfonso Fernandez for helping with the ultraviolet ozone surface treatments, and Mr. Jorge Ramirez for constructing some of the demonstration pieces included in this thesis. Additionally, I would like to thank Dr. Benjamin Flores, Mrs. Ariana Arciero, and Mrs. Sara Rodriguez of the University of Texas System Louis Stokes Alliance for Minority Participation (LSAMP) program for supporting me via the National Science Foundation Bridge to the Doctorate Fellowship (NSF grant number HRD-1139929). A special thank you is also owed to Bob Zinniel and Terry Hoppe of Stratasys, Inc. for providing support via materials, equipment, and advice regarding the development of the multi-material, multi-technology FDM system.

Finally, I would like to thank my wife, Elissa Espalin, and family for supporting and encouraging my continued education. In particular, I would like to acknowledge the memory of my brother “Luisito” which has inspired me to continually better myself and those around me.

Abstract

Over the last three decades, developments within the area of Additive Manufacturing (AM) have resulted in novel technologies capable of producing highly customized, complex part geometries in a fraction of the lead time required by traditional manufacturing methods (e.g., injection molding, metal casting). In particular, fused deposition modeling (FDM), a material extrusion AM process, can produce parts using production-grade thermoplastics like acrylonitrile butadiene styrene, polycarbonate, and polyetherimide. Additionally, non-commercial materials (e.g., polycaprolactone, ceramic loaded polymers, carbon nanotube loaded polymers) have been processed using FDM in part to demonstrate the potential diversity in material selection.

Recently, a myriad of personal 3D Printers using material extrusion processes have received much attention because they resemble the initial steps towards transforming AM technologies into a home consumer item. These steps were also taken during the 1980s by inkjet printing technologies when they were first entering the home consumer market. However, before inkjet printers became a home consumer item, challenges related to the controlled flow of inks and the clogging of print heads needed to be resolved. Synonymously, FDM technologies need to resolve issues related to part accuracy, surface roughness, build time, and mechanical properties before they can be fully adopted by industry and home consumers.

A multi-material, multi-technology (MMMT) FDM system was developed to enable experimental methods related to the FDM attributes in need of improvement. The MMMT FDM system consists of two legacy FDM systems, a pneumatic slide, and an overall control system. The FDM systems were modified so that they mimic a gantry system enabling a work piece to be transported between each FDM system. A build platform was attached to the pneumatic slide to enable the transportation of the workpiece. A software program named FDMotion was developed to control each FDM system and the pneumatic slide via a graphic user interface as well as provide in-process instructions to the user. The functional MMMT FDM system was used to explore build process variations, the effect of ultraviolet ozone surface treatments at

every layer on mechanical properties, and the development of a novel heat treatment for multi-material parts produced via FDM. Additionally, the system was employed to demonstrate the fabrication of multi-colored parts as well as multi-material parts made from discrete similar and dissimilar thermoplastics.

The build process variation consisted of depositing fine contours to promote dimensional accuracy and reduce surface roughness while depositing larger internal fill rasters to decrease build time. The internal roads were four times thicker and five times wider than the outer roads. A 55% improvement in surface roughness was measured on a plane that was inclined 10° from vertical and a 35% reduction in build time was observed when fabricating a simple square prism (50.8mm by 50.8mm and 25.4mm tall). Additionally, a student's *t*-test confirmed that the tensile properties of tensile specimens were not significantly altered by the build process variation

Multi-material fabrication was demonstrated with the MMMT FDM system by depositing different materials (similar and dissimilar) into different layers and different regions within a layer. This fabrication method was performed to construct simple geometries requiring little to no support material as well as complex geometries that required support material for a majority of the layers.

An interlayer bond improvement strategy was explored in which an ultraviolet ozone (UV/O_3) surface treatment was implemented before the deposition of a new layer. The UV/O_3 treatment was intended to increase surface energy and reduce the local glass transition temperature, which in turn was expected to increase interlayer bonding. A design of experiments (DOE) and analysis of variance (ANOVA) was conducted using six UV/O_3 exposure times (0, 0.5, 1.0, 1.5, 2.0, or 3.0 minutes) to determine their effect on surface energy and mechanical properties (ultimate tensile stress (UTS), strain at UTS, and modulus of elasticity). While the surface energy increased by 26% when exposing ABS P400 for 1 minute, the mechanical properties remained unchanged. The UV/O_3 surface treatment, however, can be used to increase the surface energy and wettability of FDM-fabricated parts for adhesive bonding processes requiring clean and chemically active surfaces.

To improve the tensile properties of FDM-fabricated specimens, a novel multi-material fabrication method and heat treatment were developed; the result being an increase of 25% in ultimate tensile strength with minor dimensional changes. A shell-and-core configuration was used wherein the shell material (PC) exhibited a higher glass transition temperature (T_g) than that of the core (ABS). The specimens were heat-treated at a temperature above the T_g of the core material but below the T_g of the shell material. This heat treatment removed the interstices between roads of the core material while limiting dimensional changes of the shell material.

Table of Contents

List of Tables

List of Figures

Chapter 1

Introduction

1.1 Background

Additive Manufacturing (AM), also known as layer manufacturing, rapid prototyping, solid freeform fabrication, and 3D printing, is a relatively new fabrication process which entered the commercial platform in the late 1980's. Technologies within AM are able to produce parts directly from computer-aided design (CAD) data and are well suited for low volume production and mass customization. These parts have found applications as prototypes, structural parts, tooling, biomedical implants and fashion attire, just to name a few (Bourell *et al*., 2009). As an example, large amounts (in the order of millions) of customized dental crowns and housings for hearing aids are currently being produced by AM technologies (The Economist, 2012). Still, AM technologies have yet to reach a level of wide acceptance for producing customer or engineering products.

Fused deposition modeling (FDM) is a heated material extrusion AM process that uses thermoplastics (ASTM F2792, 2012). The process entails driving a thermoplastic filament into a liquefier to produce a semi-molten plastic. While scanning a horizontal plane, the plastic is extruded through a small diameter nozzle and selectively deposited onto a build platform to produce a cross section or layer (Figure 1.1). The build platform is lowered after the completion and thermal fusion of each layer until the part is fabricated in its entirety. To enable the fabrication of complex parts, a sacrificial support material is also deposited for overhanging features. Although this fabrication process produces geometrically complex parts, several attributes need to be improved to enable the everyday use of FDM in many industries. In

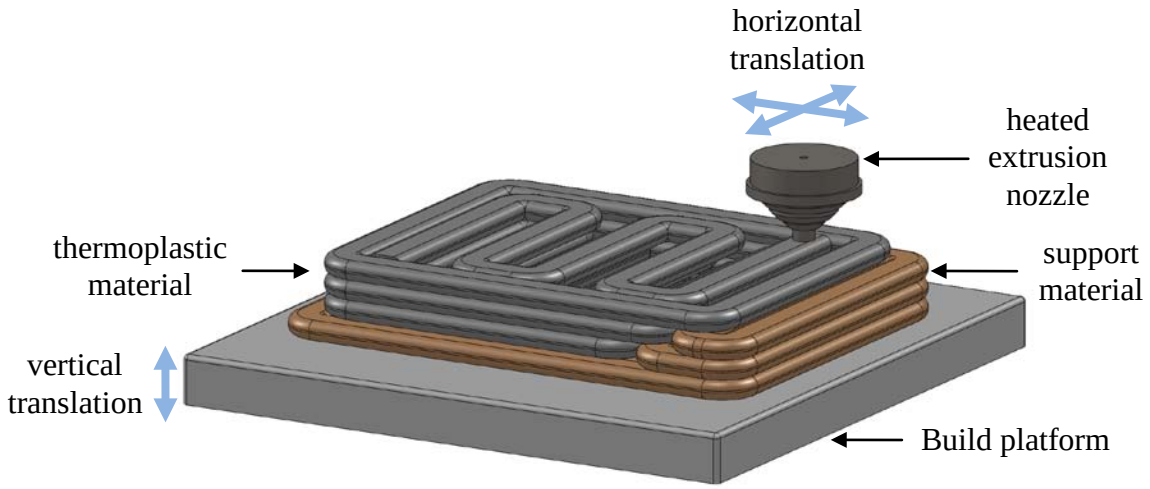

Figure 1.1 Schematic of FDM process for legacy systems.

particular, improvements are needed to resolve issues related to poor surface quality, limited feature resolution, weak bonds between adjacent filaments, and relatively slow build times.

1.2 Motivation

The sustained success of FDM has allowed this technology to evolve since its commercialization through continuous process enhancements including dimensional accuracy improvements and material selection expansion. However, much work is required before FDM can become entirely competitive with traditional plastic manufacturing processes like injection molding or screw extrusion. Therefore, the main motivation of the present research is to develop and construct an FDM system that facilitates experimental methods that address the current FDM aspect in need of improvement: surface quality, feature resolution, bonds between adjacent filaments, and build times. The developed FDM system will enable the evaluation of three hypotheses for improving FDM technology. First, it is hypothesized that having access to more than two extrusion tips will enable the rapid and accurate deposition of both model and support material using variable layer thicknesses and road widths to improve surface quality, part accuracy, and reduce build time. Second, it is hypothesized that employing an ultraviolet ozone

surface treatment will increase surface energy, which will strengthen interlayer bonding and in turn improve mechanical properties. Lastly, it is hypothesized that fabricating discrete multi-materials parts will allow heat treatments for the improvement of mechanical properties and density (i.e., reduce porosity).

1.3 Thesis Objectives

There are six thesis objectives and are listed as follows:

1. Incorporate two previously modified legacy FDM machines into a single system.
2. Design and develop a software program to control the two modified FDM machines and enable the fabrication of novel AM parts.
3. Develop and evaluate a process for fabricating geometrically complex parts with fine contours and coarse internal rasters to improve surface quality, part accuracy, and build time.
4. Develop a fabrication process using discrete multi-materials to produce novel AM parts and enable the heat treatment of FDM-manufactured parts for improving mechanical properties and density.
5. Experimentally determine the effects of ultraviolet ozone surface treatments on surface energy and mechanical properties.

1.4 Thesis Outline

The subsequent material was divided into the five chapters. Chapter 2 is composed of an overview of FDM as well as a literature review of topics pertinent to the hypothesis statements in section 1.2. These topics include the anisotropic mechanical properties of FDM-manufactured parts, FDM building strategies, previous interlayer bonding improvement processes, and the nature of amorphous polymers. In Chapter 3 the developed multi-material, multi-technology (MMMT) FDM system is described including the hardware and software. Chapter 4 consists of the experimental methodology employed for (1) determining the processing time, surface

roughness, and mechanical properties of specimens built using varying layer thicknesses and road widths (from this point forward referred to as build process variations), (2) determining the effects of ultraviolet ozone surface treatments on surface energy and mechanical properties, and (3) determining the effects of heat treatments on the mechanical properties of discrete multi-material specimens. The results of these experiments are discussed in Chapter 5. Additionally, multi-material demonstrations and parts produced using the build process variations are described in Chapter 5. Finally, conclusions and recommendations for future work are offered in Chapter 6.

Chapter 2

Literature Review

2.1 Introduction

Additive Manufacturing (AM) refers to the rapid production of complex objects in a layer-by-layer fashion directly from three-dimensional Computer Aided Design (CAD) data and in doing so effectively circumvents the costly production steps associated with traditional manufacturing (e.g., process planning, long lead times, expensive tooling). Initially, AM technologies and their products were primarily used for prototyping purposes, but recent advancements have altered the focus of AM to include the production of end-use parts in the pursuit of making a shift to Direct Digital Manufacturing (DDM) (Bellini and Guceri, 2003). Generally, an AM technology will employ seven steps in the fabrication of a part; 1) generating a CAD model, 2) converting the CAD model to stereolithography (STL) file format, 3) generating tooling commands from the STL file and transferring them to the AM system, 4) setting up the AM system, 5) building the part layer by layer, 6) removing the fabricated part from the AM system, and 7) post-processing the part. The duration of the building process (step 5) is dependent on the AM technology being used and its process parameters as well as the shape and orientation of the part. The AM technology options include those that use a system of liquid polymers, discrete particles, molten materials, or solid sheets where each uses a unique technology to deposit or solidify materials – lasers, liquefiers, electron beams, or print heads (Gibson, Rosen, and Stucker, 2010). The application of the finished product dictates the material and technology to be used as well as the degree of post-processing – some parts may require little or no post-processing while others may require machining, sanding, priming, and painting.

Although initial applications of AM were limited to prototyping, the more recent improvements of mechanical properties and surface finish have allowed the mass customization of structural parts, tooling, biomedical parts, architectural design representations, and artwork (Bourell *et al*., 2009 roadmap). Within this method of manufacturing, several technologies have been introduced including stereolithography, fused deposition modeling (FDM), laser sintering, laser melting, laminated object manufacturing, laser engineered net shaping, and electron beam melting with capabilities of processing thermoplastics, ceramics, photoreactive resins, metals, and biocompatible materials.

2.2 Fused Deposition Modeling (FDM)

Fused Deposition Modeling (FDM), a registered trademark of and a technology developed by Stratasys, Inc. (commercialized in 1990), is a material extrusion process that fabricates components in a layer-by-layer fashion using thermoplastics (ASTM F2792, 2012). According to the Wolhers Report (2012), Stratasys, Inc. is the leader among manufacturer of industrial AM systems indicating that FDM is the most utilized AM technology. As such, much effort has been devoted to finding novel applications for FDM-manufactured parts and resolving issues related to feature resolution, part accuracy, interlayer bonding, and surface finish.

FDM follows a variation of the general steps described above: 1) generate a CAD model, 2) convert the CAD model to STL file format, 3) import the STL file into Insight software for slicing and generating toolpaths in the form of a SML file, 4) build the part applying the processing parameters specified by the user, and 5) perform the required post processing (e.g., removal of support material, surface smoothing). Among the most important processing parameters are the air gap between rasters, road width, layer thickness, and raster orientation, which are illustrated in Figure 2.1. From a production standpoint, these processing parameters

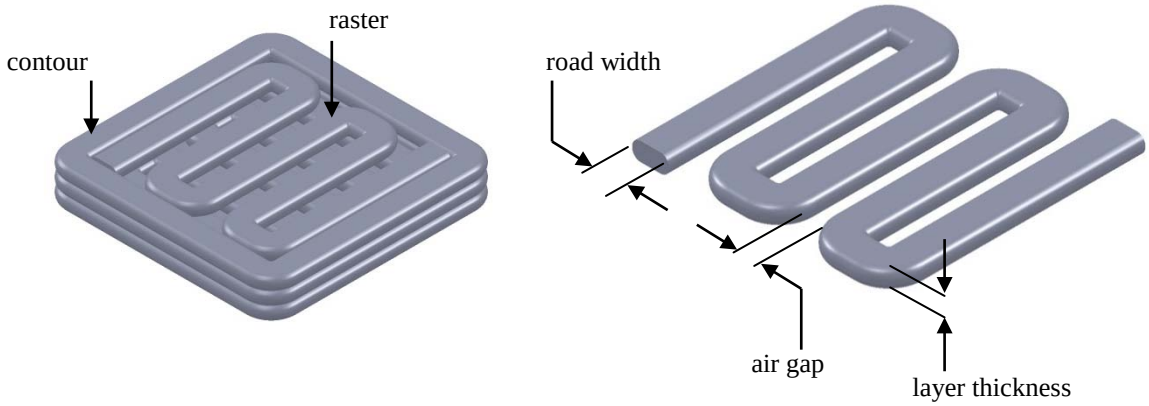

Figure 2.1. Features of deposited material produced by FDM

are critical because they have a great effect on build time. Additionally, these parameters have a significant effect on the performance of FDM-manufactured parts, as is discussed in later sections.

An FDM machine builds parts by driving a thermoplastic filament (Ø = 1.77mm) into a heated liquefier and extruding a semi-molten polymer fiber through a small-diameter nozzle (Ø = 0.127, 0.118, 0.254, or 0.330mm). The liquefier is fixed on an extrusion head that traverses parallel to the *XY* plane and over a build platform (Figure 2.2). The extrusion head is equipped with two liquefiers that work in concert to deposit both a model and sacrificial support material required for the fabrication of overhanging features and complex geometries. After the layer is completed, the build platform lowers along the *Z* direction a predetermined distance equivalent to the layer thickness to allow for the deposition of the next layer. In this sense, a part is fabricated from bottom to top and is composed of concatenated layers. FDM-manufactured parts typically exhibit an accuracy of ± 0.127mm (0.005-in.). Moreover, this layered manufacturing process in carried out in a temperature controlled envelope that aids in controlling material shrinkage and development of internal stresses (Wang, Xi, and Jin, 2007).

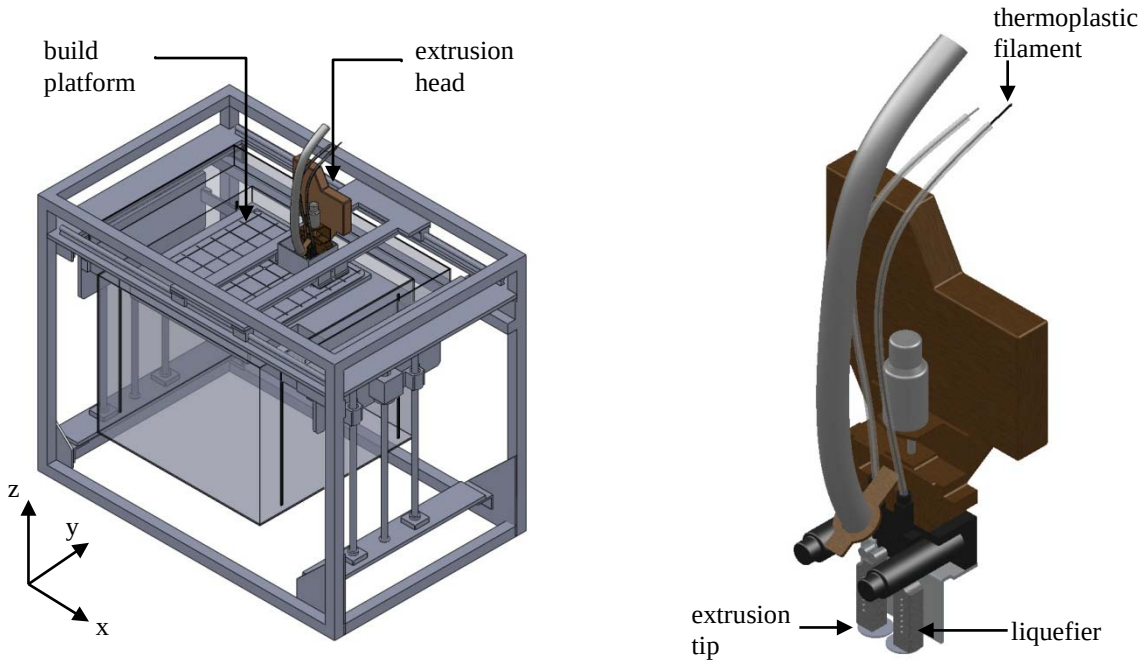

Figure 2.2. Schematic of FDM hardware (overview on left and close up of extrusion head on right)

When compared to other AM technologies that process polymers such as stereolithography and laser sintering, FDM has a clear advantage in that a variety of production grade thermoplastics may be processed – commercial materials for FDM (Table 2.1) include acrylonitrile-butadiene-styrene (ABS), polycarbonate (PC), PC-ABS blend, ABS-M30, and polyetherimide (ULTEM 9085). Additionally, non-commercial materials (e.g., poly(methyl methacrylate) (Espalin *et al*., 2010), poly(ε-caprolactone) (Zein, *et al*., 2002), silicon nitride ceramic (Iyer *et al*., 2008)) have also shown promise for use with FDM. The material choices

Table 2.1. Select properties for commercial FDM materials

Find datum for FDM1	Tensile Strength MPa	Tensile Modulus MPa	Glass Transition Temperature °C	Coefficient of Thermal Expansion mm/mm/°C	Specific Gravity
ABS	22.00	1,627	104	10.08 X 10^{-5}	1.05
ABS-M30	36.00	2,413	108	8.46 X10-5	1.04
PC	68.00	2,280	161	3.80 X 10^{-5}	1.20
PC-ABS	41.00	1,917	125	7.40 X10^{-5}	1.20
ULTEM 9085	71.64	2,220	186	----	1.34

for stereolithography and laser sintering are limited and lack the robust mechanical and thermal properties as well as high chemical resistance of materials used with FDM.

Despite this clear advantage, the transition to Direct Digital Manufacturing (DDM) and industry-wide adoption of FDM technology has not occurred due to poor surface quality (Pandey, Reddy, and Dhande, 2003a), low feature resolution (when compared to SL), weak bonds between adjacent filaments (Bellini and Guceri, 2003; Rodriguez, Thomas, and Renaud, 2003), and relatively long build times. Poor surface quality is a result of "stepping" or the unsmooth transition from one layer to the next. Weak interlayer bonds give rise to anisotropic material properties. As an example, tensile strength is greater along the axial direction of the deposited filament when compared to loads carried across filaments or layers (Ahn, *et al*., 2002). This is primarily due to weak bonds between adjacent filaments. While many users of FDM commonly orient filaments along the load bearing direction, the fabrication of functional parts is limited and sometimes prohibited by their anisotropic mechanical properties that lack the ability to withstand transverse loading. As such, any improvement to bonds between adjacent filaments would enable the production of functional FDM-manufactured parts.

2.3 Anisotropic mechanical properties of FDM-manufactured parts

The layer-by-layer manufacturing process employed by FDM results in parts exhibiting anisotropic mechanical properties. This behavior is of utmost importance in the fabrication of functional parts and as a response, much research has been performed to identify the design and processing parameters that have a significant effect on performance criteria. Work performed by Es-said *et al*. (2000) analyzed the effect of layer orientation (0°, 45/-45°, 45°, 90°, and 45/0°) on three mechanical properties. This study demonstrated that layer orientation had an effect on tensile strength, flexural strength, and absorbed energy during Izod impact testing as well as

fracture path. Similar work performed by Ahn *et al*. (2002) employed a design of experiments to conclude that the air gap between rasters and orientation of rasters are process variables that have an effect on tensile strength. In particular, this work noted that tensile strength had a dependence on build orientation resulting in tensile strength anisotropy. Other studies performed by Bellini and Guceri (2003) tested filaments before and after the FDM extrusion process and conclude that the process does not have a significant influence on tensile strength and modulus, but does affect maximum strain – possibly due to the viscoelastic nature of polymers. Lee *et al*. (2005) utilized the Taguchi method (FDM parameters: air gap, raster angle, raster width, and layer thickness; each at three levels) to determine the optimal process parameters that yielded the best performance from a fabricated catapult. This work indicated that application-specific parameters may be determined by considering the main effects revealed through a statistical analysis. Sun *et al*. (2008) noted that the bond quality between adjacent polymer filaments is dependent on the degree of neck growth as well as the randomization of polymer chains across the interface and molecular diffusion. Through in-process monitoring, it was determined that the temperature history of the interfaces was a major contributor to bond quality. Specifically, microphotographs of cross-sections revealed that bottom-most layers achieved larger neck growth when compared to top layers. When considering the part location on the build platform, it was concluded that both the location and immediate surroundings (i.e., presence or absence of adjacent parts) have an effect on the temperature history, and therefore bond quality. Sood *et al*. (2010) implemented a central composite statistical design to determine the effect of five processing parameters (part orientation, layer thickness, raster angle, raster width, and air gap between rasters; each at three levels) on tensile, flexural, and impact strength. Results included the use of response surfaces to identify relationships between the processing parameters of interest.

From the aforementioned works it can be concluded that anisotropic properties are due to 1) the alignment of polymer molecules along the raster direction, 2) the presence of voids between adjacent rasters, 3) residual stresses caused by volumetric shrinkage, and 4) weak interlayer bonding. Research has shown that FDM-manufactured parts fail under a fraction of the tensile stress that an injection molded ABS P400 parts is capable of withstanding (10 - 73% of 26 MPa) (Ahn *et al*., 2002). Furthermore, research related to the anisotropy of FDM-manufactured parts has mostly been devoted to determining the optimum FDM processing parameters and little work has been devoted to developing an interlayer bonding improvement method independent of the FDM processing parameters.

2.4 Previous interlayer bonding improvement strategies

The anisotropic mechanical properties associated with FDM-manufactured parts are often mitigated by designing and orientating the part so that the layers and fibers can accommodate the mechanical loading. However, this strategy cannot always accommodate every loading scenario and as a result anisotropic mechanical properties inhibit FDM-manufactured parts from being used in many applications (e.g., pressure vessels, structural components undergoing multi-direction mechanical loading). Having realized this limitation, several research groups have attempted to find a permanent solution that addresses bonding between layers. Parker *et al*. (2009) utilized hot pressing to evaluate if hot isostatic pressing (HIP) could be an effective method for eliminating the voids present between adjacent polymer fibers. Polyphenylsulfone (PPSU), PC, and ULTEM 9085 were tested at pressures up to 150 MPa and at temperatures below their associated glass transition temperatures. Results from these studies demonstrated that the volume of voids may be reduced at optimum pressure and temperature conditions; however, dimensional distortion may arise if either pressure or temperature is too high. Despite

the reduction in volume fraction of voids, the corresponding ultimate tensile strength did not consistently increase. This behavior lead the authors to conclude that the reduction in volume fraction of voids does not necessarily strengthen the produced parts.

Other work performed by Partain (2007) used a pre-deposition heating system in an attempt to increasing the degree of material bonding between polymer fibers and layers. The pre-deposition heating system was designed with the intent of increasing the temperature at the layer-layer interface by using localized forced air at the recently deposited material before the deposition of additional material. Essentially, one can imagine a hot air welder tool aimed directly at the material being deposited. Single factor and multiple factor design of experiments were performed and the results were processed through an analysis of variance. The authors concluded that parts produced with the pre-deposition heating system did not exhibit higher flexural strength that those produced without the pre-deposition heating system. Evidently, significantly and consistently improving interlayer bonding for FDM-manufactured parts has been unsuccessful and more efforts in this area are required.

2.5 Amorphous Polymers

Polymers can be generally characterized based on their structure, arrangement and physical form (Stevens 1999, 61). As a result, polymers are typically grouped into one of two morphologies – amorphous or crystalline. The discussion here is solely focused on the amorphous state since ABS polymer (commonly accepted as amorphous) was used in this study. Amorphous polymers are characterized by a physical state in which molecules, for the most part, are ordered randomly, and the polymer resembles a glass. Conversely, molecules in crystalline polymers are aligned in regular patterns or arrays that are in part analogous to lattice crystals, for

example, of solid crystalline metals. However, crystalline polymers never reach a complete crystalline state and therefore are often referred to as semicrystalline.

To a great extent, the properties of polymers are dependent on molecular weight and chemical structure. This argument is supported by the fact that specific molecular weights must be achieved before attaining a desired set of mechanical properties (Stevens 1999, 61). These specific molecular weights are highly dependent on the polymer's molecular structure. Furthermore, mechanical properties in part arise from the attractive forces between the polymer molecules. These intermolecular forces can generally take form as induction forces, dipole-dipole interactions (including hydrogen bonding), dispersion, London forces among nonpolar molecules, ionic bonding, or ion-dipole interactions. These secondary bonding forces contribute to achieving the desired mechanical properties for polymers (Stevens 1999, 62).

Fused deposition modeling uses both amorphous and some semi-crystalline polymers. Amorphous polymers behave as viscous pastes and retain their extruded shape due to the absence of an explicit melting temperature as noted in Figure 2.3. On the other hand, the thermal properties of crystalline polymers induce shrinkage during the crystallization process which hinders shape retention after extrusion (Gibson, Rosen, and Stucker, 2010). ABS is an amorphous polymer and one of the most common commercial FDM materials (chemical structure shown in Figure 2.4). The deposition of semi-molten thermoplastics, as done with FDM, creates a thermal bond to the previous layer. Nonetheless, the bonding mechanism fails to eliminate all interfacial regions, and interstices between adjacent material roads and layers produce domains of decreased strength –this limits the application of FDM-manufactured parts.

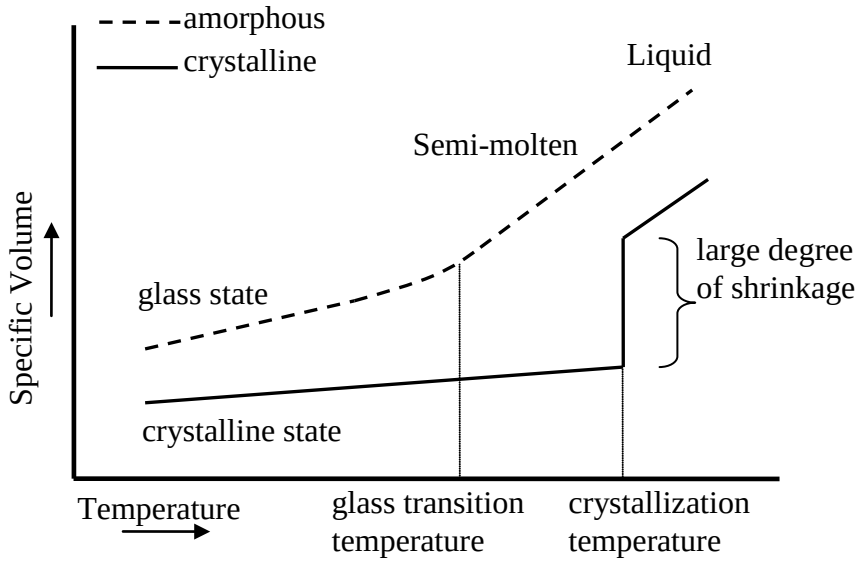

Figure 2.3. Typical thermal properties for crystalline and amorphous polymers. Note the large degree of shrinkage for crystalline materials.

2.6 Glass Transition Temperature

The transition of an amorphous polymer from solid to liquid is of great interest to the polymer's industry. The thermal history of an amorphous polymer is described below:

1. The kinetic energy of the molecules increases as the polymer is heated from room temperature. As a result, molecular short range vibrations and rotations occur but are limited if the polymer still resembles a glasslike structure.
2. The additional increase in temperature causes an evident change whereby the polymer no longer resembles a glasslike structure. The temperature at this point

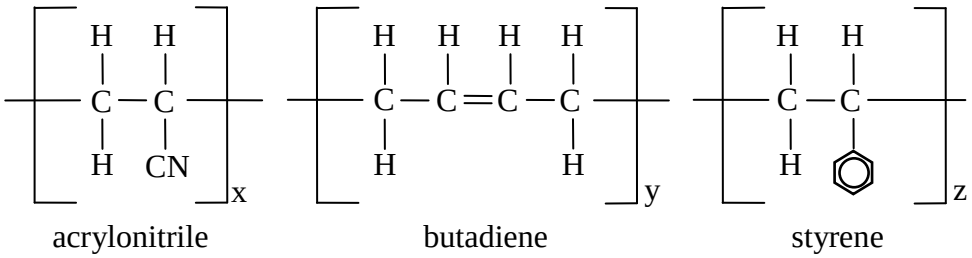

Figure 2.4. Chemical structure of ABS – $(C_8H_8)_x \cdot (C_4H_6)_y \cdot (C_3H_3N)_z$

is commonly referred to as the glass transition temperature and is denoted by T_g.

3. If the polymer is heated further, a loss of elasticity is experienced and a flowable liquid is produced

At a molecular level, the glass transition temperature signifies a condition where the following occur: 1) long-range molecular motion, 2) rotational freedom, and 3) segmental motion of the chains. Upon reaching the glass transition temperature, the segmental motion is estimated to involve ~20-50 chain atoms, which indicates that there must be an increase of free volume (the space between atoms) and therefore an increase of specific volume. Several studies have recorded other notable behaviors such as a change in enthalpy, modulus, stiffness, refractive index, and thermal conductivity (Stevens 1999, 70).

2.7 Alternative interlayer bonding improvement strategies

The successful decomposition of photoresist polymers via ultraviolet (UV) irradiation by Bolon and Kuns in 1972 lead to the development of a dry cleaning method wherein surface contaminants are decomposed by the UV irradiation and ozone (O_3) chemical oxidation – this photo-sensitized oxidation process is known as ultraviolet ozone (UV-O_3) cleaning (Tsao and DeVoe, 2009). Although UV-O_3 was initially used to remove unwanted organic compounds (e.g., cutting oils, soldering fluxes, contaminants resulting from persistent air exposure) from substrate surfaces such as optical lenses, the process may also be used to create functional groups for enhanced bonding/adhesion of organic substrates. In terms of surface free energy, functional groups are created when polymers chains that have undergone scission due to the UV irradiation react with free oxygen (also produced by UV irradiation), which increase the polar component to its total surface free energy (Mathieson and Bradley, 1995).

formation of O_3 with 184.9 nm UV ray

$$O_2 \longrightarrow O + O$$
$$O_2 + O \longrightarrow O_3$$

dissociation of O_3 with 253.7 nm UV ray

$$O_3 \longrightarrow O_2 + O$$

Figure 2.5. Formation and dissociation reactions that take place within an ultraviolet ozone apparatus.

The UV-O_3 apparatus uses a low-pressure mercury vapor lamp to produce two principal wavelengths: 184.9 nm and 253.7 nm. The simultaneous presence of both wavelengths is critical. O_3 is generated when the 184.9 nm UV rays interact with atmospheric O_2, while the 253.7 nm UV rays dissociate the O_3 to produce atomic oxygen (Figure 2.5). The continuous formation and dissociation of O_3 ensures a steady presence of atomic oxygen that has exceptional oxidizing abilities. Concurrently, the organic compounds being irradiated with the UV rays undergo photolysis wherein ions, free radicals, excited molecules, and neutral molecules are produced.

The energy (E) available from a photon is determined by employing Planck's relation

$$E = h\nu \qquad \text{Equation 1}$$

where h is Planck's constant (6.626×10^{-34} J-s) and ν is the photon's frequency. Furthermore, the frequency is related to wavelength λ by

$$\nu = \frac{c}{\lambda} \qquad \text{Equation 2}$$

where c is the velocity of light (2.998×10^{10} cm-s^{-1}). Combining these two relations and incorporating Avogadro's constant N (6.022×10^{23} mol^{-1}) yields the energy per mol available from a photon at a particular wavelength.

$$E = \frac{Nhc}{\lambda} \qquad \text{Equation 3}$$

Calculations for the energy per mol available from the principal UV rays associated with UV-O_3 cleaning are as follows.

$$E_{184.9nm} = \frac{(6.022 \times 10^{23}\ mol^{-1})(6.626 \times 10^{-34}\ J \cdot s)(2.998 \times 10^{10}\ cm \cdot s^{-1})}{184.9 \times 10^{-7} cm} = 647\ kJ \cdot mol^{-1} \quad \text{Equation 4}$$

$$E_{253.7nm} = \frac{(6.022 \times 10^{23}\ mol^{-1})(6.626 \times 10^{-34}\ J \cdot s)(2.998 \times 10^{10}\ cm \cdot s^{-1})}{253.7 \times 10^{-7} cm} = 472\ kJ \cdot mol^{-1} \quad \text{Equation 5}$$

Typical bonds present in organic compounds and their corresponding bond energy (Blansky and Ellison, 2003) are shown in Table 2.2. The energy supplied through the UV-O_3 process must exceed the bond energy to promote photolysis and yield free radicals. When UV-O_3 is used for removing organic contaminants, these free radicals react with the atomic oxygen to form simple, volatile molecules such as CO_2, H_2O, and O_2, which are easily removed (Truckenmuller *et al*., 2004).

As previously mentioned, UV-O_3 exposure can be used to create functional groups for enhanced bonding/adhesion of organic substrates. The composition of ABS, PC, and ULTEM

Table 2.2. Bond energy of typical bonds in thermoplastics

Bond	Bond Energy (kJ mol^{-1})	Bond	Bond Energy (kJ mol^{-1})	Bond	Bond Energy (kJ mol^{-1})
O – O	138.9	C – N	291.6	C = O	724
O = O	490.4	C ≡ N	791	C – Cl	328.4
O – H	462.8	C - O	351.5	C – F	441.0
C – C	347.7	C = C	607	H – Cl	431.8
C – H	413.4	C ≡ C	828	N – H	309.8

shaded cells indicate the bonds present in ABS, PC, or ULTEM that can be broken via UV-O_3

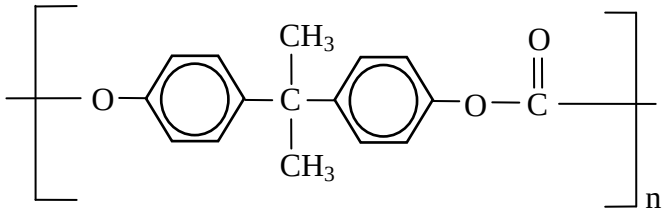

Figure 2.6. Chemical structure of polycarbonate (PC) – $C_{16}H_{18}O_3$.

(common polymers used with FDM) can be seen in Figures 2.4, 2.6, and 2.7. Based on the energy per mol available from UV rays at 184.9 nm and 253.7 nm, the bonds that can be broken with UV-O_3 are highlighted in Table 2.2. Moreover, the UV-O_3 exposure can break the polymer chains and insert functional groups containing oxygen (Tsao and DeVoe, 2009). That is, chemical bonds within hydrocarbons can be broken and oxidized with atomic oxygen to produce carbonyl and hydroxyl functional groups (Figure 2.8), which result in an increase of surface energy.

In addition to the creation of functional groups on the surface of the polymer, the glass transition temperature (T_g) of the polymer is locally reduced. Work performed by Truckenmuller *et al*. (2004) has shown that treating poly(methylmethacrylate) with UV-O_3 reduces the T_g by ~60 K. This reduction of T_g is localized to the thickness of the affected polymer layer, which is determined by the optical absorption length of the polymer. As an example, the absorption length of ABS when irradiated with 248nm wavelength is 0.11μm (Frerichs *et al*., 1995). Therefore, the bulk thermomechanical properties of the polymer (treated with OV-O_3) do not experience consequential changes. This behavior allows the bonding of polymers at temperatures below their bulk T_g without causing any noticeable changes in dimensional accuracy. It can also be argued that if substrates are bonded at the bulk T_g, then the UV-O_3 affected area will be well above the local T_g, which will promote more and quicker molecular diffusion at the bond interface. This is the foundation for the second hypothesis statement in

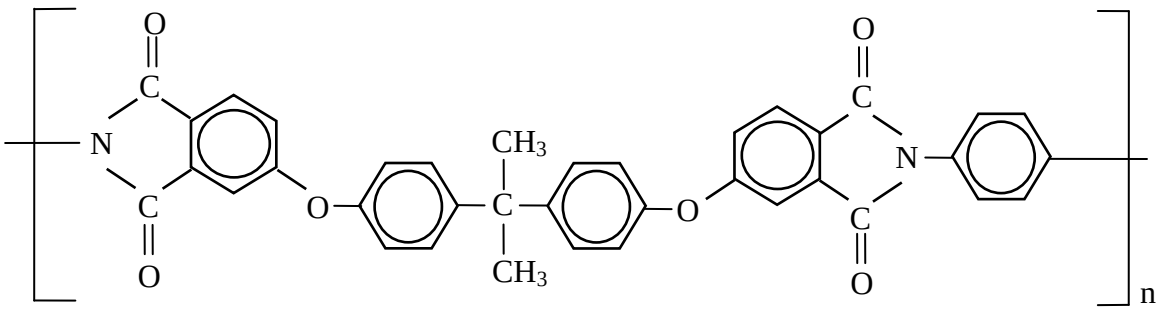

Figure 2.7. Chemical structure of ULTEM – $C_{37}H_{36}N_2O_6$

section 1.2: employing an ultraviolet ozone surface treatment will increase surface energy, which will strengthen interlayer bonding and in turn improve mechanical properties.

2.8 FDM build strategies

A CAD model is generated and converted to a stereolithography (STL) file format. In the STL model, a network of triangular facets on the surface of the solid model approximates the geometry of the CAD model. Creating slices throughout the model's height is accomplished by intersecting it with horizontal planes. The intersection of the horizontal plane and the STL model results in a polygon, which lies on the intersecting plane and is referred to as a slice. A layer is produced by depositing material at the periphery and interior of the bounding polygon. Conventional FDM processes utilize uniform layer thicknesses for the layers that make up a part.

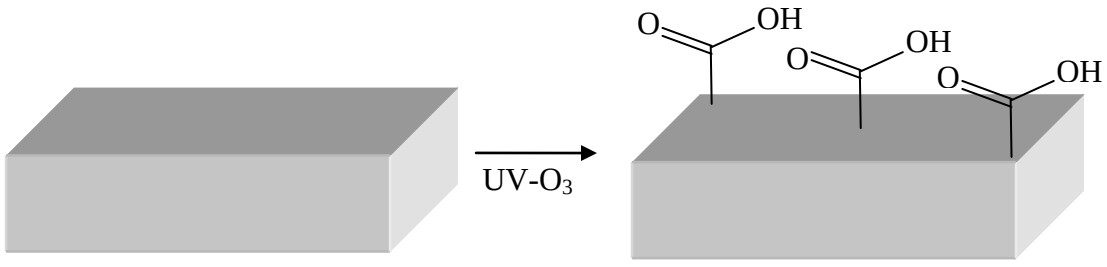

Figure 2.8. Schematic illustrating the formation of carbonyl and hydroxyl functional groups on polymer surfaces due to ultraviolet ozone (UV-O_3) exposure.

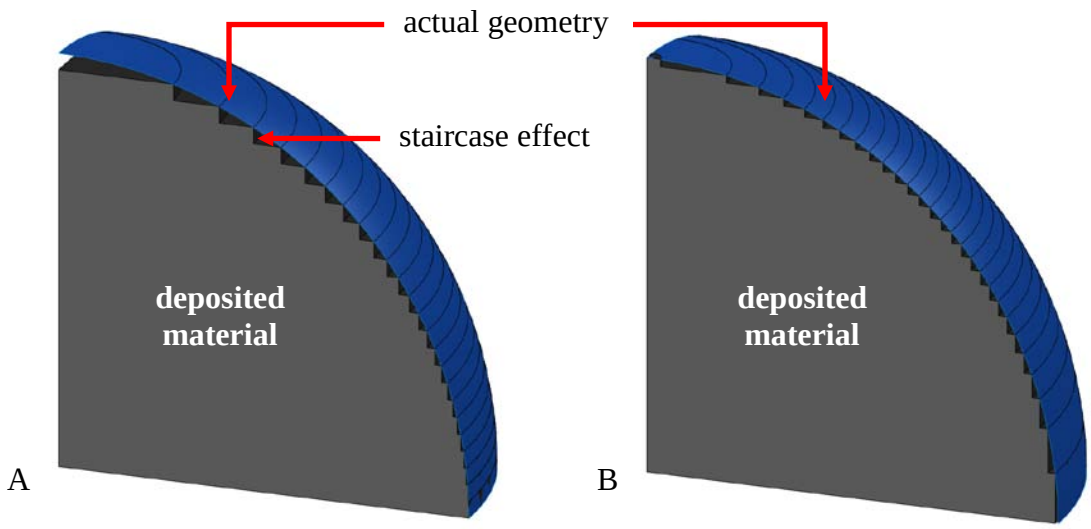

Figure 2.9. Cartoon of a sectioned dome demonstrated staircase effect and geometrical inaccuracy. A) uniform layer thickness. B) varying layer thickness produced by adaptive slicing.

For complex geometries, the bounding polygons at one slice are different from that of an adjacent slice. In the case where polygons between adjacent slices are dramatically different, the deposited layers do not represent the geometry accurately and the resulting part exhibits poor surface quality. In near horizontal surfaces, the inaccuracy is more pronounced and a series of layers, in cross-section, resemble a staircase (Figure 2.9). Therefore, this geometrical inaccuracy is referred to as the staircase effect. Moreover, the staircase effect causes undesirable surface roughness and detrimentally affects aesthetics.

In work related to FDM, several methods have been proposed to reduce the staircase effect. Adaptive slicing – a slicing method (Figure 2.9B) that assigns variable layer thicknesses based on a part's geometry to better approximate the outer surface (Kulkarni and Dutta, 1996; Pandey, Reddy, and Dhande, 2003a) – is one example of such effort at improving surface quality. The adaptive slicing method, however, is not support by commercial software or hardware. Other work that used a standard FDM machine equipped with two extrusion tips was focused on depositing model material with regular thin layers for exterior regions while using

thick layers for interior regions to reduce the build time up to 80% while preserving the surface quality (Sabourin, Houser, and Bohn, 1997). This approach has demonstrated remarkable improvements to FDM build times and has partially inspired the first hypothesis statement in Section 1.2: having access to more than two extrusion tips will enable the rapid and accurate deposition of both model and support material using variable layer thicknesses and road widths to improve surface quality, part accuracy, and reduce build time. The access to four extrusion tips with different orifice diameters not only allows build variation for the model material, but the support material can also be deposited using the same method to further reduce build time.

2.9 Additive Manufacturing and multiple materials

The use of discrete multi-materials within single components is viewed as a technically challenging and economically favorable manufacturing method that can enable unprecedented levels of functionality and adaptability (Salonitis *et al*., 2009). By utilizing multi-material components, economic and lightweight designs may be achieved via the reduction of required assembly processes and parts. The automotive industry has already begun taking advantage of multi-material designs in numerous applications (e.g., multi-colored taillights, components with compliant hinges).

Polymers and fiber reinforced polymers are widely used because they exhibit such characteristics as low density, reduced manufacturing cost, ease of manufacturing, high specific strength, and exceptional resistance to corrosion (Mangus, 2012; Young and Lovell, 2011; Zhong *et al*., 2001). Similarly, these same attributes have attracted much attention in the area of AM. Previous work has demonstrated the use of AM technologies in conjunction with multi-materials to produce a variety of functional components including electroactive polymer actuators (Malone and Lipson, 2008) and biomedical scaffolds (Arcaute, Mann, and Wicker,

2006). However, there is no indication in literature that FDM has been explored for discrete multi-material fabrication even though production-grade thermoplastics (e.g., polycarbonate, acrylonitrile butadiene styrene) are already commercially available for use with FDM, which may generate greater functionality.

In practice, joining of similar and dissimilar polymer materials can be achieved by fastening mechanically, welding, or bonding with adhesives; however, each of these methods are susceptible to failure due to various factors. For example, in the presence of humidity the development of corrosion on metallic fasteners can ultimately lead to premature failure. Components joined with adhesives can fail due to improper surface treatment, humidity and ageing (Campilho *et al*., 2012), and welding can be difficult to accomplish when the contact surfaces have complex geometries. The fusion joining performed with FDM is accomplished when thermoplastic material is deposited at a temperature sufficiently high so that the previously deposited layer is thermally activated up to a polymer chain mobility level at which the surface of the layers are chemically or covalently united (Haisma and Spierings, 2002; Sun *et al*., 2008).

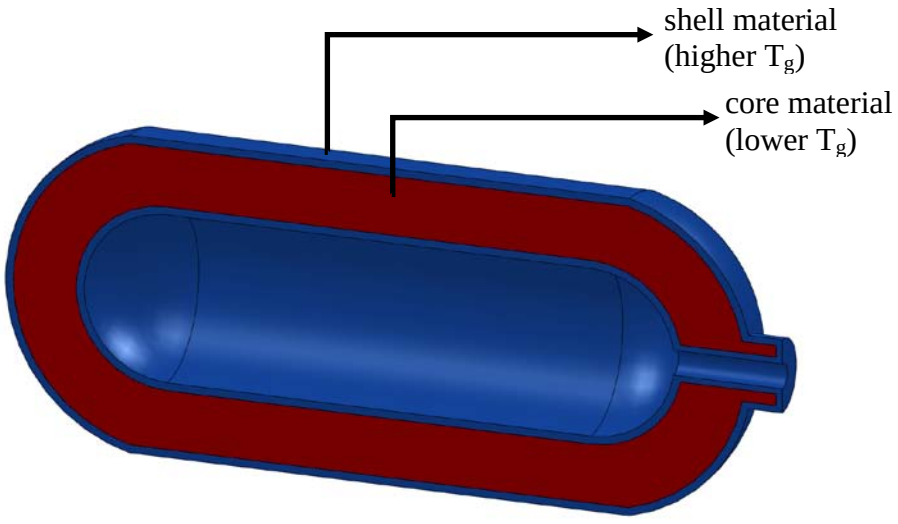

Figure 2.10. Pressure vessel example where the core and shell configuration can be heat-treated to improve mechanical properties and reduce porosity.

An FDM system with more than two extrusion tips may enable the fabrication of complex, discrete multi-material components by using at least two tips for dissimilar model materials and one tip for support material. It is anticipated that fabricating with two dissimilar materials in a shell-and-core configuration (Figure 2.10) will enable innovative heat treatments of FDM-manufactured parts. Specifically, dissimilar materials exhibiting different glass transition temperatures (T_g) can be heat-treated to improve both the density and mechanical properties of the core material without distorting the geometry. This concept is the basis for the final hypothesis: fabricating discrete multi-materials parts will allow heat treatments for the improvement of mechanical properties and density of FDM-manufactured parts. If the heat treatment is performed above the T_g of the core material but below that of the shell material, the core material will flow like a viscous fluid to eliminate interstices (Figure 2.11) commonly found in FDM-manufactured parts (Sun *et al.*, 2008) while prohibiting (1) long-range molecular motion, (2) rotational freedom, and (3) segmental motion of the shell material chains – behavior that results in physical deformation and is observed at and above the glass transition temperature of a thermoplastic (Young and Lovell, 2011).

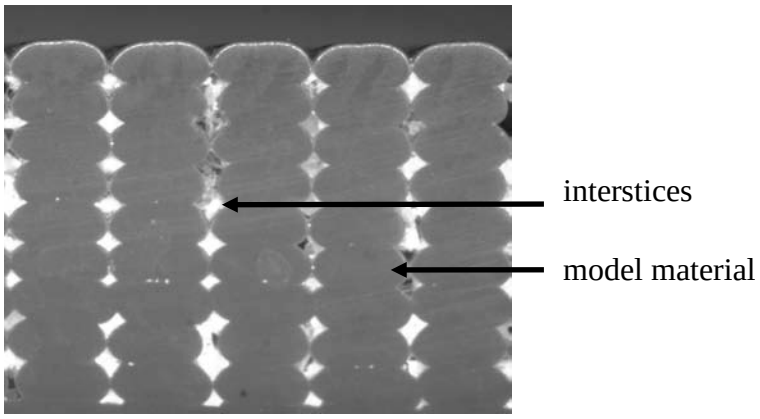

Figure 2.11. Optical image of cross-sectioned FDM-manufactured part. Note the interstices between the model material.

Chapter 3

Novel Multi-Material, Multi-Technology FDM System

3.1 Concept

FDM may be considered a multiple material fabrication process since both a model and support material is extruded within one single machine. Although the support material is sacrificial, the two extrusion tips contained in one FDM machine must work in concert to accurately fabricate the desired geometries. For the multi-material, multi-technology (MMMT) FDM system, this concept was extended to include four extrusion tips and allow the use of at least three discrete model materials in one fabricated part.

In this work, a multi-material, multi-technology FDM system, referred to as MMMT FDM system for convenience, was designed and constructed to enable experimental methods that address the current FDM aspect in need of improvement: surface quality, feature resolution, bonds between adjacent filaments, and build times. In addition, the fabrication of thermoplastic parts composed of discrete multiple materials can be explored. The MMMT FDM system includes two legacy FDM machines in which four extrusion tips were made available for the build process variations and fabrication of multi-material components. Essentially, one extrusion tip was reserved for the support material and the other extrusion tips were available for three thermoplastics. Advancements in discrete multi-material fabrication are also being performed in other polymer processing technologies to enable co-extrusion and co-molding of discrete polymers. These advancement efforts have been motivated by a variety of benefits including: 1) eliminating the need to assemble discrete polymer components, 2) increasing wearability of surfaces by including abrasion resistance polymers, 3) achieving aesthetic requirements by using polymers of different colors, and 4) attaining desired properties (e.g., bulk

tensile/compressive/flexural strength, weight, thermal conductivity) by strategically combining layers of polymers that display different properties. It should be noted that these benefits apply to the FDM of multiple polymers as well as multiple material systems with one or more discrete materials made of ceramic or a low melting temperature metal alloy (solder). Although the work presented here does not include ceramics or solders, recent work (Bellini, Shor, and Guceri, 2005; Allahverdi *et al*., 2001; Mireles *et al*., in press) has enabled the processing of these materials using FDM and as such could be implemented with the MMMT FDM system. The current state of this system (Appendix A) includes two legacy FDM systems working in concert to fabricate multi-material components. Further details regarding the hardware and software configurations are discussed in the following sections.

3.2 Hardware

The MMMT FDM system includes two legacy FDM machines, a pneumatic slide, a programmable automation controller, and a central PC. The legacy FDM machines (models FDM 3000 and 2000, Stratasys Inc., Eden Prairie, MN) were used because the standard operations of these machines allow the user to specify model, support, and envelope temperatures. This is particularly beneficial in the sense that non-commercial FDM polymers may be processed, as demonstrated with composite materials (Zhong et al., 2001) and polymethylmethacrylate (Espalin *et al*., 2010), in contrast to the current FDM machines (e.g., Fortus 400mc or 900mc), which use material-specific microchip canisters that lock-in the machine build parameters.. Moreover, each legacy FDM machine communicates using an Automove® Control Language (ACL) that is relatively easy to modify for accommodating non-commercial FDM polymers and interrupting the fabrication process.

The two legacy FDM machines were modified so that the *X/Y* traversing extrusion head was installed on the *Z* stage. The modifications to the FDM systems were performed in previous work (Choi et al., 2011). As previously mentioned, the non-modified FDM machine consists of an independent *X/Y* traversing extrusion head and a *Z* stage. Installing the *X/Y* traversing head on the *Z* stage allowed the FDM system to mimic a gantry and enabled the transportation of the work piece between the first FDM machine (FDM1) and the second FDM machine (FDM2).

A modular, multiple position pneumatic slide (series SFM, PHD, Inc., Fort Wayne, Indiana) delivering a +3.0/-0.0mm travel tolerance and ±0.04mm repeatability was used to transport the work piece between the two FDM machines. The pneumatic slide was configured with two adjustable end stops at each FDM machine and a mid-position actuator as well as corresponding magnetic, solid-state switches at each stop – the voltage output generated by the switches allowed for monitoring the build platform position and coordinated the overall programming logic. Cap and saddle mounted shock absorbers were installed to address abrupt deceleration and dispersed end-of-travel kinetic energy that could have dislodged the work piece from the build platform.

The two FDM systems and the pneumatic slide were controlled through the use of an overall control system. Table 3.1 provides a brief description of noteworthy components that constitute the control system as well as the component functions for the MMMT FDM system.

3.3 Control Software: FDMotion

3.3.1 FDMotion control and graphic user interface

A software program and graphic user interface (GUI) was developed using LabVIEW 2011 (National Instruments Corporation, Austin, TX) to control the fabrication process within the MMMT FDM system. The custom-made software program (Appendix C) was named

Table 3.1. Select properties for commercial FDM materials

Product	Model	Function
reconfigurable real-time controller	National Instruments cRIO-9074	communicate with control software and individual modules
digital Output Module	National Instruments 9472	provide voltage signals to pneumatic valves and switches
digital Input Module	National Instruments 9411	detect logic levels from pneumatic switches and FDM pause indicator
solid-state relay outputs	National Instruments 9485	emulate the pressing of front panel buttons on FDM system

FDMotion for convenience. Through this interface, the user is able to control the pneumatic slide (Figure C3), each of the two extrusion heads (Figure C4), and send the toolpath commands to the MMMT FDM system. The block diagram in Appendix B illustrates the sequence of actions that are performed by FDMotion.

FDMotion was designed to provide users with two operating modes – *Single FDM operation* and *Multiple FDM operation*. The original standalone software supplied with each technology is used within FDMotion. For instance, FDMotion interfaces with both FDM systems via the FDM Status software (Stratasys, Inc., Eden Prairie, MN).

3.3.2 Modifying SML files and sending ACL commands to the legacy FDM systems

The Insight software (Stratasys, Inc., Eden Prairie, MN) that ships standard with all FDM machines is designed to import a CAD model and slice it at predetermined locations along the Z building direction. Each slice is then treated as a two-dimensional profile and toolpath commands are written for the deposition of both model and support layers. These commands are expressed in Automove® Control Language (ACL) for the FDM 2000 and 3000 systems equipped with legacy Asymtek Automove® Series of *X*-*Y* tables and motor controllers

(Asymtek, Carlsbad, CA). The commands are supplied to the FDM Status software and then buffered to the FDM machine controllers. Commands to the *X-Y* table enable the FDM extrusion head to traverse over a build platform while commands to the extrusion head motors drive the thermoplastic material into the liquefier.

Operating the MMMT FDM system in the *Single FDM Operation* mode only required one FDM system and therefore the unchanged ACL commands were delivered to the FDM system chosen by the user. To minimize the number of programs the user needed to access and operate, a batch file with the script shown below was written to open the FDM Status software and pass option arguments including the filename (%1) associated with the ACL commands, the machine name (%2) that identified the FDM system, and a "no graphics" option argument (%3) that ran the FDM Status software without graphics.

```
@echo off
C:
cd \InsightV35\nt
Fdmspd.exe %1 %2 %3
```

After the user specified a filename for the ACL code, the batch file was executed from within LabVIEW through the use of a System Exec. virtual instrument (VI).

When in *Multiple FDM operation* mode, the ACL code created by Insight needed to be modified such that tasks were delegated appropriately to each FDM system. This was accomplished by manually modifying the ACL code before supplying it to each FDM system. Noteworthy changes to the ACL code include (1) the insertion of PS (pause) commands that interrupted the build process and allowed the build platen to be transported between each FDM system, (2) the modification of MZ (relative movement in the Z direction) commands to ensure

that the extrusion head would not obstruct the transport of the workpiece and that each material was deposited at the correct Z location. The MZ commands, in particular, were modified often for the build process variation (variable layer thickness and road width) since each FDM machine was depositing different layer thicknesses.

3.3.3 Placing the extrusion tips at the start location and initiating build sequences

For conventional operations of a non-modified FDM 3000, the user is required to press the pause button on the machine's front panel after buffering the ACL code to the FDM machine. The machine then proceeds to finding a global datum for the *X*, *Y*, and *Z* axes after which the user is allowed to place the extrusion tip at the start location (local datum) by manually pressing cursor buttons on the machine's front panel. Once the tip is in place, the pause button must be pressed again to commence the building sequences. Through FDMotion, these required actions are performed via the graphic user interface that monitors and controls a series of digital inputs and solid state relays. Additionally, the FDMotion software offers a snapshot (Figure C1) of the status for each FDM system.

When operating in *Multiple FDM Operation* mode, both FDM systems were required to start building at the same *X/Y* location relative to a benchmark on the build platform. The selected benchmark for both systems was the bottom left corner of the build platform as shown in Figure 3.1. The distance between the global datum and the benchmark was measured for each FDM system. Initial measurements were performed with a ruler and fine adjustments were carried out after measuring offset distances with a stereomicroscope. These *X*/*Y* distances were used to develop a VI (Appendix C – Figures C26-27) that required the user to specify a start location relative to the benchmark. Within this VI, the *X/Y* distances between the global datum and the benchmark were subtracted or added accordingly to place the tooling head of both FDM

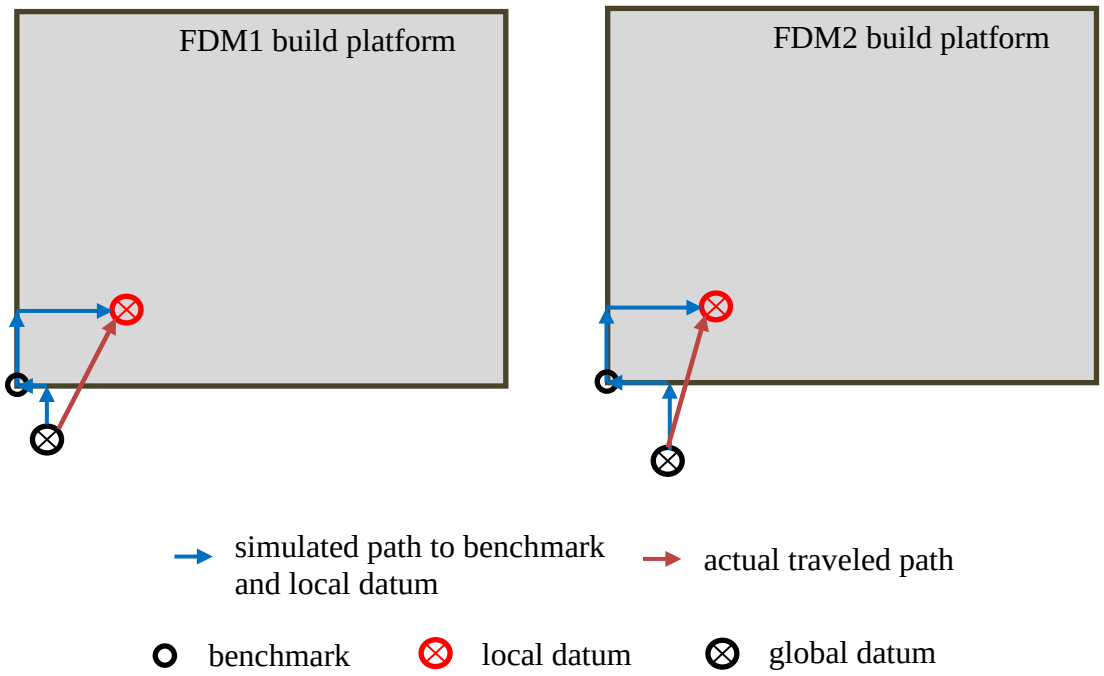

Figure 3.1. Schematic of movements for each FDM system required to arrive to the same local datum.

systems at the same local datum. In this manner the discrete materials are deposited and properly aligned to generate dimensionally accurate parts.

Chapter 4

Experimental Methodology

4.1 Surface Roughness, mechanical properties and build time of build process variation

The build process variation refers to the deposition of coarse rasters (inner fill pattern) using a T25 tip and fine contours using a T10 tip (Figure 4.1). The layer thicknesses were intended to result in a contour-to-raster thickness ratio of 4:1. The test geometry shown in Figure 4.2 has been used in similar work (Pandey, Reddy, and Dhande, 2003a) and was used here to determine the surface roughness (arithmetic average of absolute values for the surface profile, R_a) using a surface roughness tester (Mitutoyo Surftest SJ 201P, Mitutoyo, Aurora IL). The R_a of each surface was measured five times at different locations within each of the four inclined planes. For the build time study, a simple square prism (50.8mm by 50.8mm and

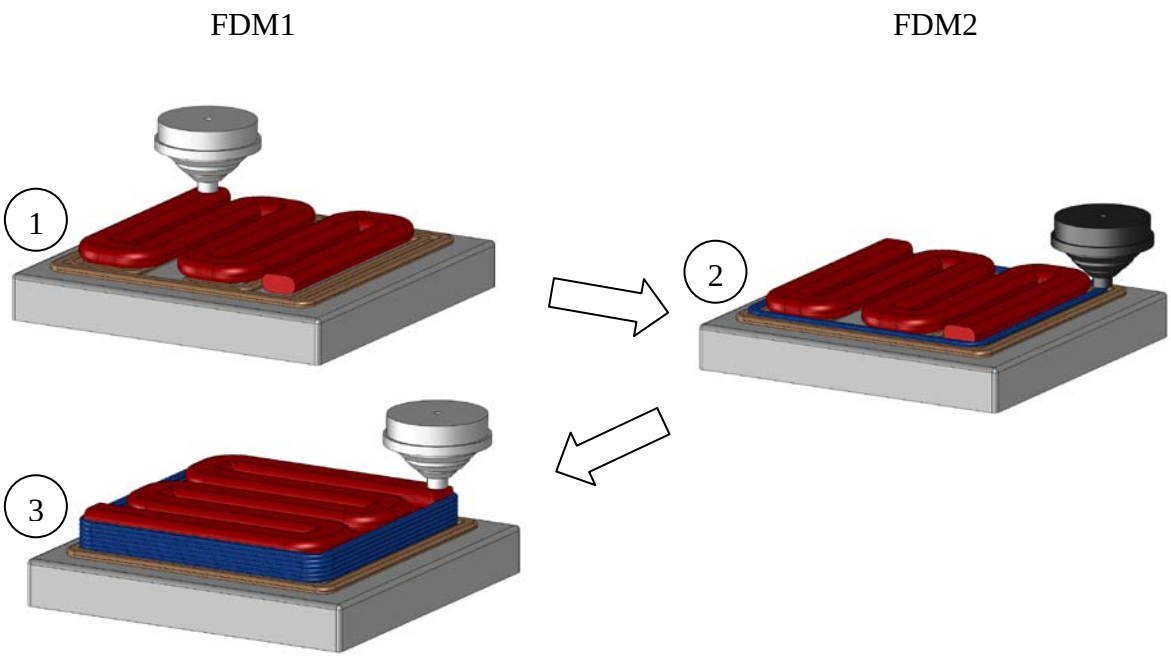

Figure 4.1. Cartoon of build process variation showing (1) the deposition of an initial coarse raster, (2) the deposition of fine contours, and (3) the deposition of a subsequent coarse raster.

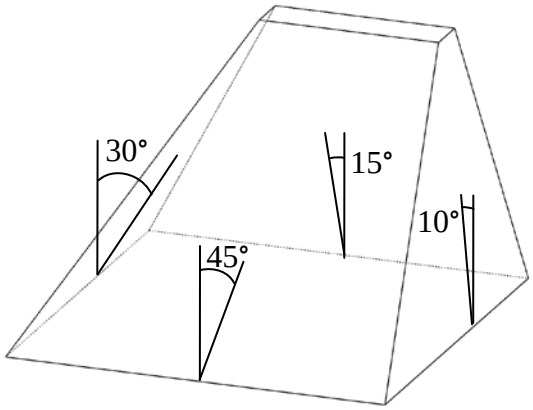

Figure 4.2. Test geometry for measuring surface roughness containing four inclined planes.

25.4mm tall) was fabricated with both a non-modfied FDM 3000 machine (using T10 tips) and the MMMT FDM system (using T10 tips for FDM1 and T25 for FDM2).

Tensile test specimens were fabricated using a non-modified FDM 3000 machine and the MMMT FDM system to compare the effect of the build process vatiation on mechanical properties. Tensile tests were conducted on an Instron 5866 system (Instron®, Norwood, MA) following guidelines provided by the ASTM D638 standard. A 10kN load cell was used and a deformation cross head speed of 5mm/min was employed. Each sample was comprised of five Type I specimens each of which was conditioned in a standard laboratory atmosphere (23±2°C and a relative humidity of 50±10%) for a minimum of 40 hours. From the collected data, the mechanical properties of ultimate tensile stress (UTS), strain at UTS, and modulus of elasticity were acquired.

4.2 Ultraviolet ozone surface treatment for interlayer bond improvements

4.2.1 Design of Experiments

4.2.1.1 Effects of UV ozone treatment on contact angle and surface energy of solid ABS P400

A design of experiments (DOE) consisting of a single factor with six levels was employed to determine the effects of UV ozone treatment on contact angles of solid ABS P400.

Table 4.1. Levels and responses for determining the effects of UV ozone treatment on contact angle and surface energy

Substrate	Exposure Time (minutes)	Response 1	Response 2
S1	0.0	water contact angle	ethylene glycol contact angle
S2	0.5		
S3	1.0		
S4	1.5		
S5	2.0		
S6	3.0		

The levels and responses for this DOE are shown in Table 4.1. Six ABS P400 substrates were produced by melting FDM stock filament and each substrate was treated with UV ozone for 0, 0.5, 1.0, 1.5, 2.0, or 3.0 minutes. Guidelines provided by ASTM D7490 were followed while using 7µL droplets of water and ethylene glycol as the working fluids. Two angle measurements were made on each droplet (one on each drop edge) Average contact angles were determined by making two angle measurements

Table 4.2 contains the total surface tension of each test liquid (γ_L) as well as the respective dispersion (γ_S^d) and polar components (γ_L^p). The Owens-Wendt-Kaelble equation shown below was used to calculate the total surface tension ($\gamma_S = \gamma_S^d + \gamma_S^p$) of solid ABS P400 for each treatment. Figure 4.3 presents a schematic of the test setup using an in-house-made goniometer.

$$\frac{\gamma_L(1+cos\theta)}{2} = \left[\left(\gamma_L^d \gamma_S^d\right)^{1/2} + \left(\gamma_L^p \gamma_S^p\right)^{1/2}\right] \qquad \text{Equation 6}$$

Table 4.2. Surface tension of water and ethylene glycol

Test Liquid	Total surface energy, γ_L (mJ/m^2)	Dispersion component, $\gamma_L{}^d$ (mJ/m^2)	Polar component, $\gamma_L{}^p$ (mJ/m^2)
water	72.8	21.8	51.0
ethylene glycol	48.0	33.8	14.2

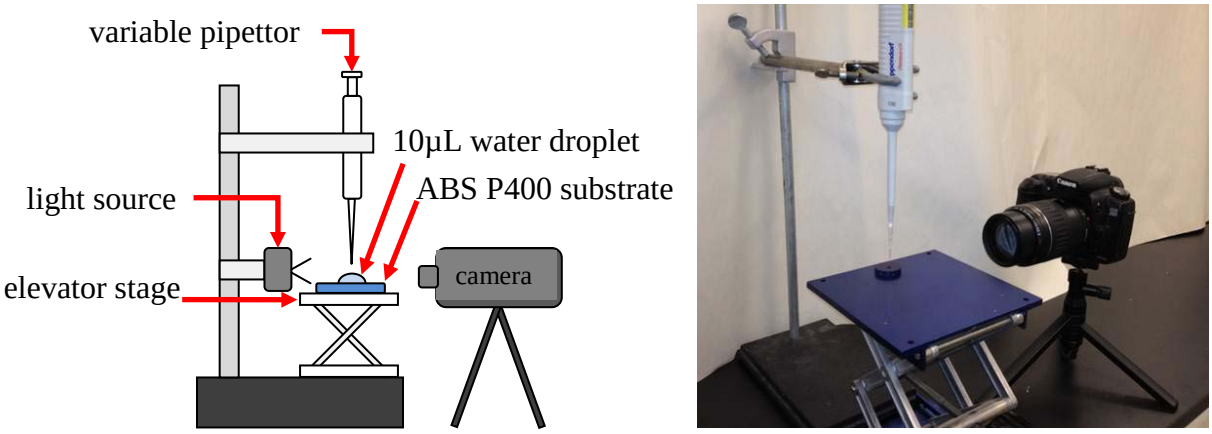

Figure 4.3. Schematic (left) and actual (right) test setup used for measuring contact angles of test liquid on ABS P400 substrate.

4.2.1.2 Effects of UV ozone treatment on mechanical properties of FDM-manufactured specimens

A single factor design of experiments containing six levels was implemented to determine the effects of UV ozone treatment on tensile mechanical properties of FDM-manufactured specimens. Each layer (except for the last one) of the tensile test specimen was exposed to UV ozone for 0, 0.5, 1.0, 1.5, 2.0, or 3.0 seconds by using a UV ozone cleaner (model 342 A, Jelight Company Inc., California). The UV ozone treated parts were mechanically tested under a tensile load according to ASTM D638 and as such the test parts were in the shape of standard tensile specimens (dog bones). Tensile testing of FDM-manufactured parts is typically done by employing the Type I specimen dimensions, however, due to the size limitations (152.4 X 152.4 X 25.4 mm) of the UV ozone cleaner, the Type V specimen dimensions were used (see Appendix D – Figure D2 for dimensions). Mechanical testing was performed with the equipment and procedure discussed in Section 4.1.

The fabrication and testing of the FDM-manufactured specimens was random, which required the fabrication of one test specimen per build sequence. Appendix E contains the order of fabrication and testing. The UV ozone treatments were carried out in the following fashion.

1. Deposit the support material and first layer of model material,
2. interrupt the build process by pausing the build sequence,
3. monitor the temperature of the deposited material with an IR thermometer (model Fluke 62 Mini, Fluke Corporation, Washington) until it cooled down to 93°C,
4. remove the specimen from the building chamber and allow it to cool down until reaching room temperature (~25°C),
5. place the specimen in the UV ozone cleaner at a distance of 5mm from the UV lamp,
6. expose the specimen for the predetermined time,
7. insert the specimen into the build chamber and allow it to heat up to 93°C,
8. continue the build sequence, and
9. repeat steps 2-8 until the test part is complete.

The last layer was not exposed to UV ozone since there were no additional layers to deposit. The test specimens were on a YXZ orientation (Appendix D – Figure D3) and fabricated on an FDM 3000 machine using the default foam build platform, support material parameters, and model material parameters, which are summarized in Table 4.3. Of the listed parameters, the employed envelope temperature (93°C) was higher than the default (70°C). Through experiments discussed in the following paragraph, the glass transition temperature (T_g) of this thermoplastic was determined to be 96.32 ± 1.49°C. The reasoning behind using 93°C as the envelope temperature is that the envelope was to be kept at a temperature where the bulk material did not experience long range molecular motion, rotational freedom, or segmental motion of the chains that result in stronger bonds between layers and reduces dimensional accuracy. However, if the surface of the layer that was exposed to the UV ozone did in fact

Table 4.3. Processing parameters used in UV ozone experiments

Model	
material	ABS P400 Blue
extrusion tip	T16
extrusion temperature	270°C
part interior style	solid-normal
part raster width	0.508 mm (0.020”)
contour width	0.508 mm (0.020”)
Support	
material	water soluble
extrusion tip	T16
extrusion temperature	235°C
support style	sparse
self-supporting angle	45°
base layers	5
Envelope	
envelope temperature	93°C

undergo a localized reduction of T_g by more than ~3°C, then at 93°C bonds between layers would be stronger and evident through mechanical testing results.

The T_g of the ABS P400 Blue thermoplastic was determined by following guidelines in ASTM E1640 (Assignment of the glass transition temperature by dynamic mechanical analysis). A dynamical mechanical analysis (DMA) instrument (model Q800, TA Instruments, Delaware) was used with the following testing parameters: 0.01N preload, 15µm amplitude, 1 Hz frequency, and 2°C/min ramp rate. The test specimen, shaped like a rectangular prism, was 35 X 10 X 4mm. Five specimens were fabricated in one build sequence using a flat layout and the default building parameters shown in Table 4.3 were used, except the default envelope temperature (70°C) was used. Each part was tested with the DMA instrument and the resulting data was averaged to represent a sample mean.

4.2.2 Statistical Analysis

The data collected from the UV ozone treatment experiments was evaluated with an analysis of variance (ANOVA) – a statistical method to test for equality of treatment effects. In general, for a single factor or treatment there may be *a* different levels. Each factor will produce a response in the form of a random variable. For each treatment there may be *n* observations that can be represented by the linear statistical model

$$Y_{ij} = \mu + \tau_i + \epsilon_{ij} \begin{cases} i = 1, 2, \dots, a \\ j = 1, 2, \dots, n \end{cases} \qquad \text{Equation 7}$$

where Y_{ij} is the (*ij*)th observation (random variable), μ is the overall mean common to all treatments, τ_i is the *i*th treatment effect, and the random error effect is denoted by ϵ_{ij}. Another form of the linear statistical model can be represented as

$$Y_{ij} = \mu_i + \epsilon_{ij} \begin{cases} i = 1, 2, \dots, a \\ j = 1, 2, \dots, n \end{cases} \qquad \text{Equation 8}$$

where $\mu_i = \mu + \tau_i$ represents the mean of the *i*th treatment. In this model, the assumption that ϵ_{ij} is normally and independently distributed with mean zero and variance σ^2 allows the evaluation of each treatment as a normal distribution with mean μ_i and variance σ^2.

In a fixed-effects model, the factor levels are chosen by the experimenter and hypotheses about the treatment means are tested. Usually, the treatment effects τ_i are described as deviations from the overall mean μ resulting in the following:

$$\sum_{i=1}^{a} \tau_i = 0 \qquad \text{Equation 9}$$

For each treatment, the total and average of the observations under the *i*th treatment are shown, respectively, as follows.

$$y_{i\,.} = \sum_{j=1}^{n} y_{ij} \qquad i = 1, 2, \ldots, a \qquad \text{Equation 10}$$

$$\bar{y}_{i\,.} = y_{i\,.}/n \qquad i = 1, 2, \ldots, a \qquad \text{Equation 11}$$

In the above equations, the period indicates the summation over the replaced subscript. Similarly, the grand total and mean of all the observations can be expressed mathematically as

$$y_{.\,.} = \sum_{i=1}^{a} \sum_{j=1}^{n} y_{ij} \qquad \text{Equation 12}$$

$$\bar{y}_{.\,.} = y_{.\,.}/N \qquad \text{Equation 13}$$

where *N* is the total number of observations (*an*).

The equality of the a treatment means $(\mu_1, \mu_2, \ldots, \mu_a)$ can be tested by using Equation 9 and noting the equivalence to the following hypothesis testing

$$H_0: \tau_1 = \tau_2 = \cdots = \tau_a = 0$$
$$H_1: \tau_i \neq 0 \text{ for at least one } i \qquad \text{Equation 14}$$

This test indicates that if the null hypothesis (H_0) is true, a normal distribution with mean μ and variance σ^2 describes all *N* observations. In other words, if the null hypothesis is true, changing the level of the factor has no effect on the mean response.

The ANOVA describes the total variability in the data with the total sum of squares (SS_T).

$$SS_T = \sum_{i=1}^{a} \sum_{j=1}^{n} \left(y_{ij} - \bar{y}_{.\,.}\right)^2 \qquad \text{Equation 15}$$

The total variability in the sample data is partitioned into two components – sum of squares of differences between treatment means and the grand mean ($SS_{Treatments}$) and sum of squares of differences of observations within a treatment from the treatment mean (SS_E). Mathematically, this partition (also known as the sum of squares identity) is shown in the following equation.

$$SS_T = SS_{Treatments} + SS_E$$

or

$$\sum_{i=1}^{a}\sum_{j=1}^{n}\left(y_{ij} - \bar{y}_{..}\right)^2 = n\sum_{i=1}^{a}(\bar{y}_{i.} - \bar{y}_{..})^2 + \sum_{i=1}^{a}\sum_{j=1}^{n}\left(y_{ij} - \bar{y}_{i.}\right)^2 \qquad \text{Equation 16}$$

In the SS_T partition, $SS_{Treatments}$ is a measure of the differences between treatments and SS_E is produced by way of random error.

In addition to the partition of the total variability, the number of degrees of freedom is also partitioned. SS_T has a total of *an*-1 degrees of freedom while $SS_{Treatments}$ has *a*-1 degrees of freedom and SS_E has *a*(*n*-1) degrees of freedom. The ratio of the sum of square to the associated degrees of freedom is called the mean square.

$$MS_{Treatments} = \frac{SS_{Treatments}}{(a-1)} \qquad \text{mean square of treatments} \qquad \text{Equation 17}$$

$$MS_E = \frac{SS_E}{a(n-1)} \qquad \text{error means square} \qquad \text{Equation 18}$$

Both $MS_{Treatments}$ and MS_E are independent and establish the test statistic F_0 for the *F*-test.

$$F_0 = \frac{SS_{Treatments}/(\mathrm{a}-1)}{SS_E/[\mathrm{a}(\mathrm{n}-1)]} = \frac{MS_{Treatments}}{MS_E} \qquad \text{Equation 19}$$

Table 4.4. The analysis of variance for the fixed-effects model and a single-factor experiment

Source of variation	Sum of squares	Degrees of freedom	Mean square	F_0
Treatments	$SS_{Treatments}$	$a-1$	$MS_{Treatments}$	$\frac{MS_{Treatments}}{MS_E}$
Error	SS_E	$a(n-1)$	MS_E	
Total	SS_T	$an-1$		

The results from an ANOVA are typically tabulated in a fashion similar to that of Table 4.4. For an *F*-test, the rejection criteria is within an upper-tail, one-tail critical region and therefore, H_0 is rejected if $f_0 > f_{\alpha,a-1,a(n-1)}$, where $f_0$is the calculated value of F_0 and α is the significance level. Since the UV ozone treatment experiments involved only one factor (UV ozone treatment) at multiple levels (exposure times), the above method for an ANOVA was employed.

4.3 Mechanical properties of PC – ABS heat-treated specimens

4.3.1 Fabrication of tensile specimens

Tensile test specimens were fabricated with dimensions of ASTM D638 Type I specimens (Appendix D – Figure D1). Four sample groups each made of PC, ABS, and discrete PC – ABS materials were fabricated. Except for the extrusion temperature of the model materials, the fabricating parameters (contour and raster widths, raster angles, air gaps, part orientation, and envelope temperature) were the same for all specimens. Figure 4.4A shows an image of a PC – ABS specimen being built, and the cross-section of the narrow section of the test specimens are shown in Figure 4.4B to illustrate the shell-and-core configuration of the multi-material specimens. For the fabrication of the PC – ABS specimens, FDM1 deposited the support material (layers 1 - 5) followed by two layers of PC (layers 6 - 7). Next, two PC

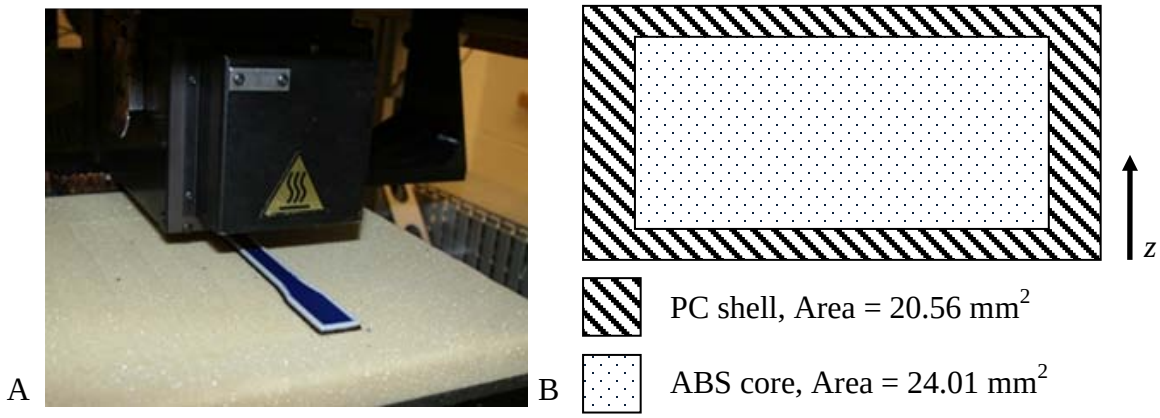

Figure 4.4. Fabrication of multi-material specimens. A) PC – ABS specimen built using multi-material, multi-technology FDM system. Note that the fabrication process used three discrete materials - PC, ABS, and a water-soluble support material. B) diagram of cross-section for the narrow section of the PC – ABS test specimens.

contours were deposited by FDM1 on layer 8 after which the build platform was moved to the FDM2 location for the deposition of ABS rasters in layer 8. Layers 9 - 15 also consisted of PC contours and ABS rasters while layers 16 and 17 were made of PC. These layers were stacked along the *z* direction indicated in Figure 4.4B.

To directly compare the effect of heat treating PC – ABS specimens, one group was heat-treated while another was left untreated. Specimens were measured for dimensions with a digital caliper before and after the heat treatment. The heat treatment consisted of placing the discrete PC – ABS specimens in an oven at room temperature and then heating to 160°C. The specimens were left at this temperature for 2 hours after which the oven was turned off and samples were removed once they reached room temperature. Referring to Table 2.1 and noting the glass transition temperature of PC (161°C) and ABS (104°C), the heat treatment was performed at 160°C to enable the flow of ABS and yield a dense core while prohibiting the PC shell from severe deformation.

4.3.2 Mechanical testing

Tensile tests were conducted following guidelines provided by the ASTM D638 standard. Section 4.1 describes the employed equipment and procedure.

4.3.3 Statistical Analysis

Student's *t*-tests were performed on the data collected for the heat-treated and untreated specimens to determine if the mean of the ultimate tensile strength, modulus of elasticity, and strain at ultimate strength were equal. The significance level used was $\alpha = 0.05$.

Chapter 5

Results and Discussion

5.1 Demonstration: FDM using multi-colors and a build process variation

The MMMT FDM system provided access to four extrusion tips that allowed fabrication using multi-colors and build process variations (variable layer thickness and road width). To demonstrate these capability, several parts were produced in which ABS P400 thermoplastic was deposited in either the blue or red variation in the form of relatively high resolution contours (ie., thin layers and narrow roads) and low resolution fill patterns or rasters. As will be discussed later, the fine contours were intended to improve surface roughness when compared to the default contours, which contain a layer thickness of 0.254mm for T10 tips. Figure 5.1 contains images of several demonstration pieces in which all parts (1-4) were fabricated using multi-colored thermoplastics and parts highlighted with labels 1-2 were fabricated with the build

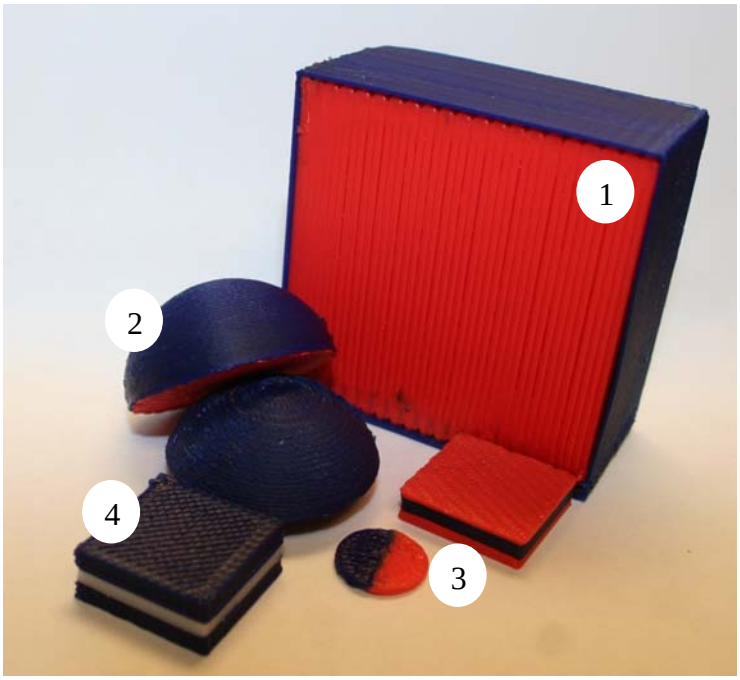

Figure 5.1. Demonstration pieces produced with the multi-color fabrication and build process variation.

process variation. Note that in most of these demonstration pieces, different colored thermoplastics are deposited not only at different layers, but at different regions within a layer.

5.2 Demonstration: FDM using discrete multi-materials

The constructed MMMT FDM system demonstrated the successful fabrication of discrete PC – ABS parts by utilizing three extrusion tips – one for each material (ABS, PC, and water-soluble support material). Hypothetically, geometrically complex multi-material parts made from three discrete thermoplastics (or four thermoplastics for self-supporting geometries) may be fabricated by this MMMT FDM system. As an example of the complexity that may be achieved by this process, a sandwich structure (Figure 5.2) was fabricated using the MMMT FDM system. Included were two ABS skins and a PC core composed of tetragonal truss elements (Figure 5.2C). This type of structure cannot be manufactured with conventional multi-material thermoplastic processing techniques such as overmolding or multi-shot injection molding.

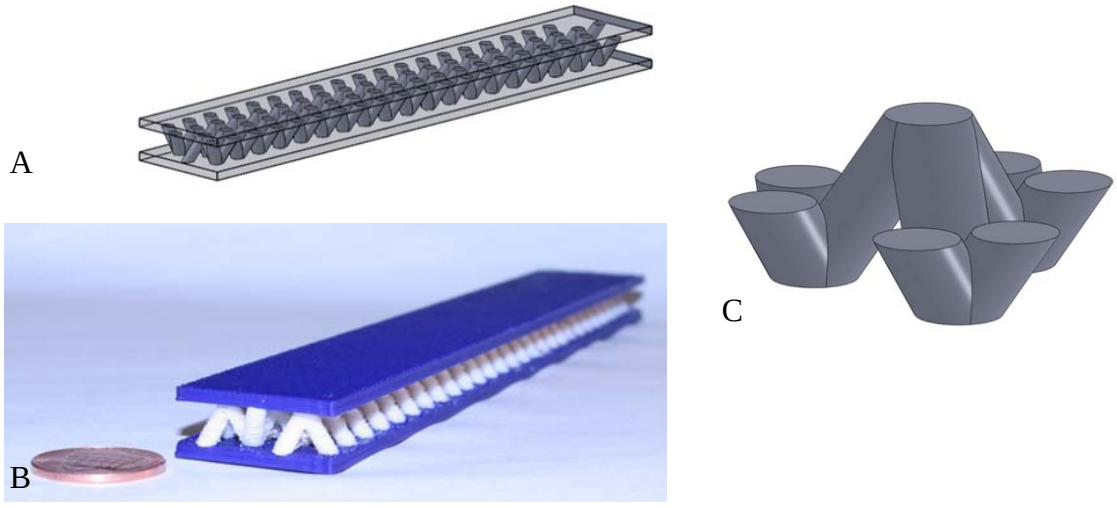

Figure 5.2. FDM-manufactured sandwich structure. A) CAD of sandwich structure. B) sandwich structure composed of ABS skins and PC core (U.S. penny used for scale). C) CAD of tetragonal truss core element.

5.3 Properties of parts produced using the build process variation

Optical images shown in Figure 5.3 were captured with a stereomicroscope (model: MZ 16, Leica Microsystems Inc., Buffalo Gove, Illinois) equiped with a digital CCD camera (model: Retiga-2000R, QImaging, Surrey, British Columbia). For the fill pattern roads (rasters), measurements ($\mu \pm \sigma$) showed a $1200 \pm 39\mu m$ road width and $497 \pm 11\mu m$ layer thickness. Contour measurements displayed a $269 \pm 18\mu m$ road width and $133 \pm 3\mu m$ layer thickness. The mechanical properties of the parts produced with the non-modified FDM 3000 (standard build process) and the MMMT FDM system are shown in Table 5.1. There was no statistical evidence that the mechanical properties (ultimate tensile stress and associated strain as well as the modulus of elasticity) of the specimens produced with the standard and build process variation were different (p-values > 0.05 for student's t test, μ_1-$\mu_2 = 0$, n = 5). That is, the build process variation did not significantly reduce or alter the mechanical properties of the produced parts when compared to the standard build process.

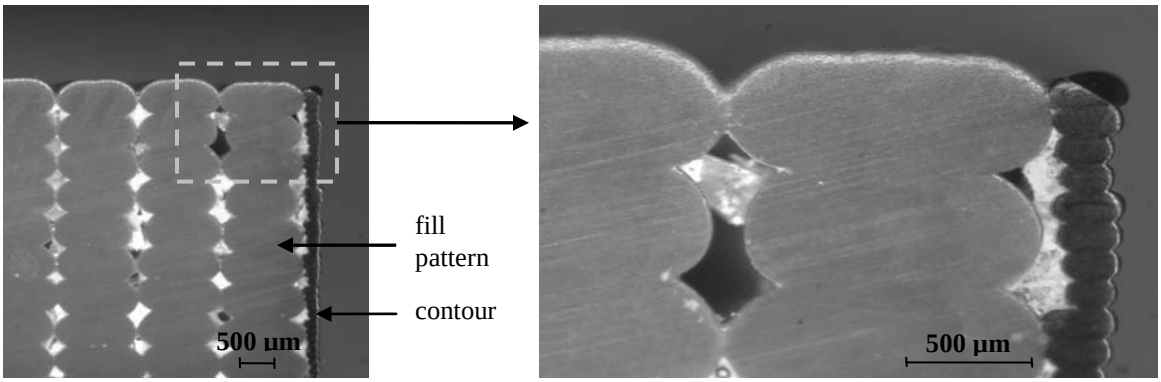

Figure 5.3. Optical image of cross-sectioned part produced with the build process variation.

Table 5.1. Tensile properties of specimens built using the standard process and the build process variation.

	Ultimate Tensile Stress, UTS (MPa)	Strain at UTS (%)	Modulus of Elasticity (MPa)
Standard Build Process	18.61	1.63	540.03
Build Process Variation	18.23	1.51	517.9

Surface roughness measurements in the form of R_a values are reported in Figure 5.4. The R_a values decreased on all four planes. In particular, there was a 55% reduction in surface roughness on the plane that was inclined 10° from vertical. Reducing the layer thickness to achieve high resolution contours was anticipated to increase the total build time, and as such compensatory rasters for the internal fill pattern were built using a larger layer thickness and wider road width. In fact, using this build variation reduced the build time by approximately 35%. The time required to build a simple square prism (50.8mm X 50.8mm and 25.4mm tall) using the standard process and the build process variation was 6.2 hr and 4.0 hr, respectively. It

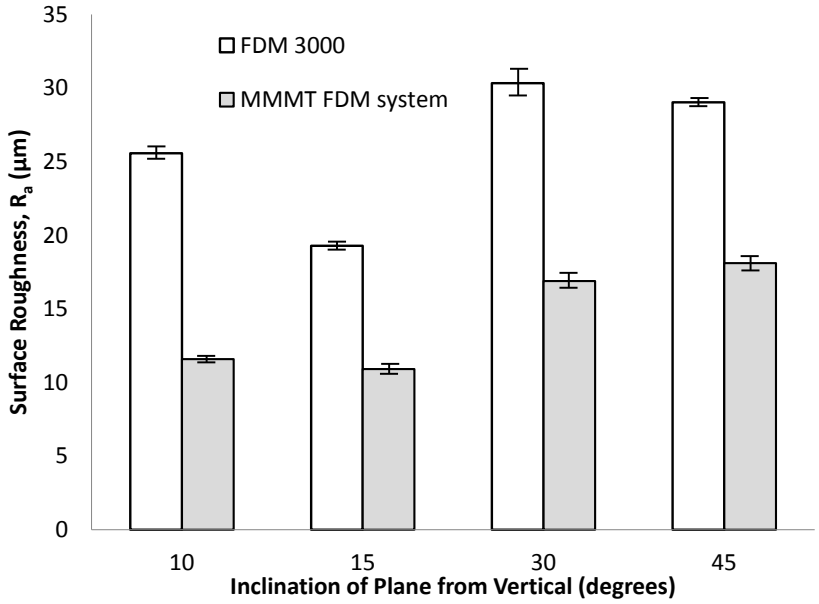

Figure 5.4. Average surface roughness of specimens built using the standard process and build process variation (each bar is the average of five measurements and the standard deviation was used for error bars).

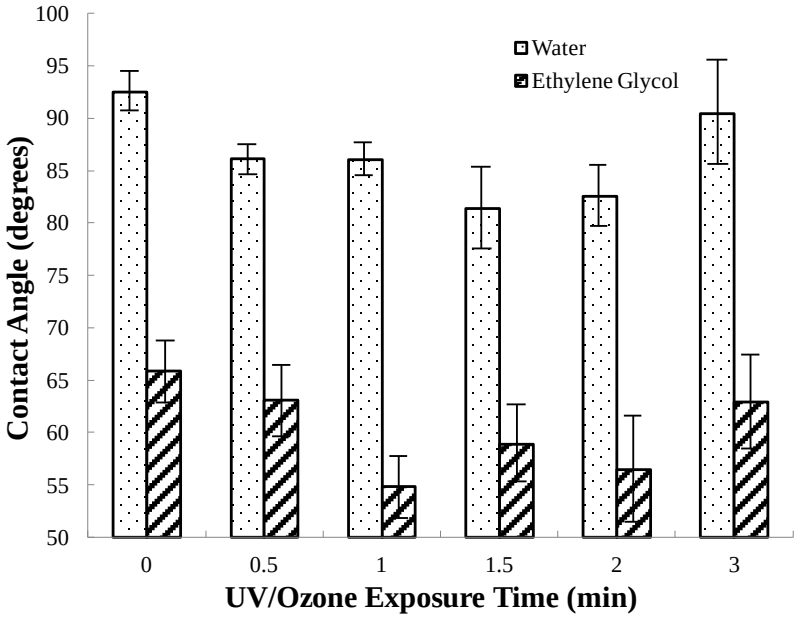

Figure 5.5. Contact angle of water and ethylene glycol on UV/O_3 treated ABS (six measurements were used to calculate the average and standard deviation for error bars).

should be noted that the build process variation included the translation of the workpiece between the FDM systems.

5.4 Contact angle and surface energy of ABS P400 treated with ultraviolet ozone

Contact angles on UV/O_3-treated ABS P400 for both water and ethylene glycol are presented graphically in Figure 5.5. An ANOVA was performed for both data sets (water and ethylene glycol) and results can be found in Table 5.2. For water, since $f_0 = 11.77 > f_{0.05,5,30} = 2.53$, the null hypothesis was rejected and therefore, it was concluded that the UV/O_3 treatment significantly affected the mean contact angle of water on solid ABS P400. Similarly for ethylene glycol, since $f_0 = 7.65 > f_{0.05,5,30} = 2.53$, the null hypothesis was rejected and it was concluded that the UV/O_3 treatment significantly affected the mean contact angle of ethylene glycol on solid ABS P400. The minimum mean contact angle for water on ABS P400

was 81.38° and was achieved with a UV/O_3 exposure time of 1.5 minutes. This constituted an approximate 12% reduction in mean contact angle when compared to untreated ABS P400, which displayed a mean contact angle of 92.54°. Similarly, the mean contact angle between ethylene glycol and solid ABS P400 experienced an approximate 17% reduction when the ABS P400 was treated with UV/O_3 for 1 minute and compared with an untreated specimen.

The mean contact angle for each test liquid and UV-O_3 treatment were used in conjunction with the Owen-Wendt-Kaelble relationship (Equation 6) to determine the dispersion and polar components of the ABS P400 surface tension. Results can be found in Figure 5.6. The polar component displayed a general increasing trend between an exposure time of 0-1.5 minutes indicating that functional groups were being formed at the polymer surface. The decreasing trend in surface energy after the 1 minute UV-O_3 exposure is most likely due to the production of low molecular weight, broken-down fragments that in essence began to contaminate the polymer surface. Also, the total surface tension of an untreated ABS P400 was 21.4mJ/m^2 and a surface

Table 5.2. Single factor ANOVA results for contact angles on solid ABS P400 at six treatment levels ($\alpha = 0.05$)

Test liquid: Water				
Source of variation	*SS*	*df*	*MS*	f_0
UV ozone exposure time	565.58	5	113.12	11.77
Error	288.20	30	9.61	
Total	853.77	35		
Test liquid: Ethylene glycol				
UV ozone exposure time	554.38	5	110.88	7.65
Error	434.96	30	14.50	
Total	989.34	35		

tension of 26.9mJ/m^2 was achieved with a UV-O3 exposure time of 1 minute constituting an increase of ~26%.

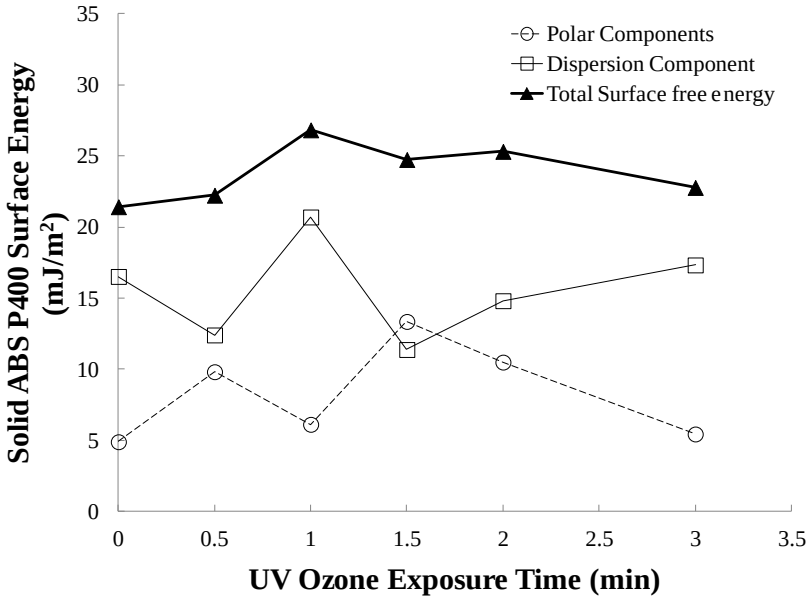

Figure 5.6. Surface energy of UV/O_3 treated ABS substrates

5.5 Mechanical properties of ABS P400 specimens manufactured using FDM and ultraviolet ozone

The ASTM D638 type V tensile test specimens were treated with UV/O_3 and characterized based on their mechanical properties. The resulting ultimate tensile stress (UTS), strain at UTS, and modulus of elasticity are shown in Figure 5.7, 5.8, and 5.9, respectively. Note that visually comparing the results for the untreated specimens (exposure time equal to zero) to the other specimens leads to the observation that the mechanical properties are unchanged. In fact, the results from an ANOVA (Table 5.3) also support the observations arrived to by inspecting Figure 5.7-5.9. Since $f_0 < f_{0.05,5,24} = 2.62$ for the three mechanical properties, the null hypothesis was not rejected and it was concluded that the UV/O_3 treatment did not have a significant effect on the tensile mechanical properties.

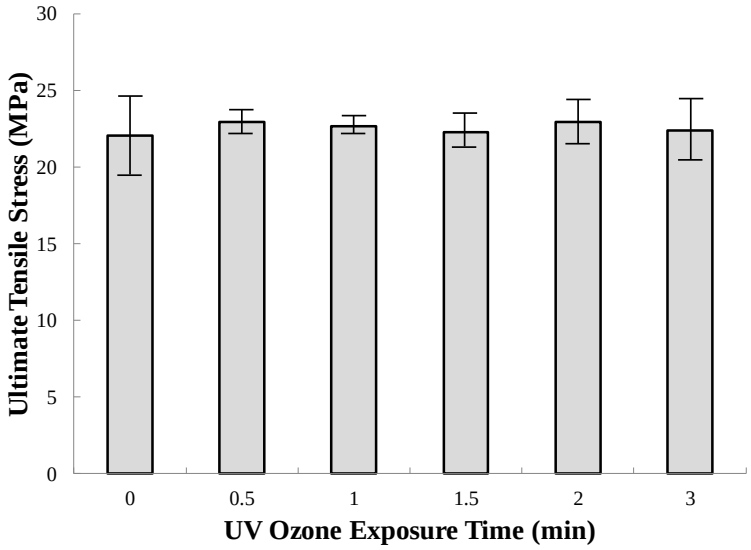

Figure 5.8. Ultimate tensile stress of FDM-manufactured P400 ABS specimens treated with UV/O_3 at each layer.

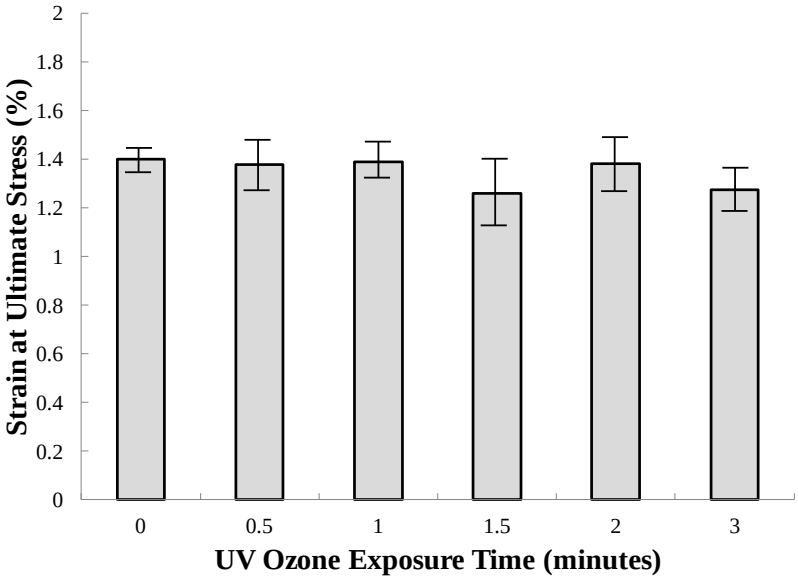

Figure 5.7. Strain at ultimate tensile stress of FDM-manufactured P400 ABS specimens treated with UV/O_3 at each layer.

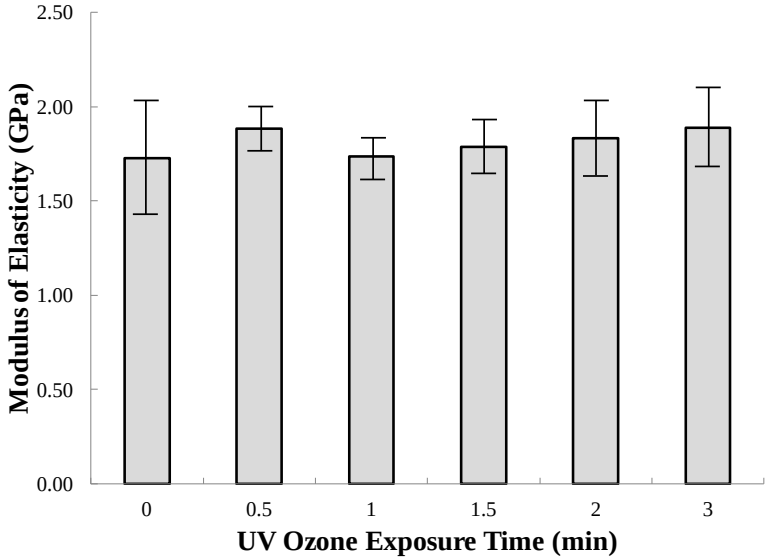

Figure 5.9. Modulus of elasticity of FDM-manufactured P400 ABS specimens treated with UV/O_3 at each layer.

5.6 Mechanical properties of heat-treated multi-material specimens

Results for ultimate tensile strength, strain at ultimate strength, and modulus of elasticity are presented in Figure 5.10. Note that the experimental ultimate tensile strength and modulus of elasticity for ABS and PC groups are lower than those reported by the manufacturer (Table 2.1). For ABS, the experimentally determined UTS is 20% lower than the tensile strength reported by the manufacturer and the modulus is 67% lower than the manufacturer value. Likewise for PC, the UTS is 34% lower than the tensile strength reported by the manufacturer and the modulus is 74% lower than the manufacturer value. The difference is due in part to the part orientation during fabrication. That is, using the orientation notation in ASTM F2921 (2011) the manufacturer constructed test specimens using either the XZY or YZX orientations while for this study the test specimens were built using the YXZ orientation. Additionally, the raster angles may have been different – this study used a starting angle of 0° and delta angle of 90°.

The student's *t*-test revealed that the means for the ultimate tensile strength of heat-treated and untreated specimens were significantly different ($p = 0.004 < 0.05$). In fact, the heat treatment resulted in ~25% increase of ultimate tensile strength. Likewise, the means for the modulus of elasticity of heat-treated and untreated specimens were significantly different ($p = 0.006 < 0.05$) – an ~18% increase due to the heat treatment was observed. There was no statistical evidence that the means of the strain for the heat-treated and untreated specimens were different, however, the standard deviation does seem to decrease with the heat treatment.

Optical microscopy images of the fracture surfaces are also shown in Figure 5.10. Note that in the untreated specimen (left image in Figure 5.10D) the roads are still distinguishable. Spaces between roads and layers are also present that result in stress concentrators known to

Table 5.3. Single factor ANOVA results for tensile testing on solid ABS P400 at six treatment levels ($\alpha = 0.05$)

Ultimate Tensile Strength				
Source of variation	*SS*	*df*	*MS*	f_0
UV ozone exposure time	3.51	5	0.70	0.27
Error	61.76	24	2.57	
Total	65.27	29		
Strain at Ultimate Stress				
UV ozone exposure time	0.096	5	0.019	2.02
Error	0.22	24	0.0095	
Total	0.32	29		
Strain at Ultimate Stress				
UV ozone exposure time	0.12	5	0.025	0.67
Error	0.89	24	0.037	
Total	1.01	29		

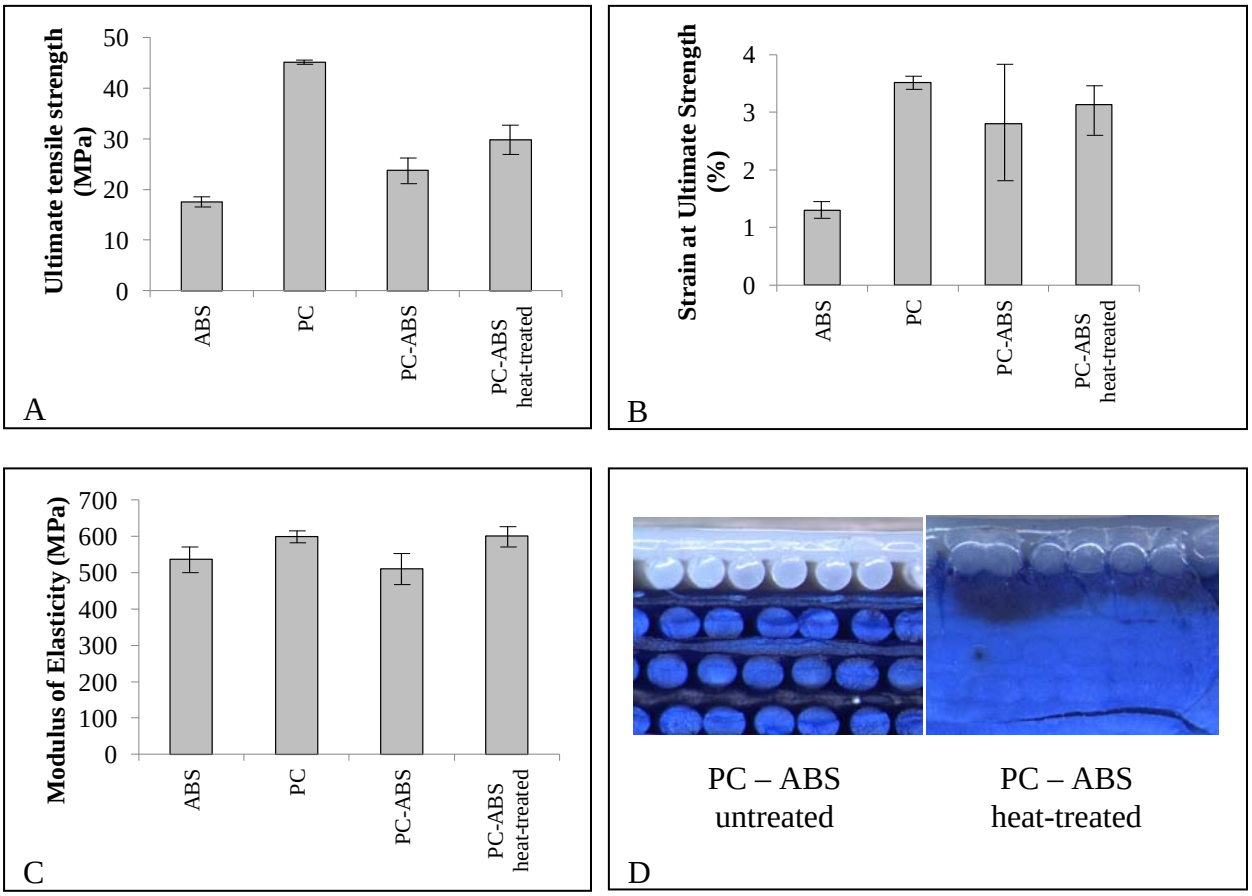

Figure 5.10. Results from ASTM D638 tensile testing (error bars represent ± σ calculated from five specimens). A) mean ultimate tensile strength. B) mean strain at ultimate strength. C) mean modulus of elasticity. D) optical microscopy images of fracture surfaces for untreated and heat-treated PC – ABS specimens.

reduce the tensile strength of FDM-manufactured parts (Bellini and Guceri 2003; Rodriguez, Thomas, and Renaud 2003). On the other hand, the heat-treated specimens (right image of Figure 5.10D) show a fully dense ABS region. This densification resulted in the ~25% increase in ultimate tensile strength.

5.7 Dimensional Accuracy of heat-treated multi-material specimens

The dimensional change for the specimen's features (thickness, width, and length) caused by the heat treatment is shown in Figure 5.11. Note that a negative dimensional change indicates a reduction in dimension for the comparison. In general, the difference between heat-treated and untreated dimensions for all features decreased due to the heat treatment in which the largest change was in length (-1.4mm) – the width change was -0.5mm and thickness change was -0.3mm. In terms of percentages, the dimensions of the width, thickness, and length decreased by 3.4%, 7.3%, and 0.8%, respectively.

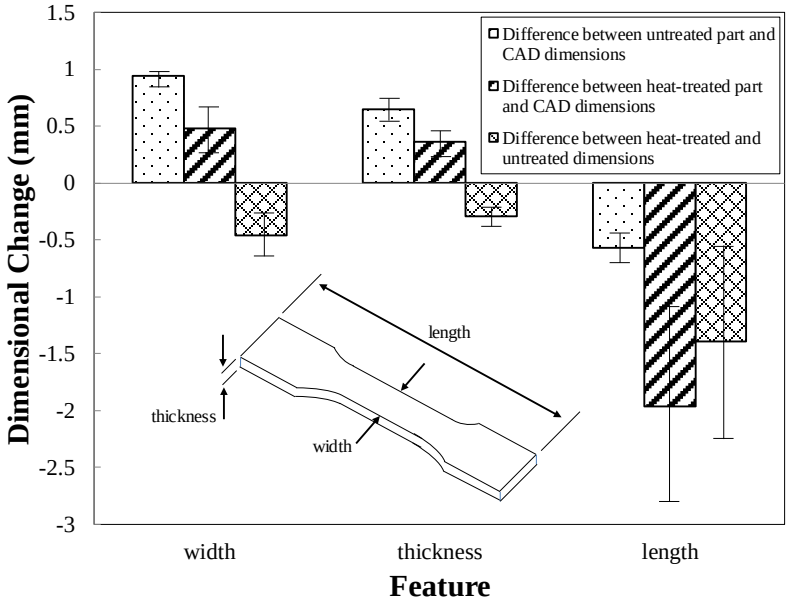

Figure 5.11. Mean dimensional changes caused by heat treating PC – ABS specimens (error bars represent ± σ calculated from five specimens).

Chapter 6

Conclusion and Recommendations

6.1 Conclusions

A multi-material, multi-technology FDM system was designed and constructed. The developed FDMotion software allowed the control of hardware through a series of GUI's. FDMotion also allowed the use of two modes (*Single FDM operation* and *Multiple FDM operation* mode) with easy to follow in-process instructions. The MMMT FDM system gave access to four extrusion tips that allowed the fabrication of novel thermoplastic parts including multi-colored parts made from similar and dissimilar materials as well as a novel process for fabricating complex geometries using FDM and subsequently performing a heat treatment that improved mechanical properties and density.

Multi-material fabrication was used to produce multi-colored parts and demonstrate the deposition of discrete materials at any layer and within different regions of a layer. Several geometries were constructed that used blue and red ABS P400 thermoplastic to easily identify the different regions. This use of multi-colored thermoplastics can be used to fabricate aesthetically pleasing and highly attractive 3D parts that may contain a company's logo, provide another level for mass customization, and easily identify mating surfaces for complex assemblies. Dissimilar thermoplastics were also used in a single build sequence to construct a sandwich structure composed of ABS skins and a complex PC core constructed from tetragonal truss elements. The geometric complexity of this structure is such that it is impossible to fabricate using injection molding. These types of structures may be employed by the transportation and aerospace industries since sandwich structures can exhibit high strength to weight ratios and result in less overall fuel consumption.

A build process variation using variable layer thicknesses and road widths was used to reduce the surface roughness of planes that were inclined 10, 15, 30, and 45° from vertical by 55, 43, 44, and 38%, respectively. The mechanical properties of parts produced with the build

process variation were not compromised and the build time was reduced by 35% for the fabrication of a simple rectangular prism (50.8mm by 50.8mm and 25.4mm tall). However, it is noted that the reduction in build time is highly dependent on the geometry and as such time savings are expected to vary. The maximum reduction in build times, therefore, will be achieved when the volume ration of internal fill to contour is highest. The FDM build process variation improved both surface roughness and build time – two FDM aspects commonly viewed in need of improvement.

The developed MMMT FDM system also allowed the ultraviolet ozone treatment at every layer to determine its effect on mechanical properties. Although it was determined that the surface energy increased by 26% when ABS was exposed for 1 minute, this increase did not translate to an increase in mechanical properties. However, this method of increasing surface energy and wettability may be useful for adhesive bonding processes that require clean and chemically active surfaces. Also, since the MMMT FDM system allows the FDM process to be easily interrupted and supplemented by other technologies (like UV/O_3 in this case), experimentation with other interlayer improvement strategies can be easily implemented.

A novel heat treatment method was developed using parts fabricated with the MMMT FDM system. The parts were made of discrete PC – ABS materials and a shell-and-core configuration. Fabricating the shell using a material with higher glass transition temperature (PC) than the core material (ABS) allowed the heat treatment of the core without drastically changing the overall dimensions of the part. The heat treatment, although not optimized, demonstrated a substantial increase in ultimate tensile strength (~25%). Optical images also showed that the density of the core increased. This multi-material and heat treatment method in combination is very promising in that the tensile and potentially fatigue properties of FDM-manufactured parts may be improved. The densification of FDM-fabricated parts can also expand FDM into applications of high pressures – an area that has not been explored in detail due to porous parts.

6.2 Recommendations for Future Work

Future work should include the use of the developed MMMT FDM system to explore other mechanical and chemical interlayer bonding improvement strategies. Also, the build process variation demonstrated in this work should be applied to the deposition of support material to determine the additional time savings. In regard to the heat treatment of multi-material parts, a design of experiments can be developed to determine the effect of temperature and time on mechanical properties and density. This study may reveal improvements in ultimate tensile strength greater than the 26% improvement shown in this work. Additionally, parts fabricated with this heat treatment method should be tested for their pressure withstanding capabilities to identify other application of FDM-fabricated parts. The integration of complementary technologies such as CNC or laser micro-machining and direct-write into the MMMT FDM system should also be pursued in the future. These technologies would aid in achieving microscale features and heterogeneous structures.

References

Ahn, S., Montero, M., Odell, D., Roundy, S., Wright, P., 2002. Anisotropic material properties of fused deposition modeling ABS. Rapid Prototyping Journal 8 (4) pp. 248-257.

Allahverdi, M., Danforth, S.C., Jafari, M., Safari, A. 2001. Processing of advanced electroceramic components by fused deposition technique. Rapid Prototyping Journal 21 (10-11), 1485-1490.

Arcaute, K., Mann, B.K., Wicker, R.B. 2006. Stereolithography of three-dimensional bioactive poly(ethylene glycol) constructs with encapsulated cells. Annals of Biomedical Engineering 34 (9), 1429-1441.

ASTM Standard D638-10. 2010. "Standard Test Method for Tensile Properties of Plastics". ASTM International, West Conshohocken, PA.

ASTM Standard D7490-08. 2008. "Standard Test Method for Measurement of the Surface Tension of Solid Coatings, Substrates and Pigments using Contact Angle Measurements". ASTM International, West Conshohocken, PA.

ASTM Standard E1640-09. 2009. "Standard Test Method for Assignment of the Glass Transition Temperature By Dynamic Mechanical Analysis". ASTM International, West Conshohocken, PA.

ASTM Standard F2792-12a. 2012. "Standard Terminology for Additive Manufacturing Technologies". ASTM International, West Conshohocken, PA.

ASTM Standard F2921-11. 2011. "Standard Terminology for Additive Manufacturing – Coordinate Systems and Test Methodologies". ASTM International, West Conshohocken, PA.

Bellini, A., Guceri, S. 2003. Mechanical characterization of parts fabricated using fused deposition modeling. *Rapid Prototyping Journal* 9 (4), 252-264.

Bellini, A., Shor, L., Guceri, S. 2005. New developments in fused deposition modeling of ceramics. *Rapid Prototyping Journal* 11 (4), 214-220.

Blanskby, S.J., Ellison, G.B. 2003. Bond dissociation energies of organic molecules. *Accounts of Chemical Research* 36 (4), 255-263.

Bourell, D.L., Beaman, J.J., Leu, M.C., Rosen, D.W. 2009. A brief history of Additive Manufacturing and the 2009 Roadmap for Additive Manufacturing: Looking back and looking ahead. Proceedings from the RapidTech 2009 US-Turkey Workshop on Rapid Technologies.

Campilho, R.D.S.G., Pinto, A.M.G., Banea, M.D., da Silva, L.F.M. 2012. Optimization study of hybrid spot-welded/bonded single-lap joints. International Journal of Adhesion & Adhesives 37, 86-95.

Choi, J., Medina, F., Kim, C., Espalin, D., Rodriguez, D., Stucker, B., Wicker, R., 2011. Development of a mobile fused deposition modeling system with enhanced manufacturing flexibility. Journal Of Materials Processing Technology 211 (3) pp. 424-432.

The Economist. "A Third Industrial Revolution." *The Economist* 21 April 2012. Print.

Espalin, D., Arcaute, K., Rodriguez, D., Medina, F., Posner, M., Wicker, R., 2010. Fused deposition modeling of patient-specific polymethylmethacrylate implants. Rapid Prototyping Journal 16 (3) pp. 164-173.

Es-said, O.S., Foyos, J., Noorani, R., Mendelson, M., Marloth, R. 2000. Effect of layer orientation on mechanical properties of rapid prototyped samples. Materials and Manufacturing Processes 15 (1) pp. 107-122.

Frerichs, H., Stricker, J., Wesner, D.A., Kreutz, E.W. 1995. Laser-induced surface modification and metallization of polymers. Applied Surface Science 86 (1-4) pp. 405-410.

Gibson, I., Rosen, D.W., Stucker, B. 2010. Additive manufacturing technologies: Rapid prototyping to direct digital manufacturing. New York: Springer.

Haisma, J., Spierings, G.A.C.M. 2002. Contact bonding, including direct-bonding in a historical and recent context of material science and technology, physics, and chemistry: Historical review in a broader scope and comparative outlook. Materials Science and Engineering Vol. 37 (1-2), 1-60.

Iyer, S., McIntosh, J., Bandyopadhyay, A., Langrana, N., Safari, A., Danforth, S.C., Clancy, R.B., Gasdaska, C., Whalen, P.J., 2008. Microstructural characterization and mechanical properties of Si_3N_4 formed by fused deposition of ceramics. International Journal of Applied Ceramic Technology 5 (2) pp. 127-137.

Kulkarni, P., Dutta, D. 1996. An accurate slicing procedure for layered manufacturing. *Computer-Aided Design* 28 (9), 683-697.

Lee, B.H., Abdullah, J., Khan, Z.A. 2005. Optimization of rapid prototyping parameters for production of flexible ABS object. Journal of Materials Processing Technology 169 (1) pp. 54-61.

Malone, E., Lipson, H. 2008. Multi-material freeform fabrication of active systems. Proceedings of the 9th Biennial ASME Conference on Engineering Systems Design and Analysis, July 7-9, Haifa, Israel.

Mangus, C., 2012. Feasibility study of metal to polymer hybrid joining. Master's thesis, Lappeenranta University of Technology.

Mathieson, I., Bradley, R.H. 1996. Improved adhesion to polymers by UV/ozone surface oxidation. International Journal of Adhesion and Adhesives 16 (1), 29-31.

Mireles, J., Kim, H., Lee, I.H., Espalin, D., Medina, F., MacDonald, E., Wicker, R. (in press). Development of a Fused Deposition Modeling system for low melting temperature metal alloys. *Journal of Electronic Packaging*.

Pandey, P.M., Reddy, N.V., Dhande, S.G. 2003a. Improvement of surface finish by staircase machining in fused deposition modeling. Journal of Materials Processing Technology 132 (1-3), 323-331.

Pandey, P.M., Reddy, N.V., Dhande, S.G. 2003b. Real time adaptive slicing for fused deposition modelling. International Journal of Machine Tools & Manufacturing 43 (1), 61-71.

Parker, M. E., Arbegast, W., Boysen, A., West, M. 2009. Eliminating voids in FDM processed polyphenylsulfone, polycarbonate, and ULTEM 9085 by hot isostatic pressing. South Dakota Schools of Mines & Technology, Research Experience for Undergraduate.

Partain, S.C. 2007. Fused deposition modeling with localized pre-deposition heating using forced air. Master's thesis, Montana State University.

Rodriguez, J.F., Thomas, J.P., Renaud, J.E. 2003. Mechanical behavior of acrylonitrile butadiene styrene fused deposition materials modeling. Rapid Prototyping Journal 9 (4), 219-230.

Sabourin, E., Houser, S.A., Bohn, J.H. 1997. Accurate exterior, fast interior layered manufacturing. *Rapid Prototyping Journal* 3 (2), 44-52.

Salonitis, K., Pandremenos, J., Paralikis, F., Chryssolouris, G. 2009. Multifunctional materials used in automotive industry: A critical review. Engineering Against Fracture 1, 59-70.

Sood, A.K., Ohdar, R.K., Mahapatra, S.S., 2010. Parametric appraisal of mechanical property of fused deposition modeling processed parts. Materials and Design 31 (1) pp. 287-295.

Stevens, Malcolm P. 1999. *Polymer chemistry: An introduction*. New York: Oxford University Press

Sun, Q., Rizvi, G.M., Bellehumeur, C.T., Gu, P. 2008. Effect of processing conditions on the bonding quality of FDM polymer filaments. Rapid Prototyping Journal 14 (2) pp. 72-80.

Truckenmuller, R., Henzi, P., Herrmann, D., Saile, V. Schomburg, W.K. 2004. Bonding of polymer microstructures by UV irradiation and subsequent welding at low temperatures. Microsystem Technologies 10 (5) pp. 372-374.

Tsao, C., DeVoe, D.L. 2009. Bonding of thermoplastic polymer microfluidics. Microfluidics and Nanofluidics 6 (1) pp. 1-16.

Wang, T., Xi, J., Jin, Y. 2007. A model research for prototype warp deformation in the FDM process. *International Journal of Advanced Manufacturing Technology* 33 (11-12), 1087-1096.

Wohlers, T. 2012. Wohlers Report 2012: Additive manufacturing and 3D printing state of the industry.

Young, R., Lovell, P.A. 2011. Introduction to polymers. New York: CRC Press, Taylor & Francis Group.

Zein, I., Hutmacher, D.W., Tan, K.C., Teoh, S.H. 2002. Fused deposition modeling of novel scaffold architectures for tissue engineering applications. *Biomaterials* 23 (4), 1169-1185.

Zhong, W., Li, F., Zhang, Z., Song, L., Li, Z. 2001. Short fiber reinforced composites for fused deposition modeling. Materials Science and Engineering: A 301 (2), 125-130.

Appendix A

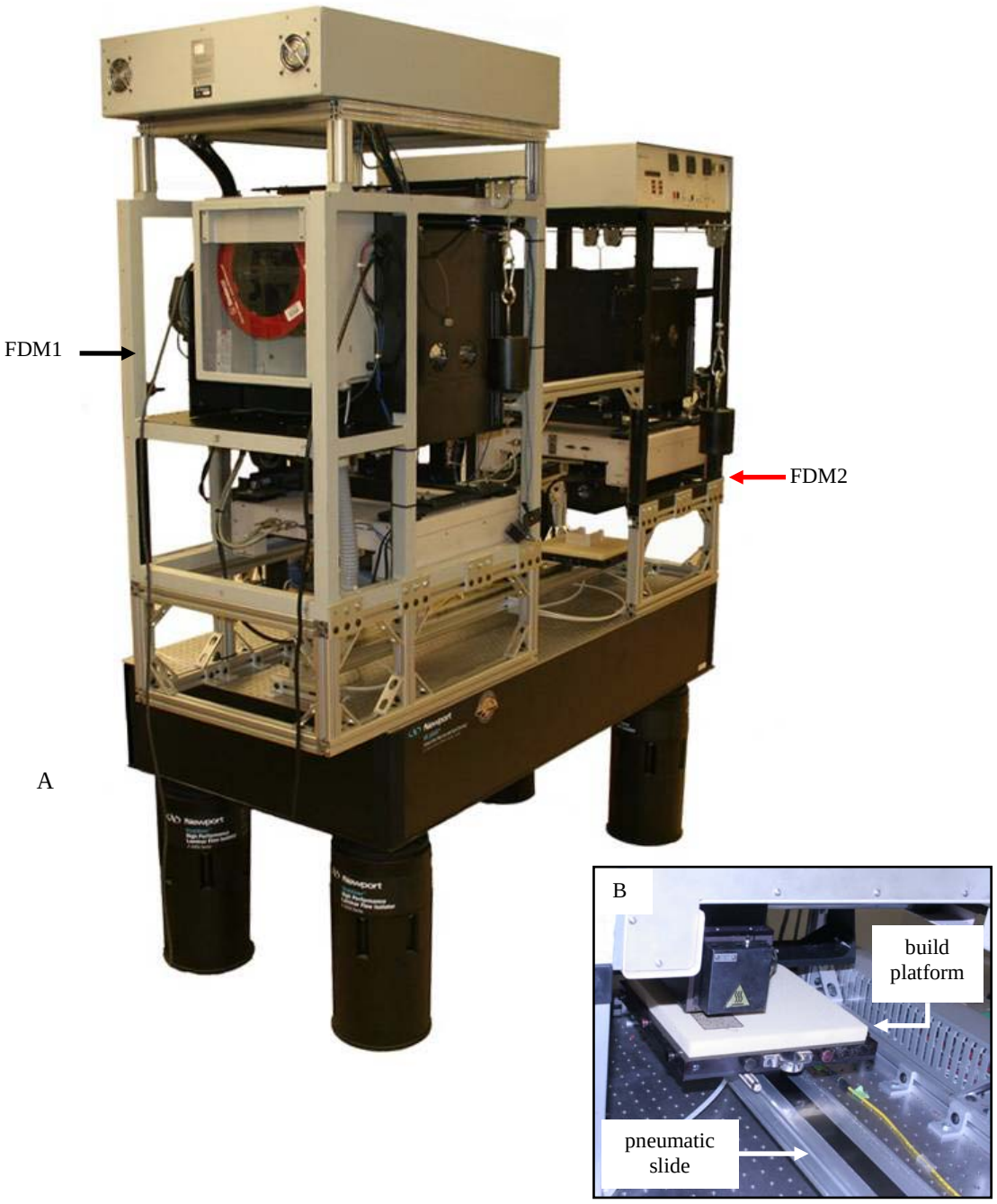

Figure A1. Multi-material, multi-technology FDM system. A) overview of entire system. B) close-up view of FDM1 building on the platform that is attached to a pneumatic slide.

Appendix B

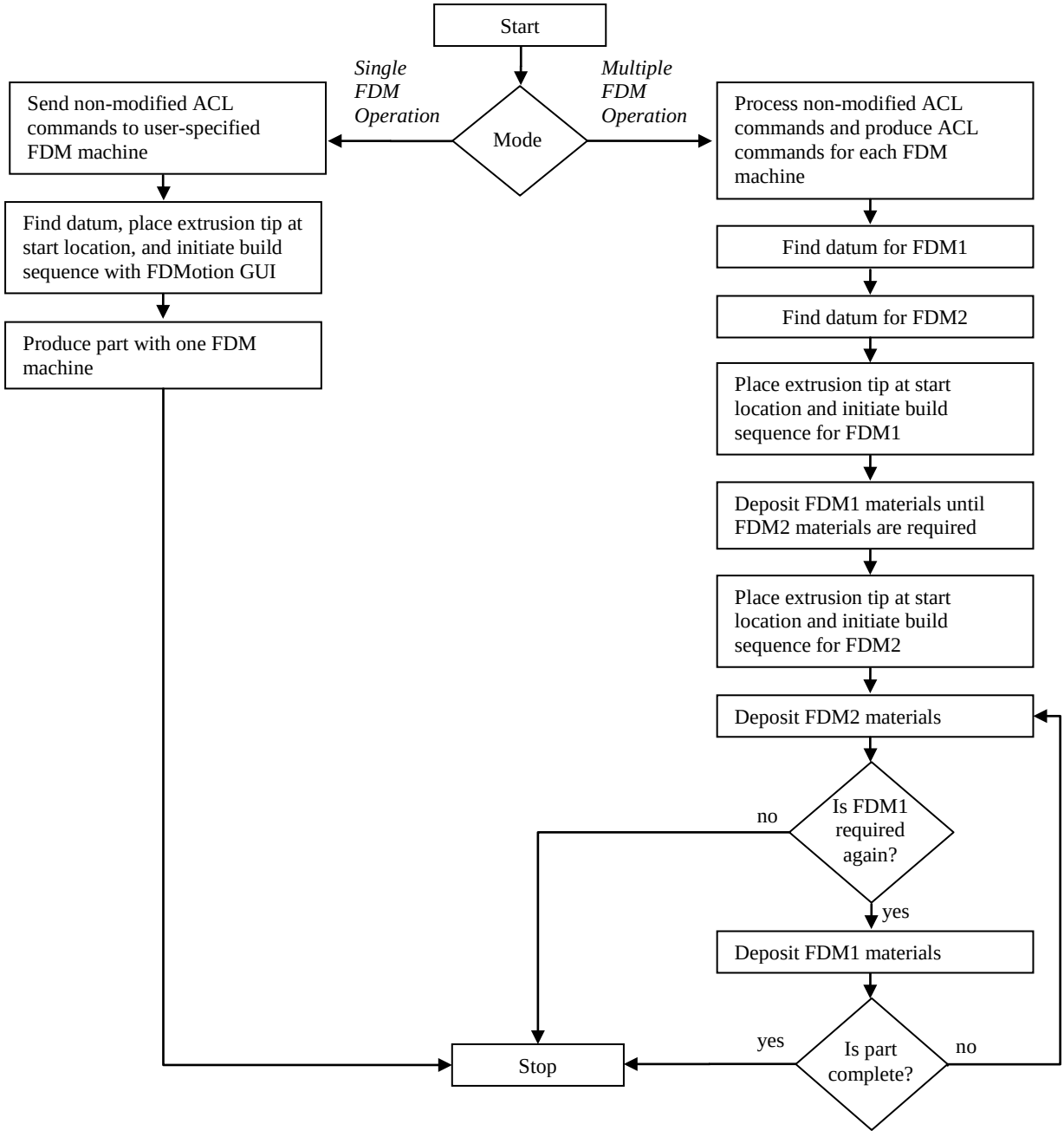

Figure B1. Sequence of actions performed by FDMotion.

Appendix C

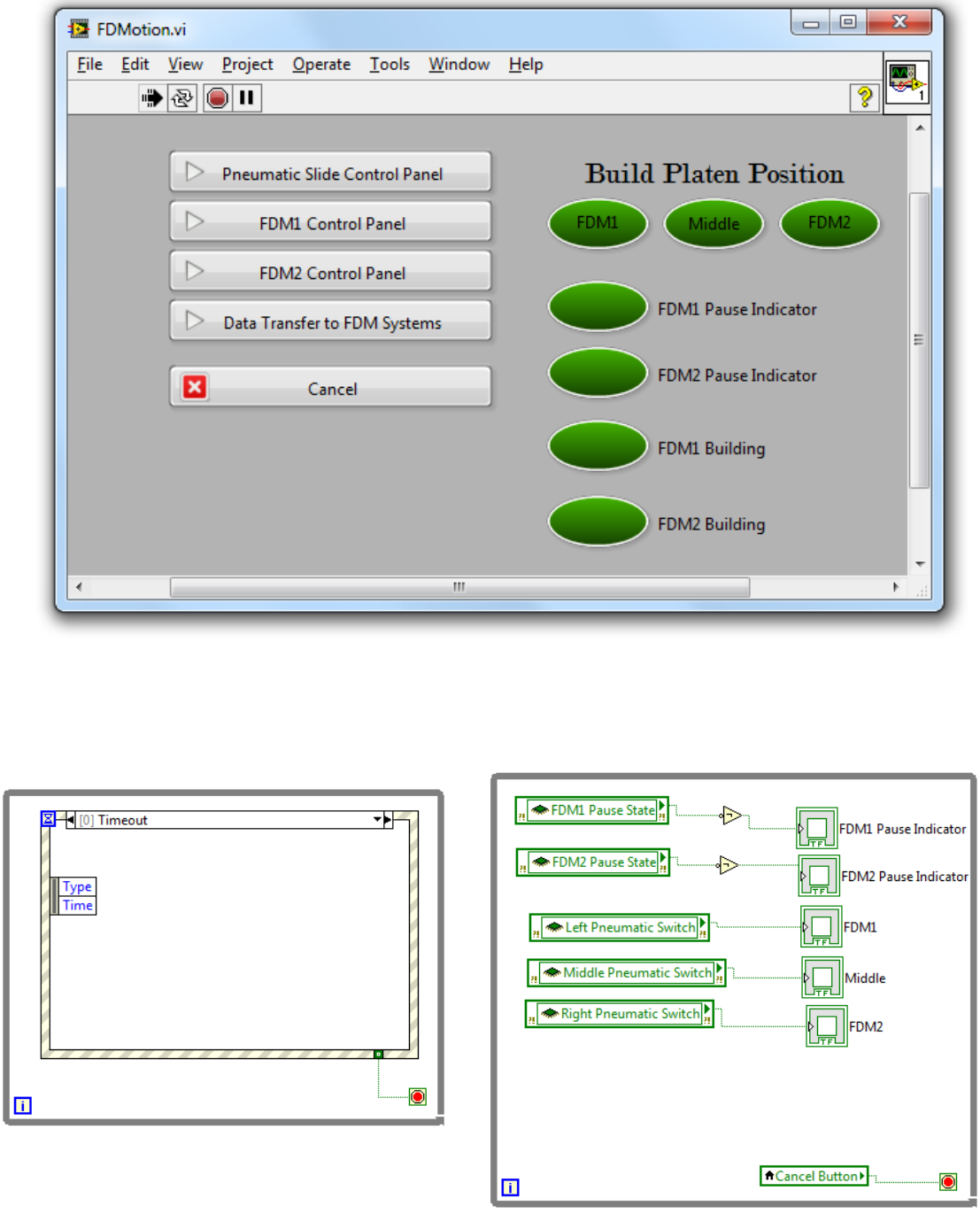

Figure C1. "FDMotion.vi" front panel and block diagram showing Case 0

Figure C2. "FDMotion.vi" block diagram showing Case 1-5

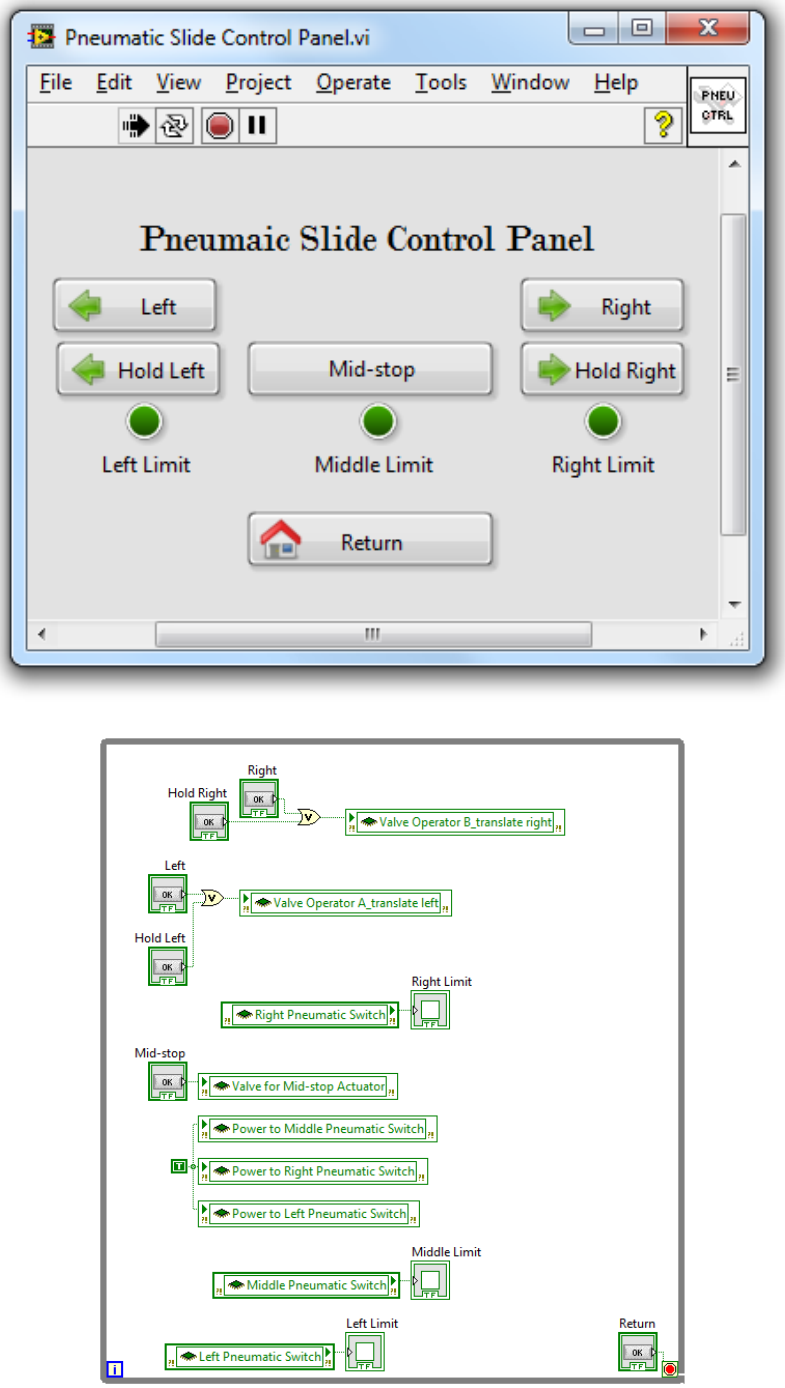

Figure C3. Front panel and block diagram for "Pneumatic Slide Control Panel.vi."

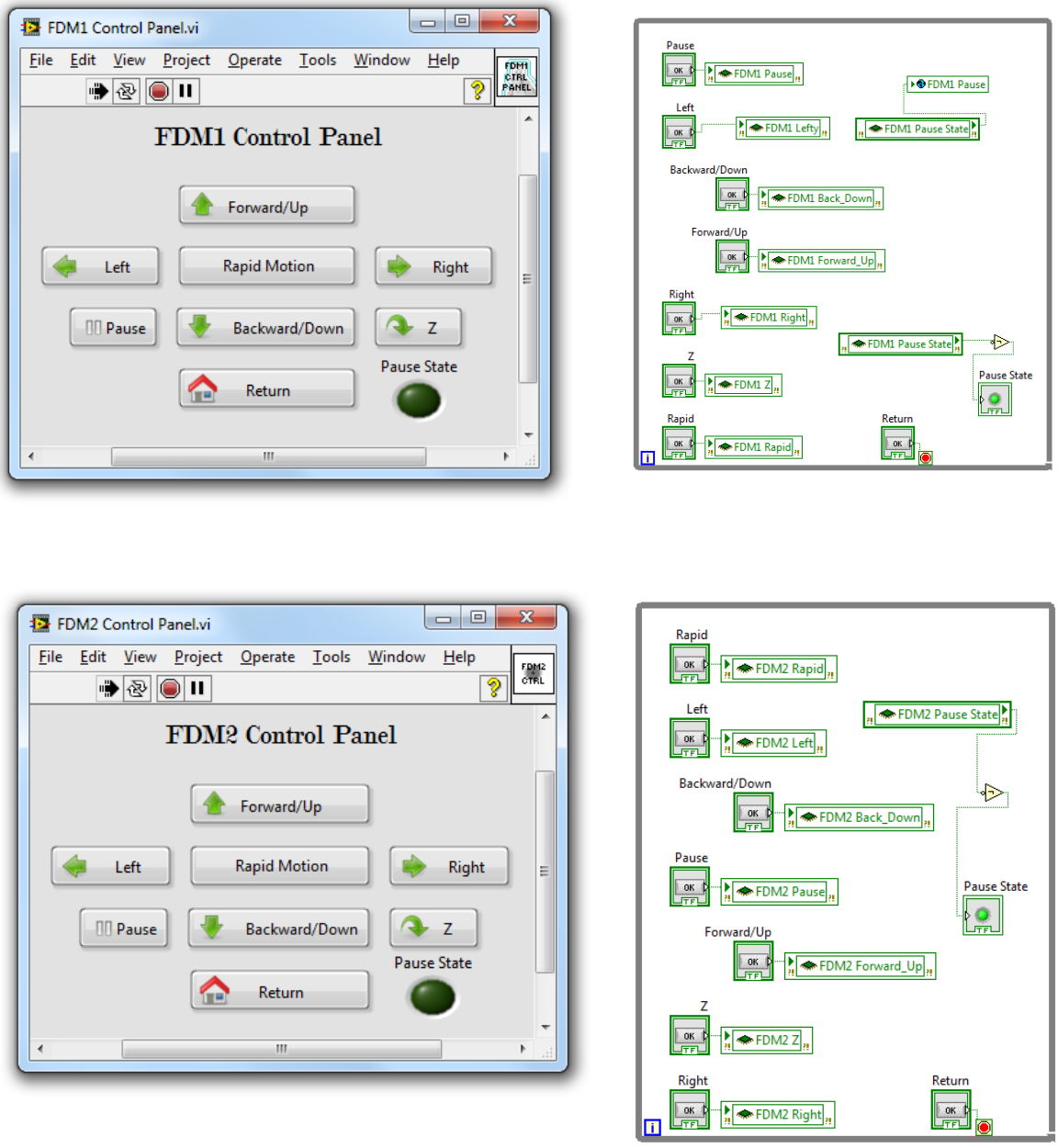

Figure C4. Front panel and block diagrm for "FDM1 Control Panel.vi" (top) and "FDM2 Control Panel.vi." (bottom).

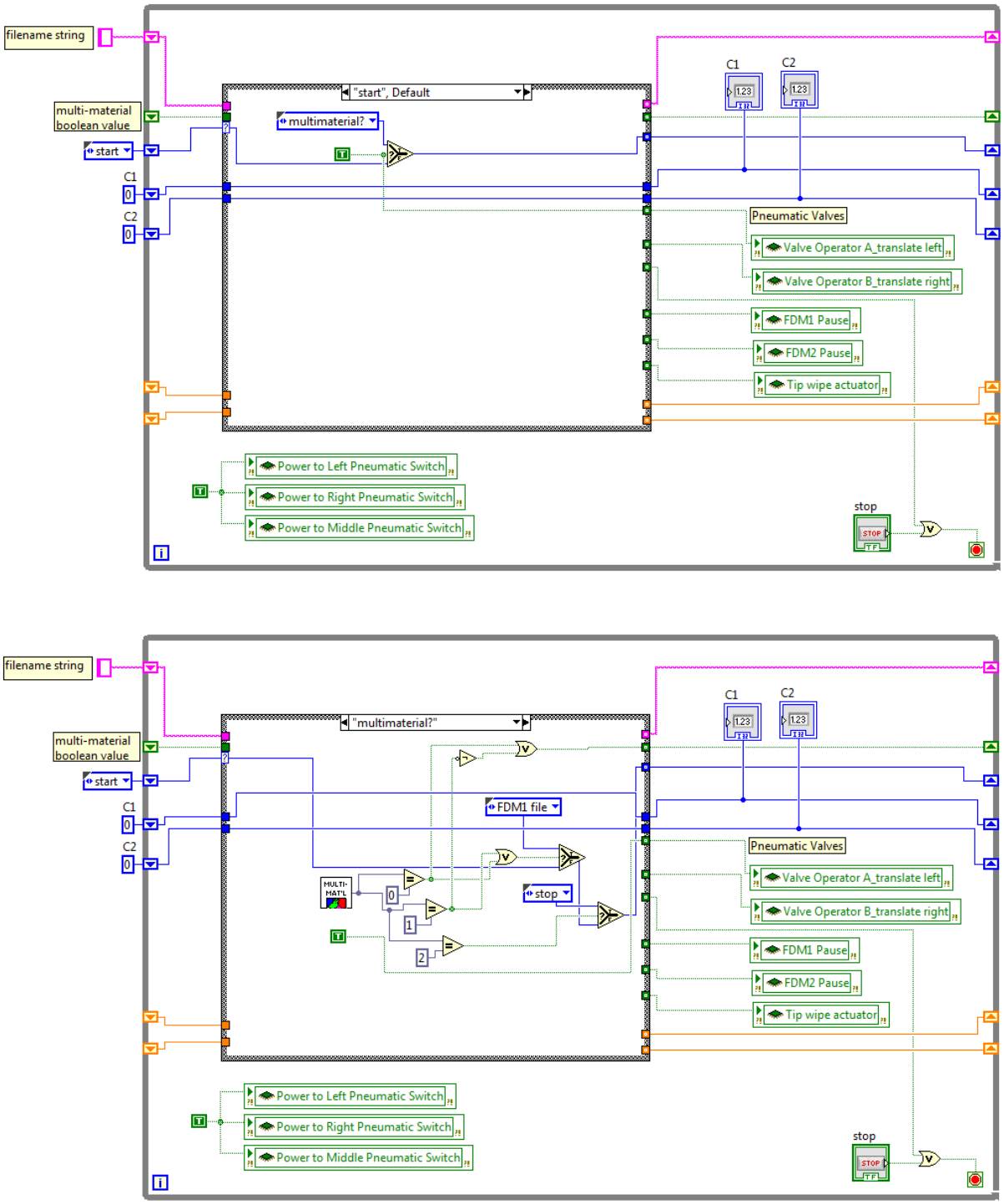

Figure C5. States within the "data transfer.vi." "Start" and "multimaterial" states are shown.

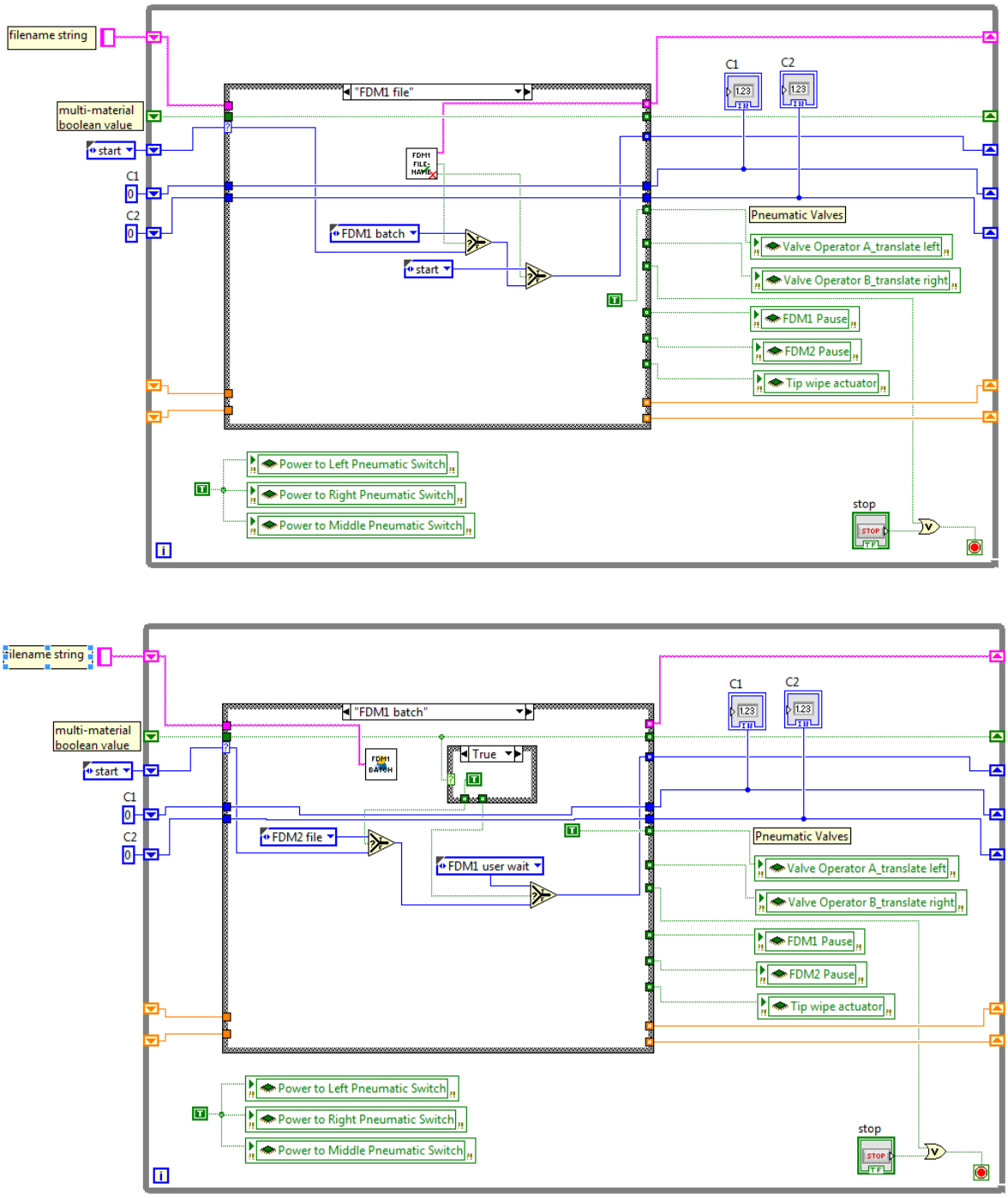

Figure C6. States within the "data transfer.vi." "FDM1 file" and "FDM1 batch (T)" states are shown.

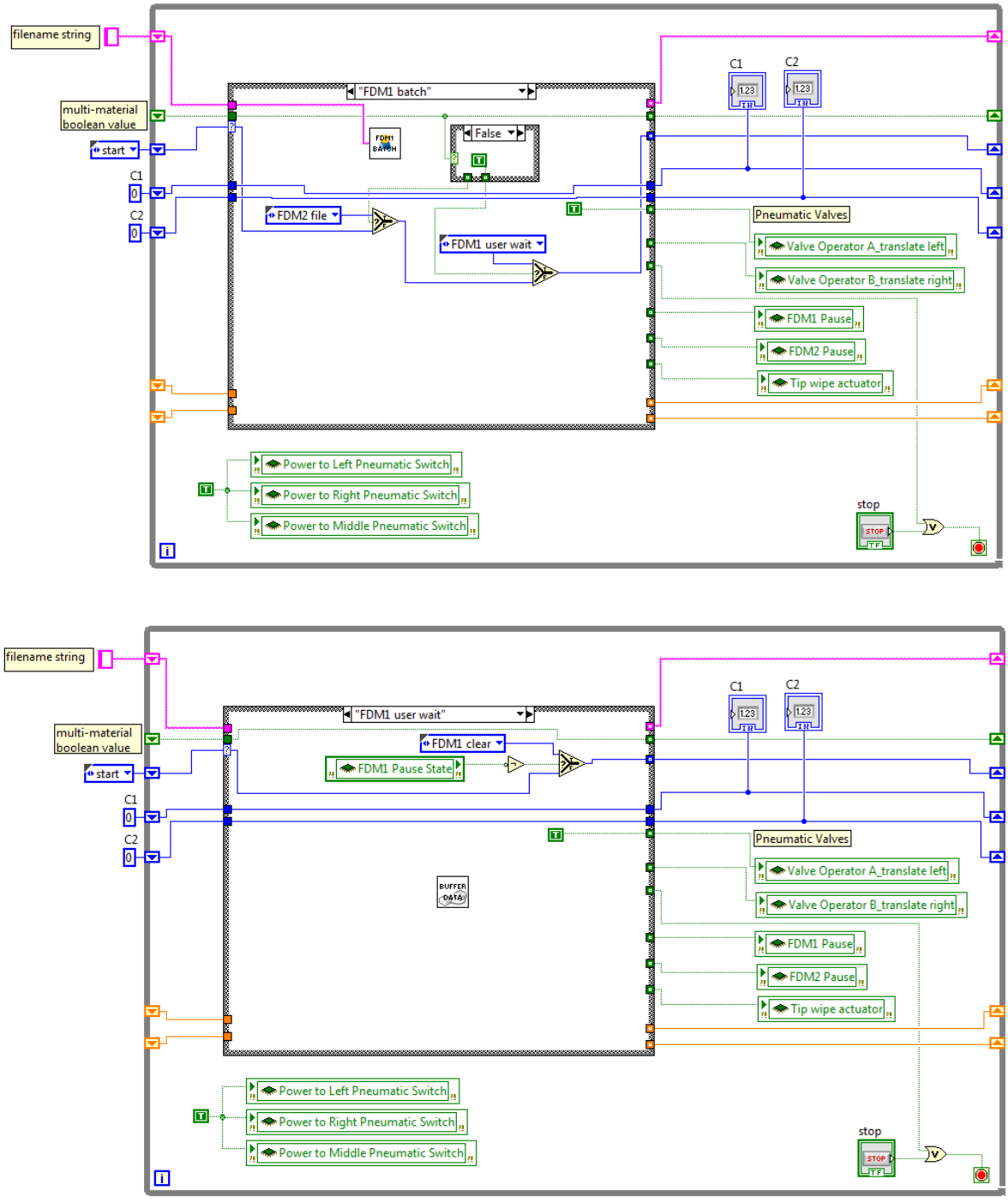

Figure C7. States within the "data transfer.vi." "FDM1 batch (F)" and "FDM user wait" states are shown.

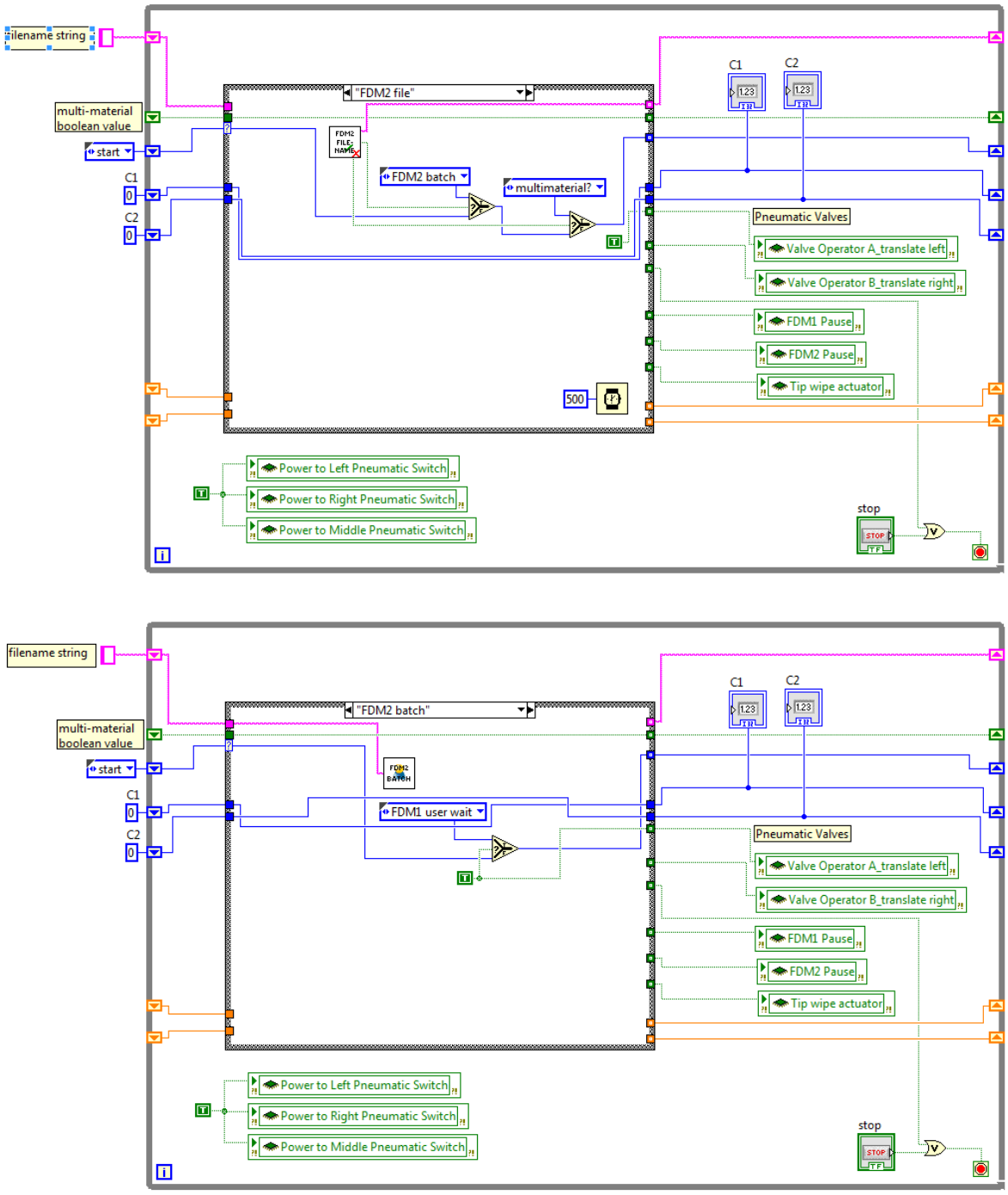

Figure C8. States within the "data transfer.vi." "FDM2 file" and "FDM2 batch" states are shown.

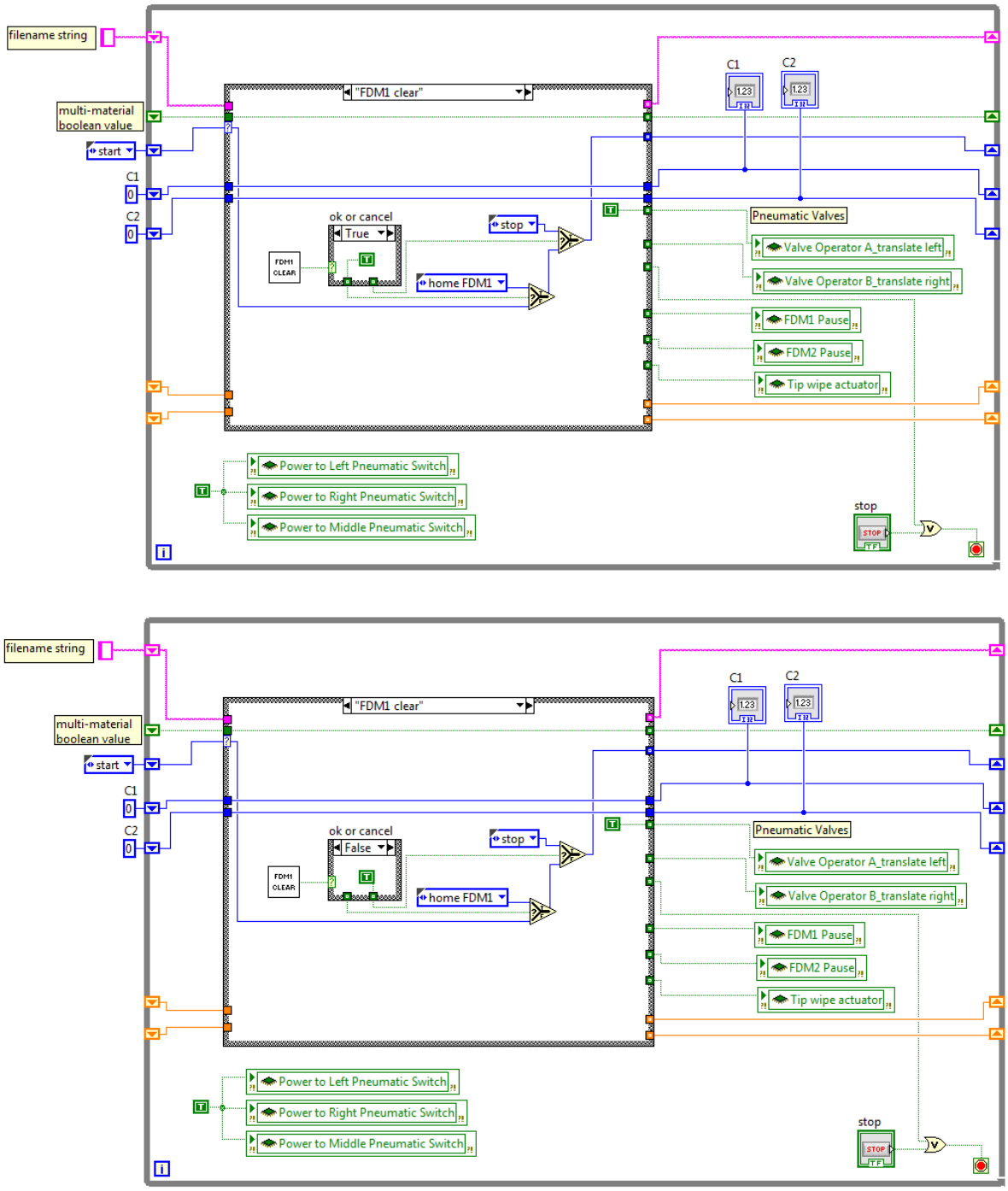

Figure C9. States within the "data transfer.vi." "FDM clear (T)" and "FDM1 clear (F)" states are shown.

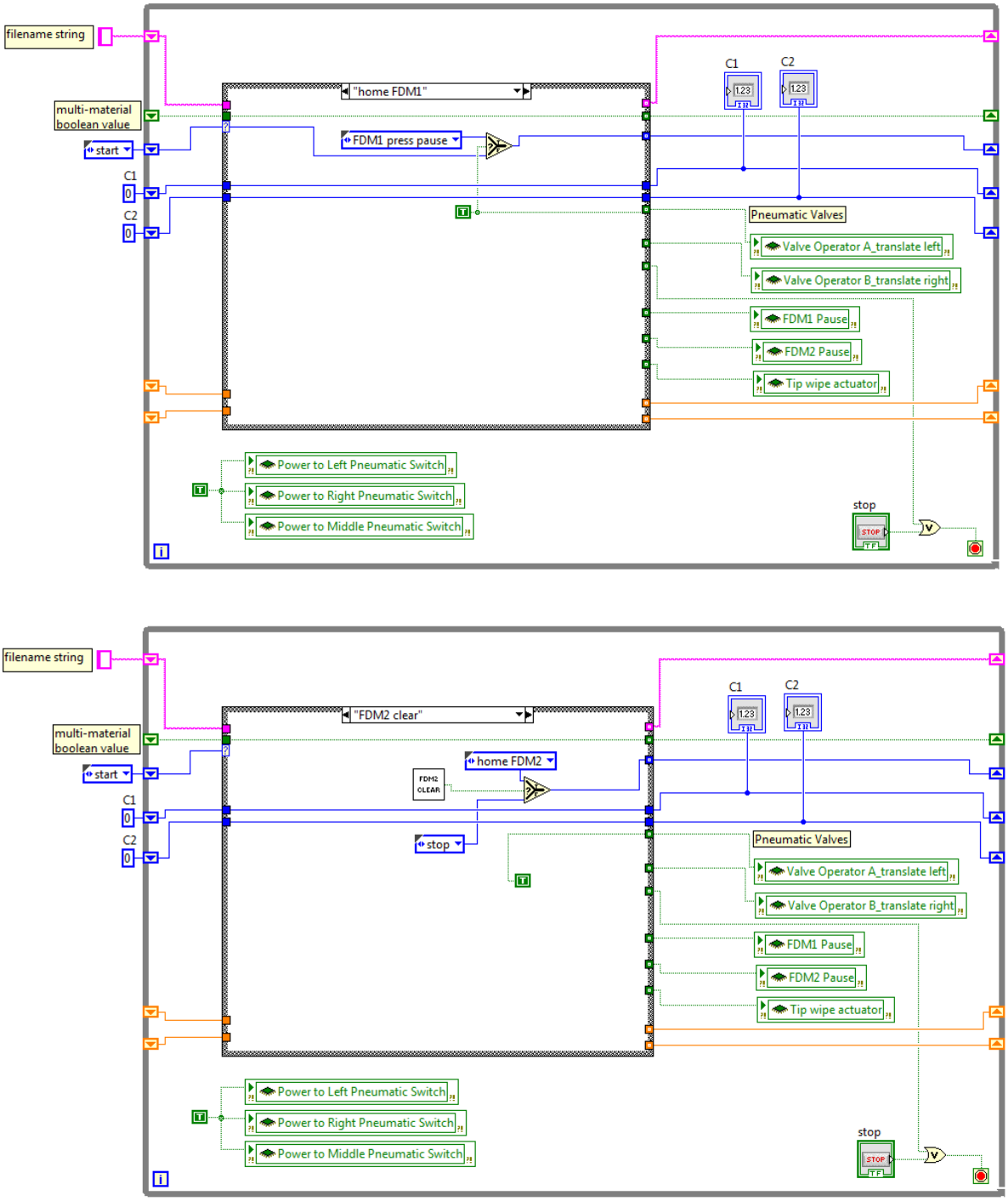

Figure C10. States within the "data transfer.vi." "home FDM1" and "FDM2 clear" states are shown.

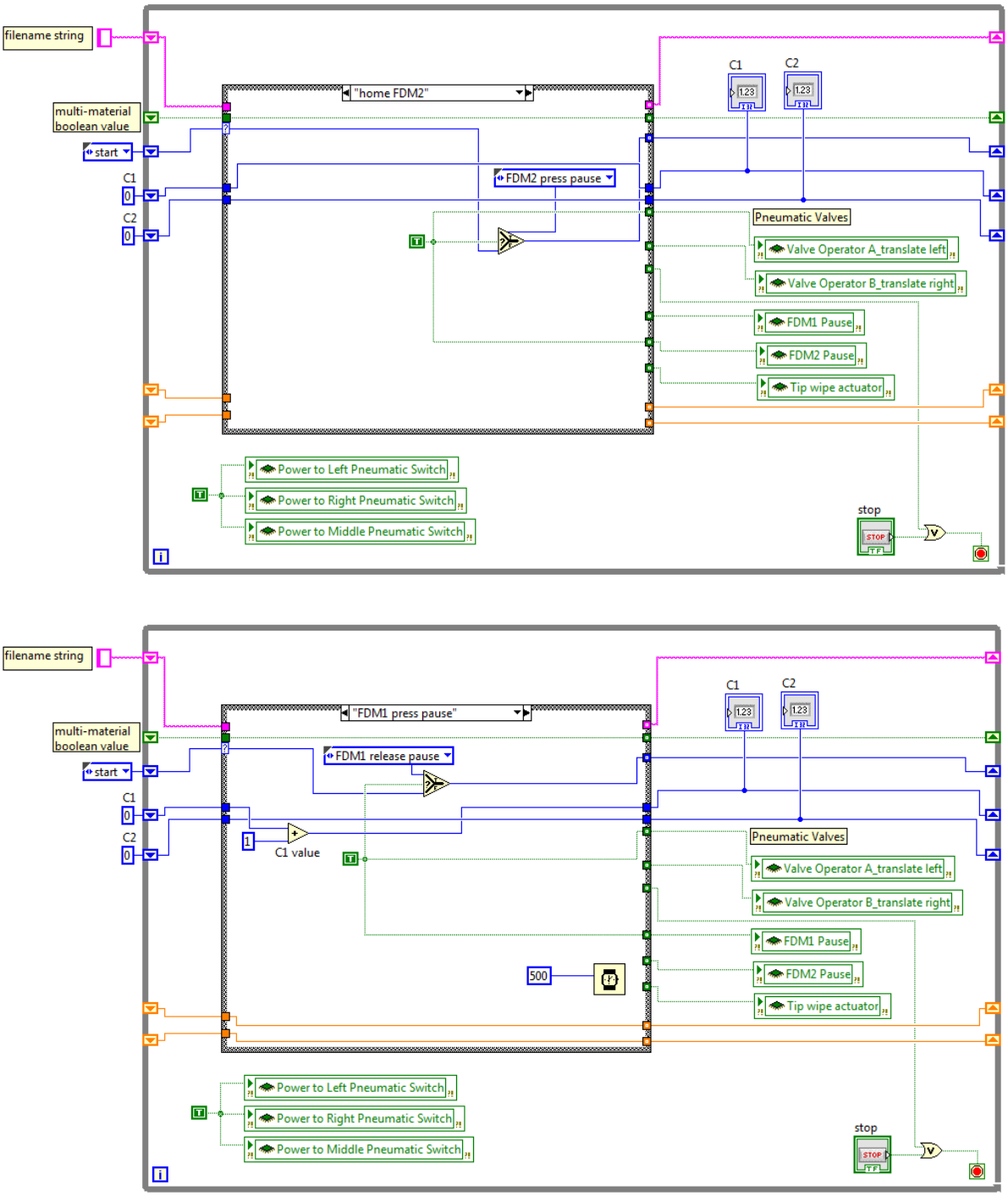

Figure C11. States within the "data transfer.vi." "home FDM2" and "FDM1 press pause" states are shown.

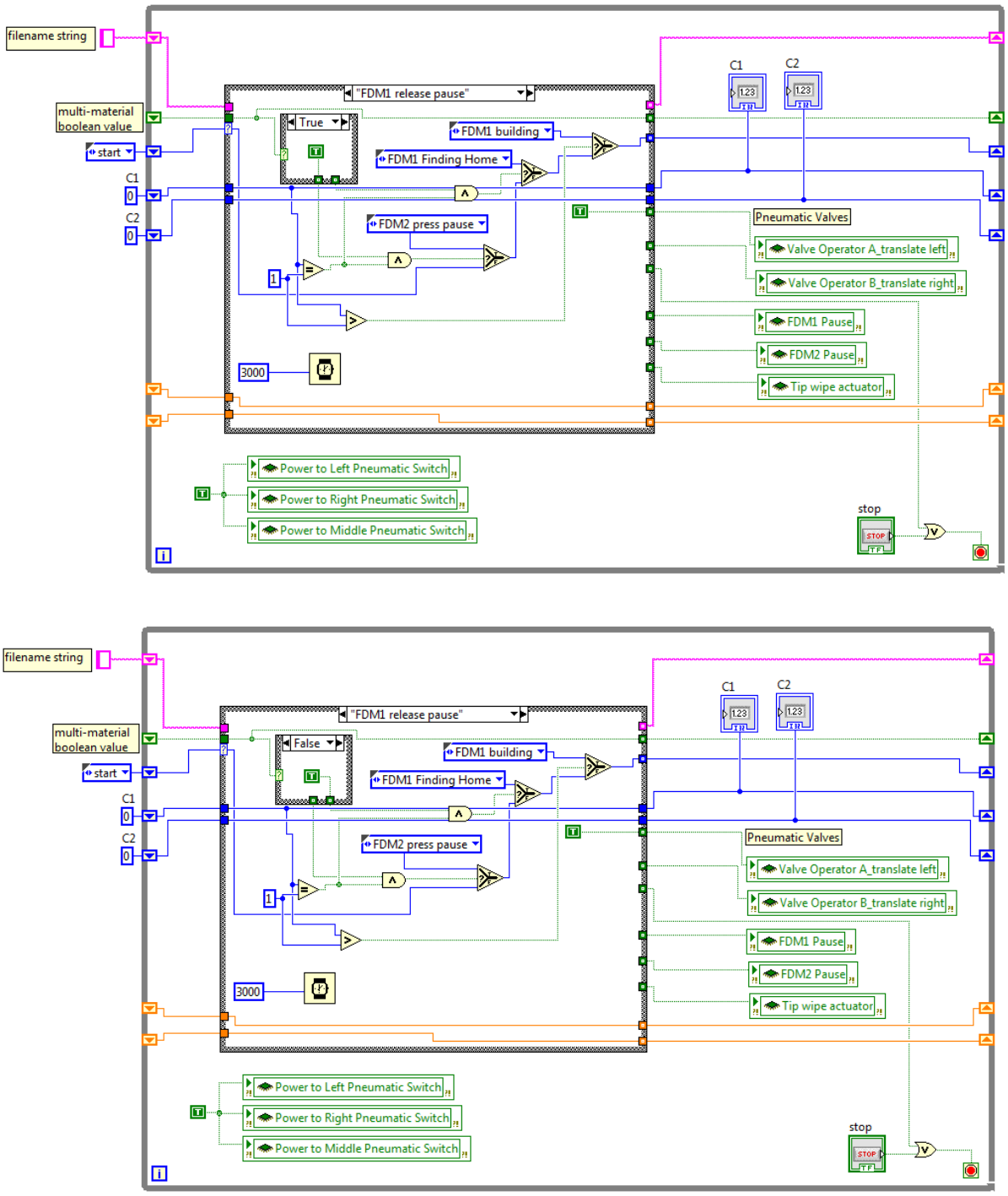

Figure C12. States within the "data transfer.vi." "FDM1 release pause (T)" and "FDM1 release pause (F)" states are shown.

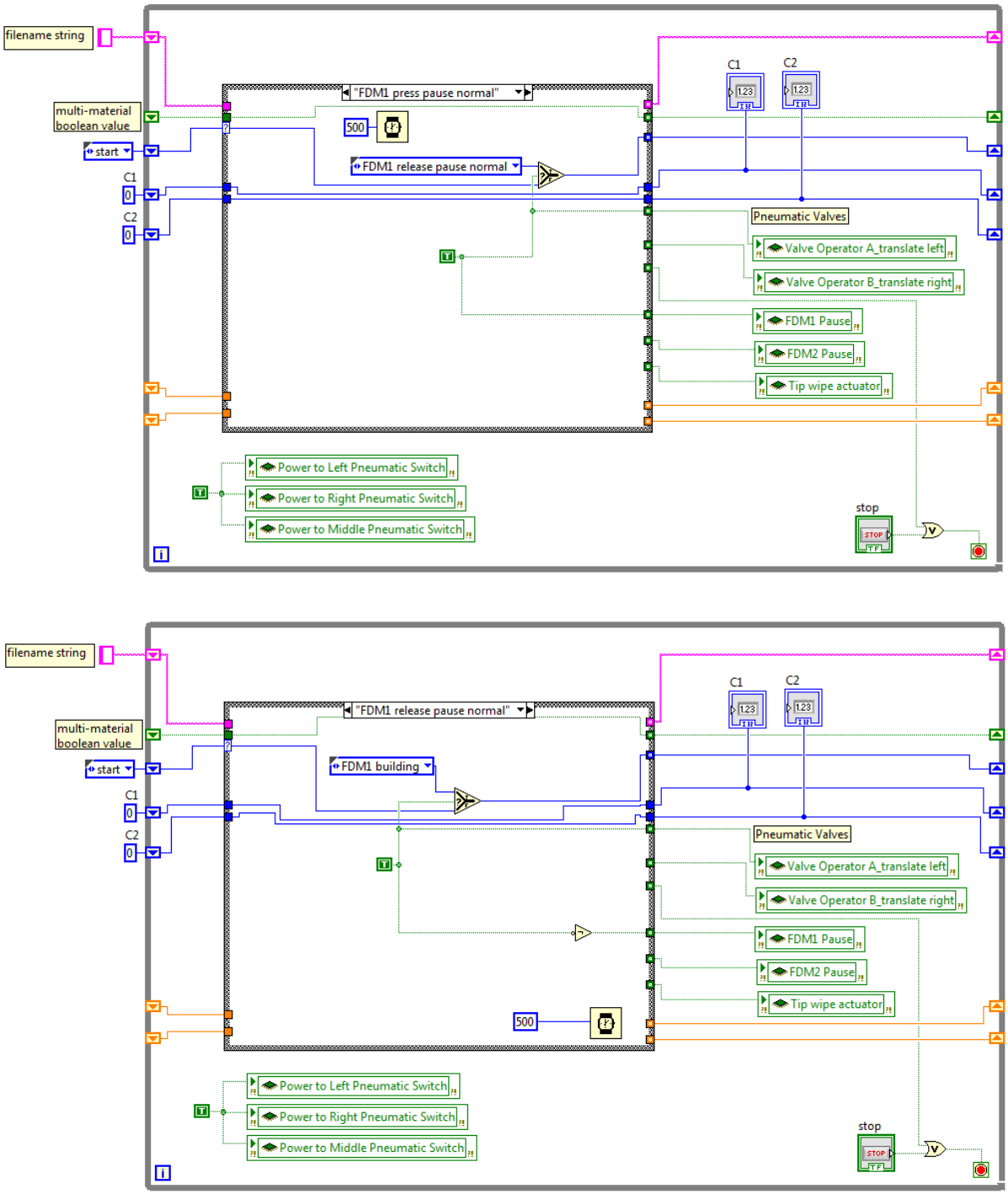

Figure C13. States within the "data transfer.vi." "FDM1 press pause normal" and "FDM1 release pause normal" states are shown.

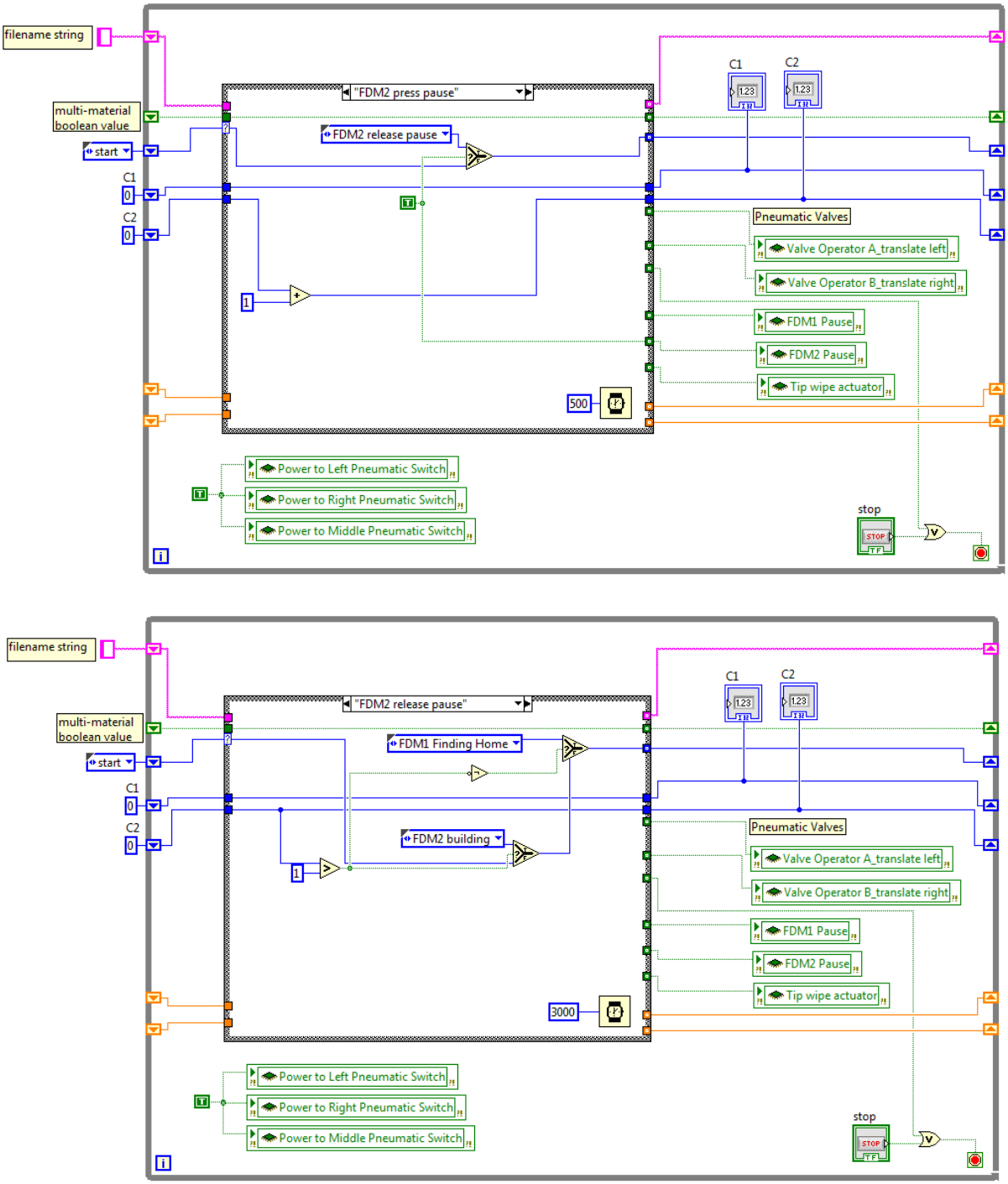

Figure C14. States within the "data transfer.vi." "FDM2 press pause" and "FDM2 release pause" states are shown.

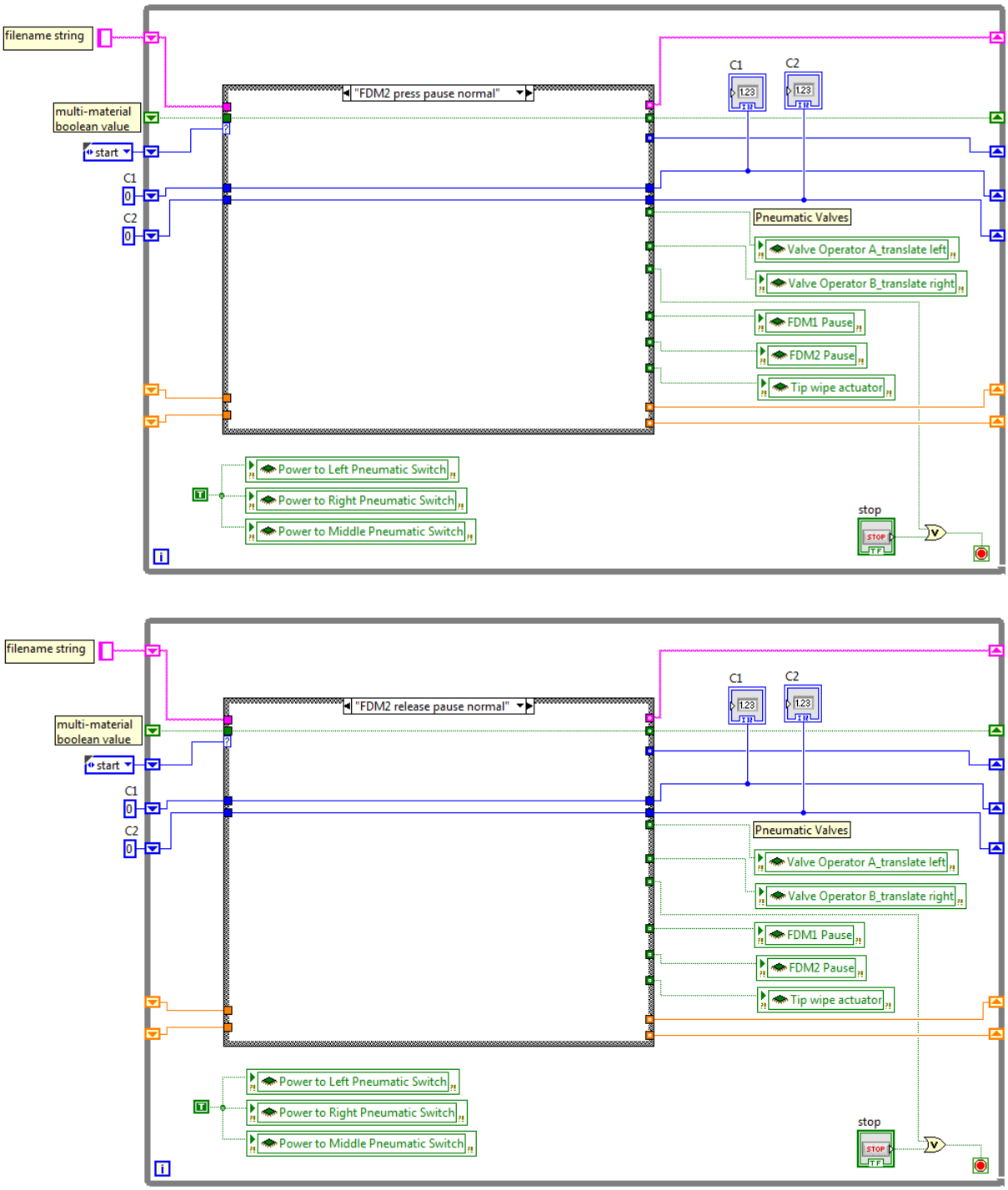

Figure C15. States within the "data transfer.vi." "FDM2 press pause normal" and "FDM2 release pause normal" states are shown.

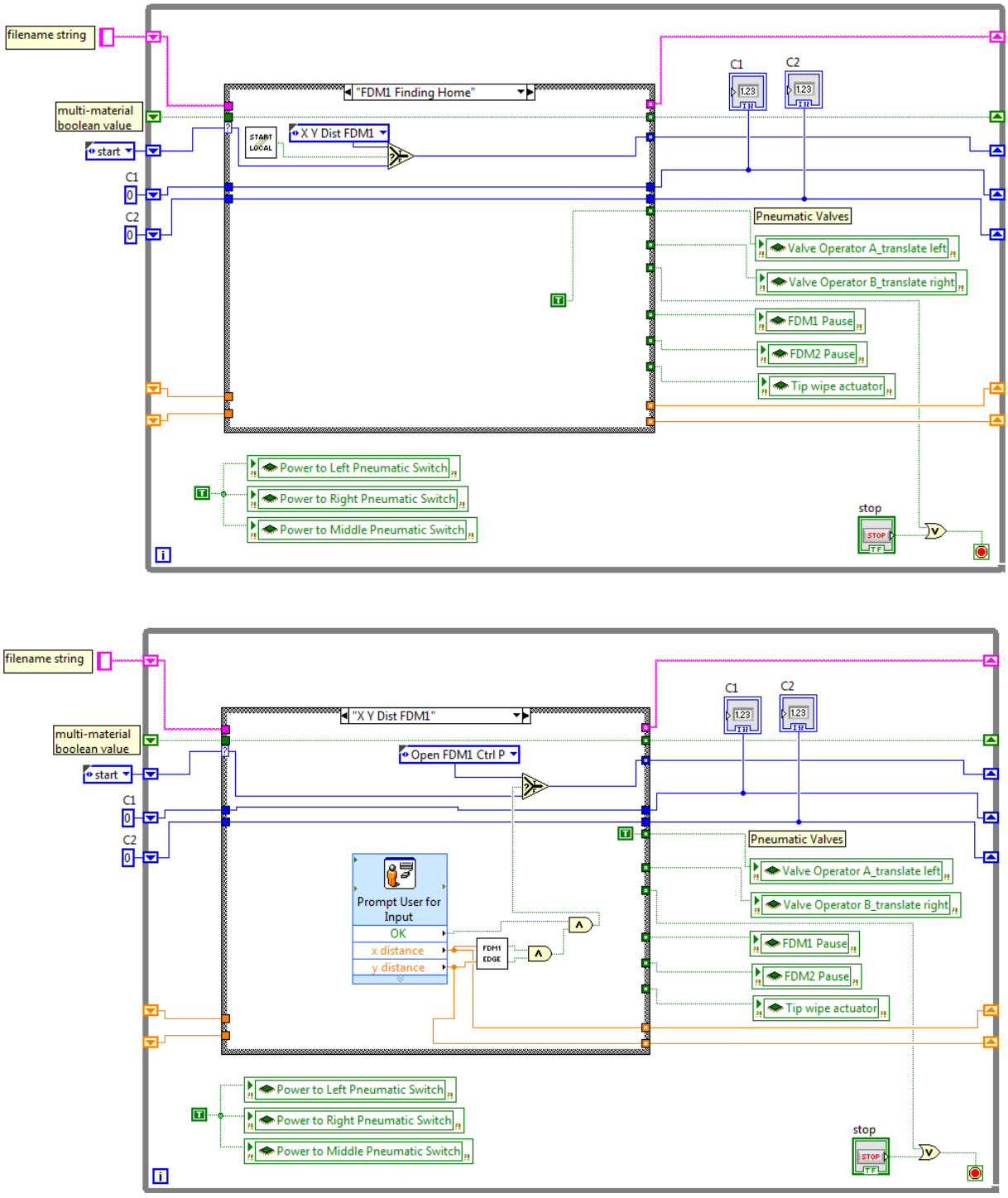

Figure C16. States within the "data transfer.vi." "FDM1 Finding Home" and "XY Dist FDM1" states are shown.

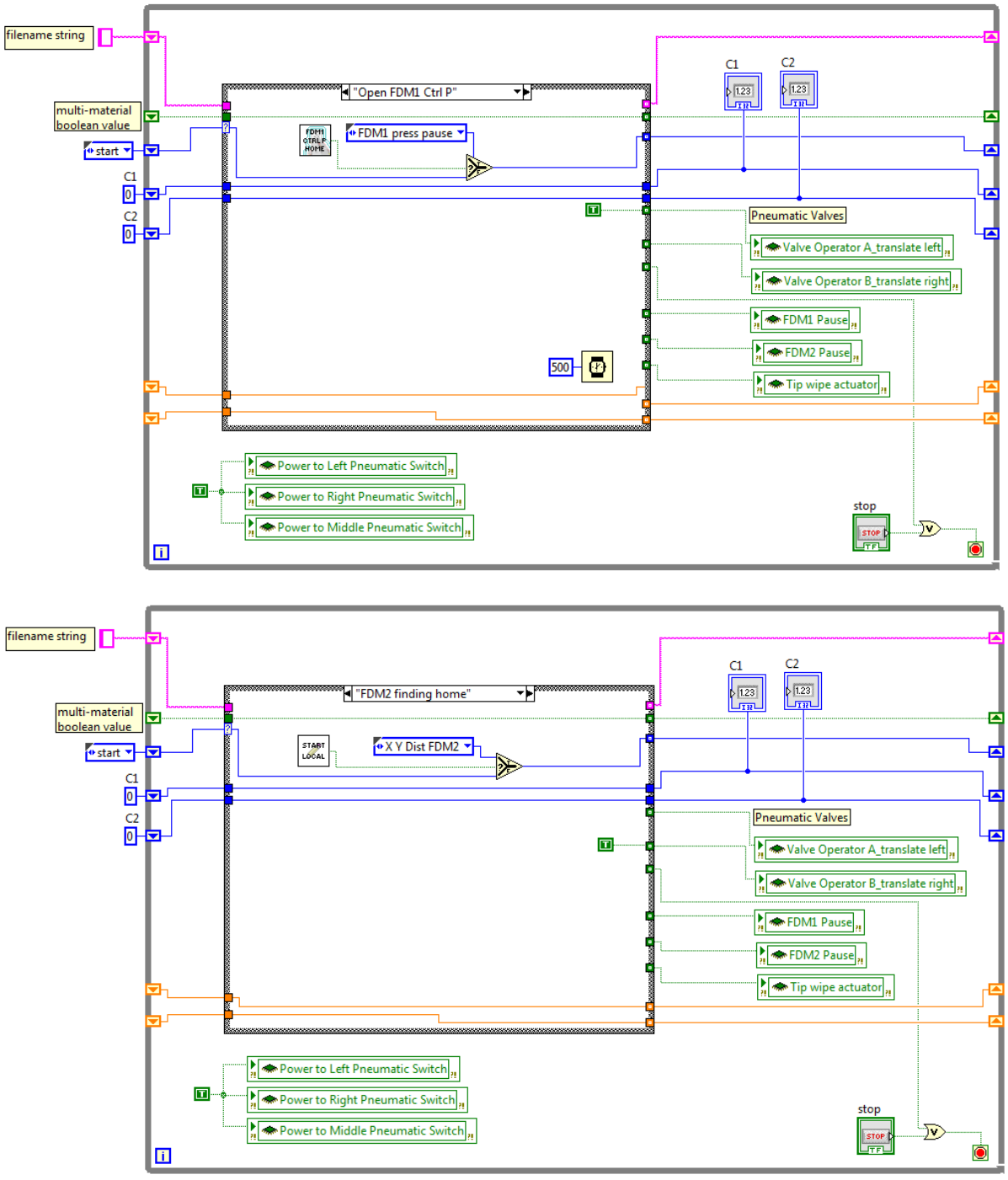

Figure C17. States within the "data transfer.vi." "Open FDM1 Ctrl P" and "FDM2 finding home" states are shown.

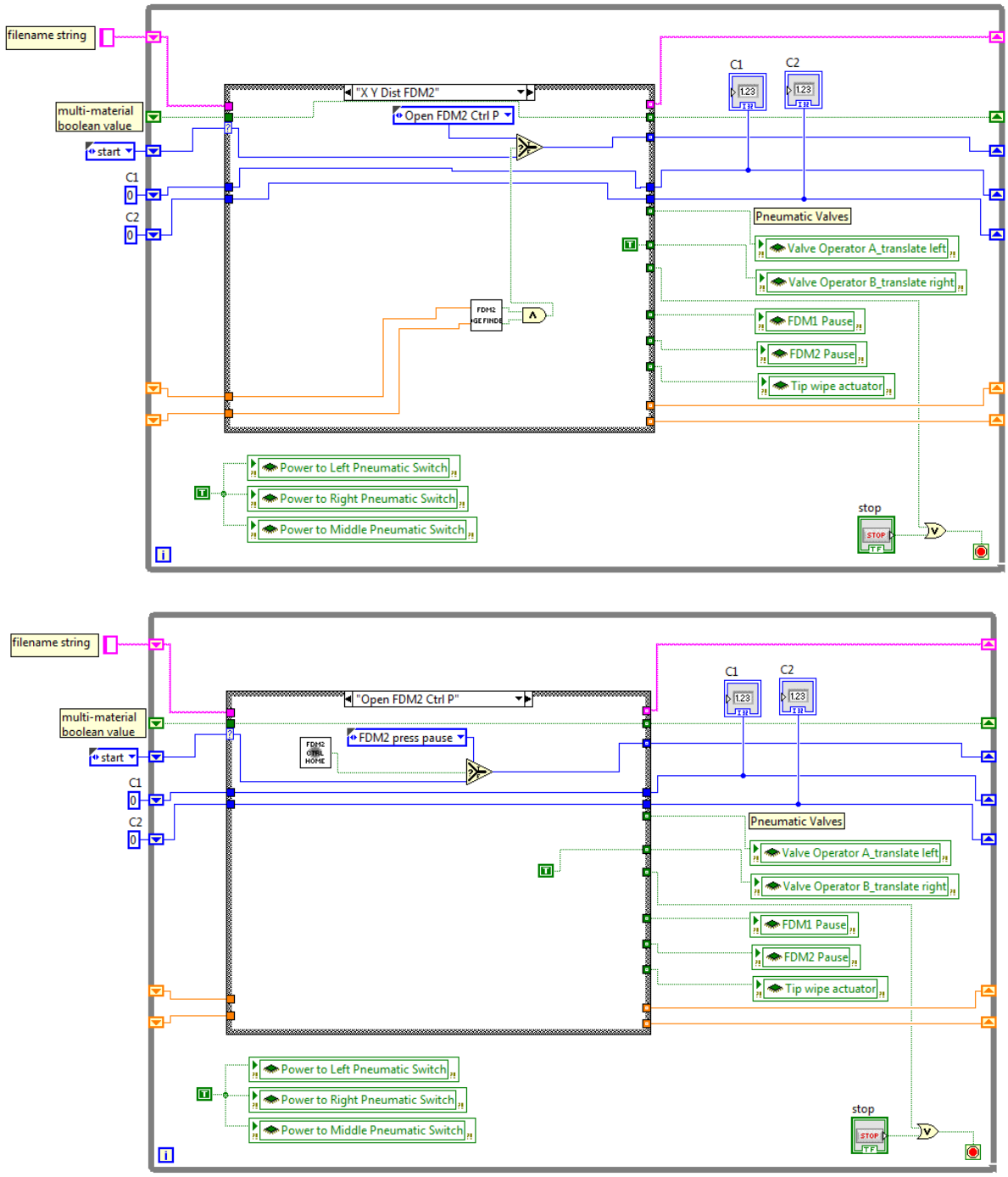

Figure C18. States within the "data transfer.vi." "XY Dist FDM2" and "Open FDM2 Ctrl P" states are shown.

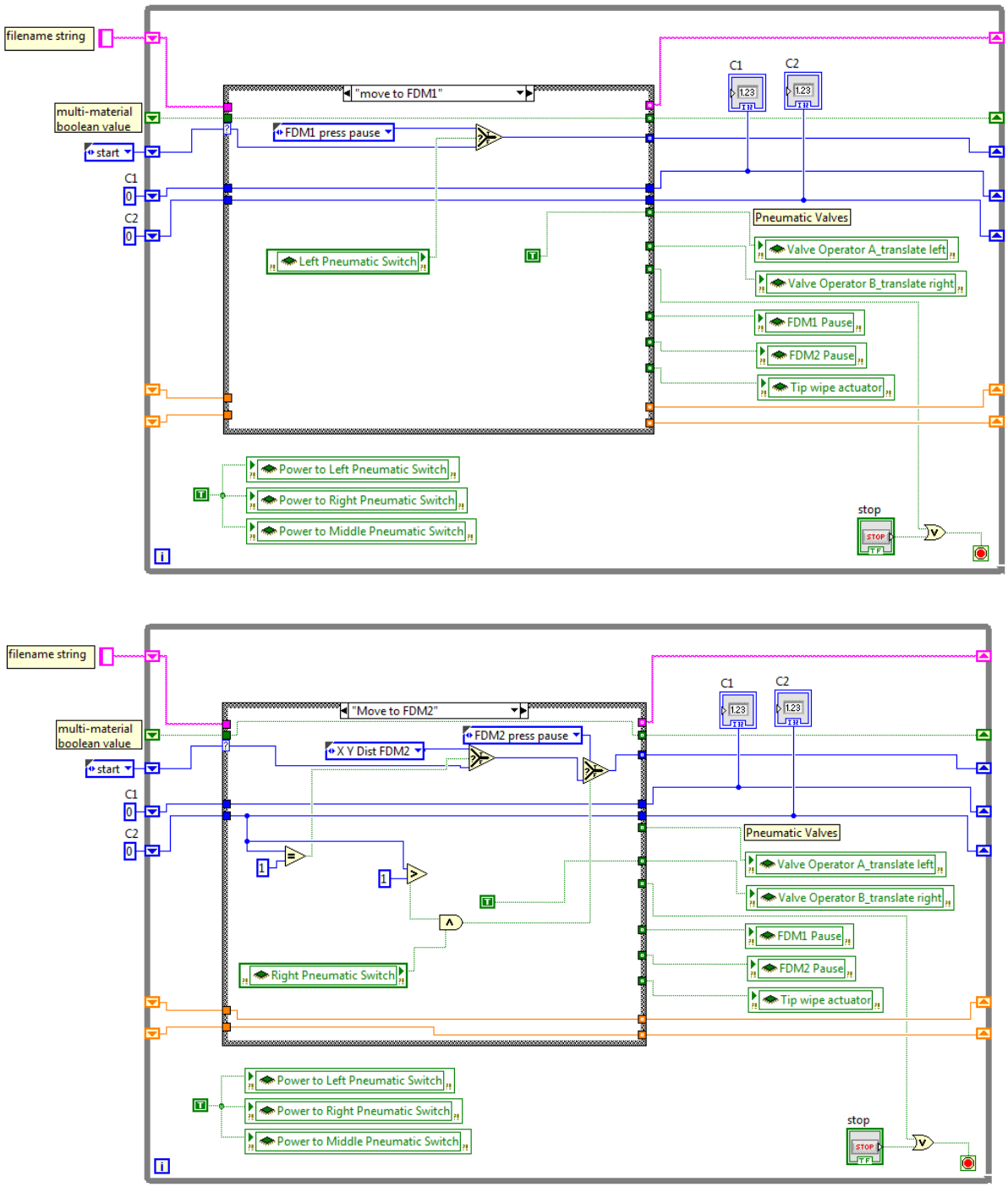

Figure C19. States within the "data transfer.vi." "move to FDM1" and "Move to FDM2" states are shown.

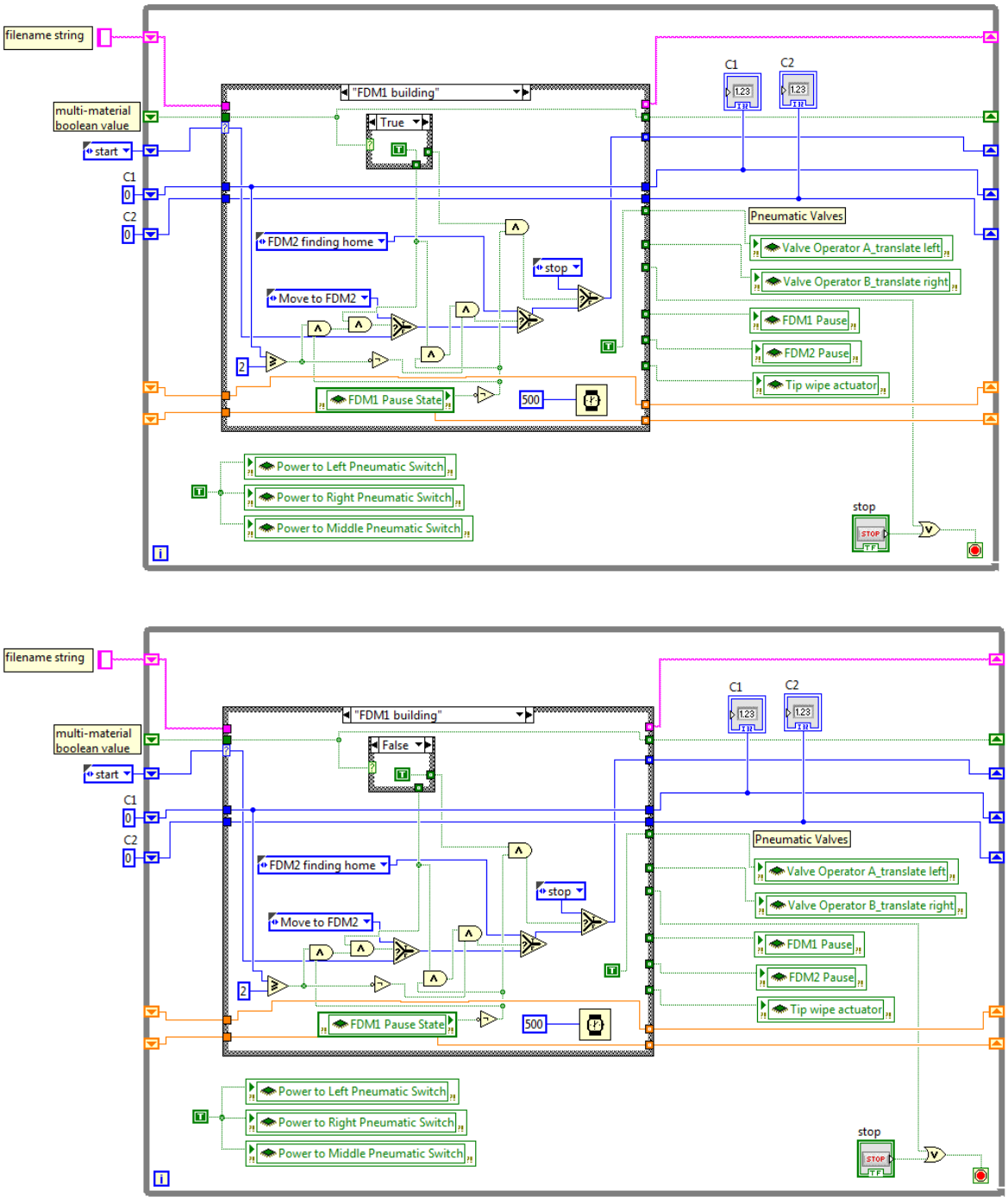

Figure C20. States within the "data transfer.vi." "FDM1 building (T)" and "FDM1 building (F)" states are shown.

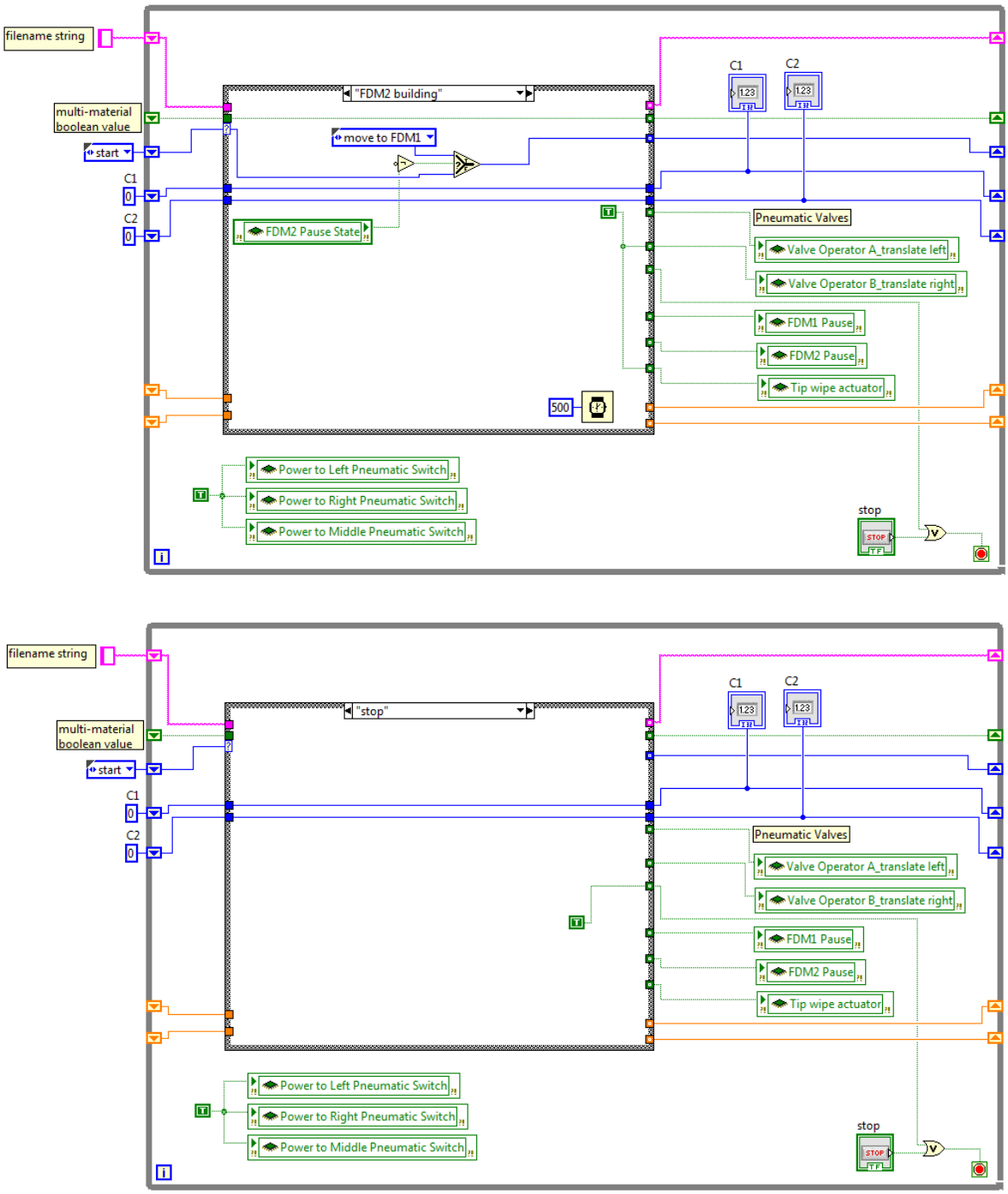

Figure C21. States within the "data transfer.vi." "FDM2 building" and "stop" states are shown.

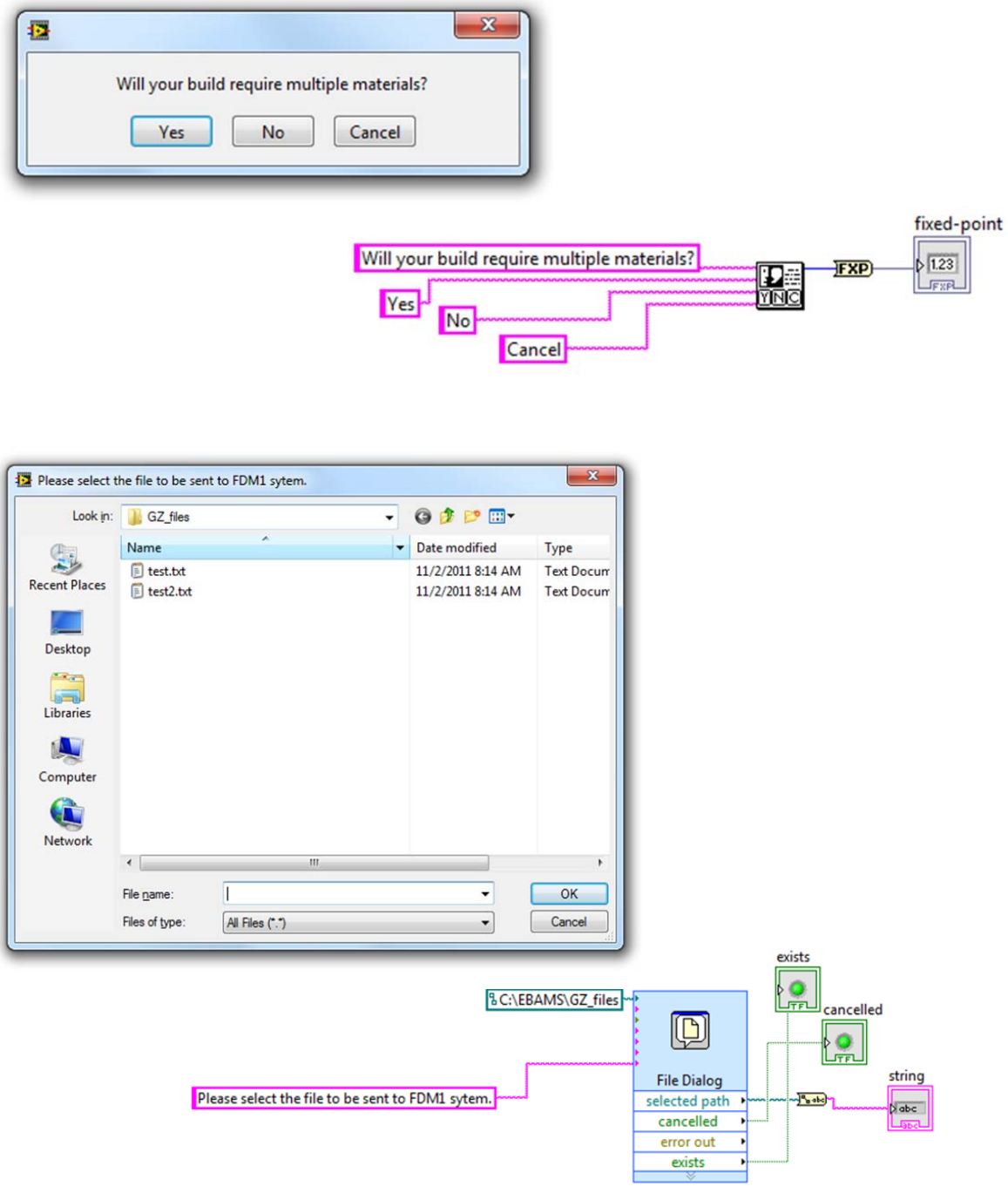

Figure C22. Front panel and block diagram for "multimaterial decision.vi" (top) and "FDM1filename.vi" (bottom).

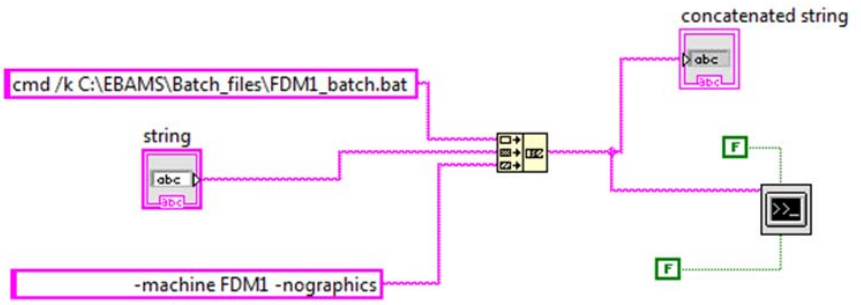

"FDM1 batch.vi"

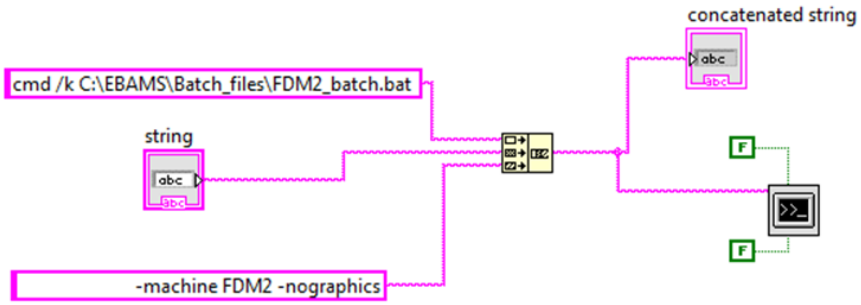

"FDM2 batch.vi"

"buffering data dialog.vi"

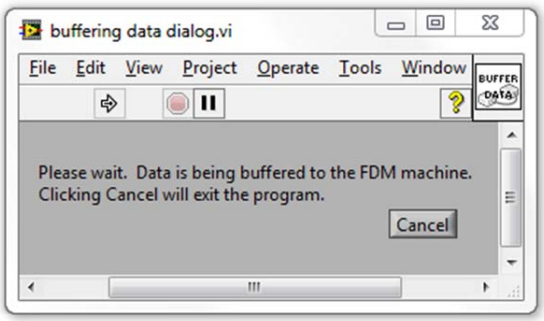

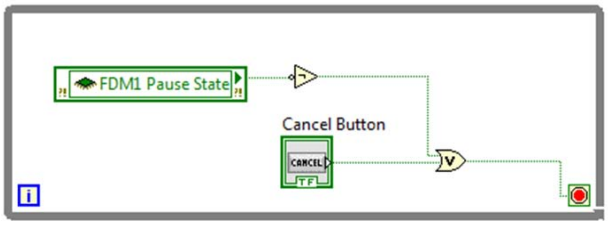

Figure C23. Block diagrams for "FDM1 batch.vi" and "FDM2 batch.vi." Front panel and block diagram for "buffering data dialog.vi."

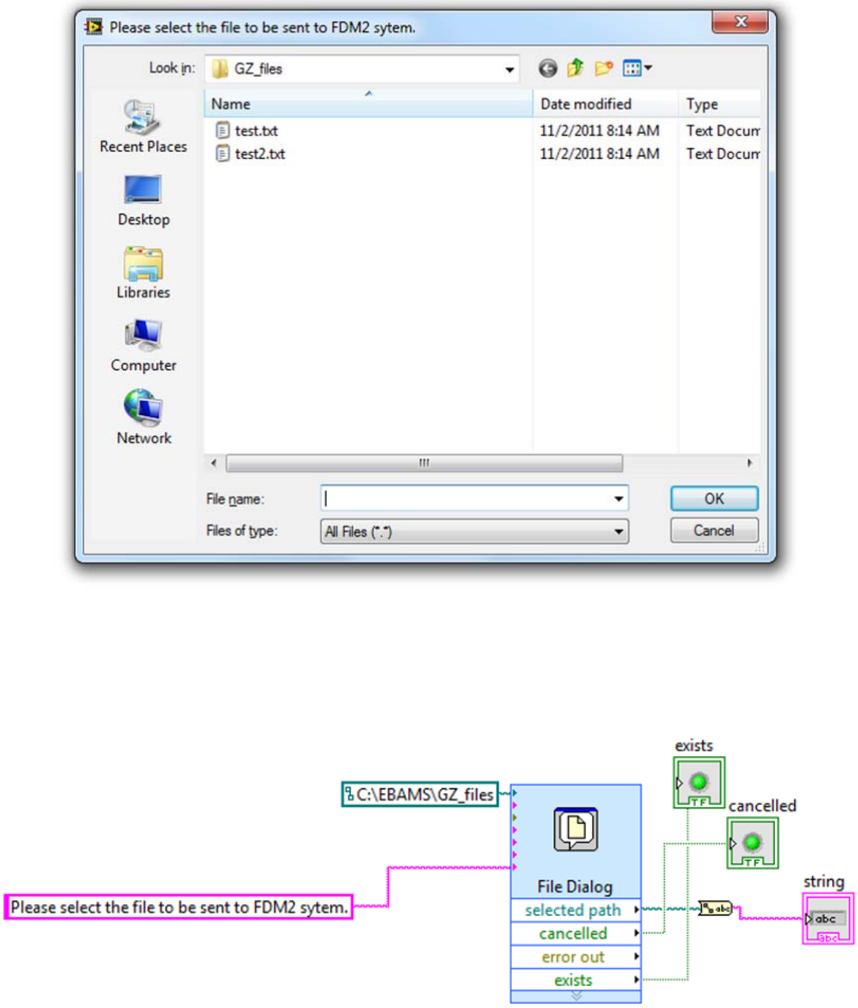

Figure C24. Front panels and block diagrams for “FDM2 filename.vi”.

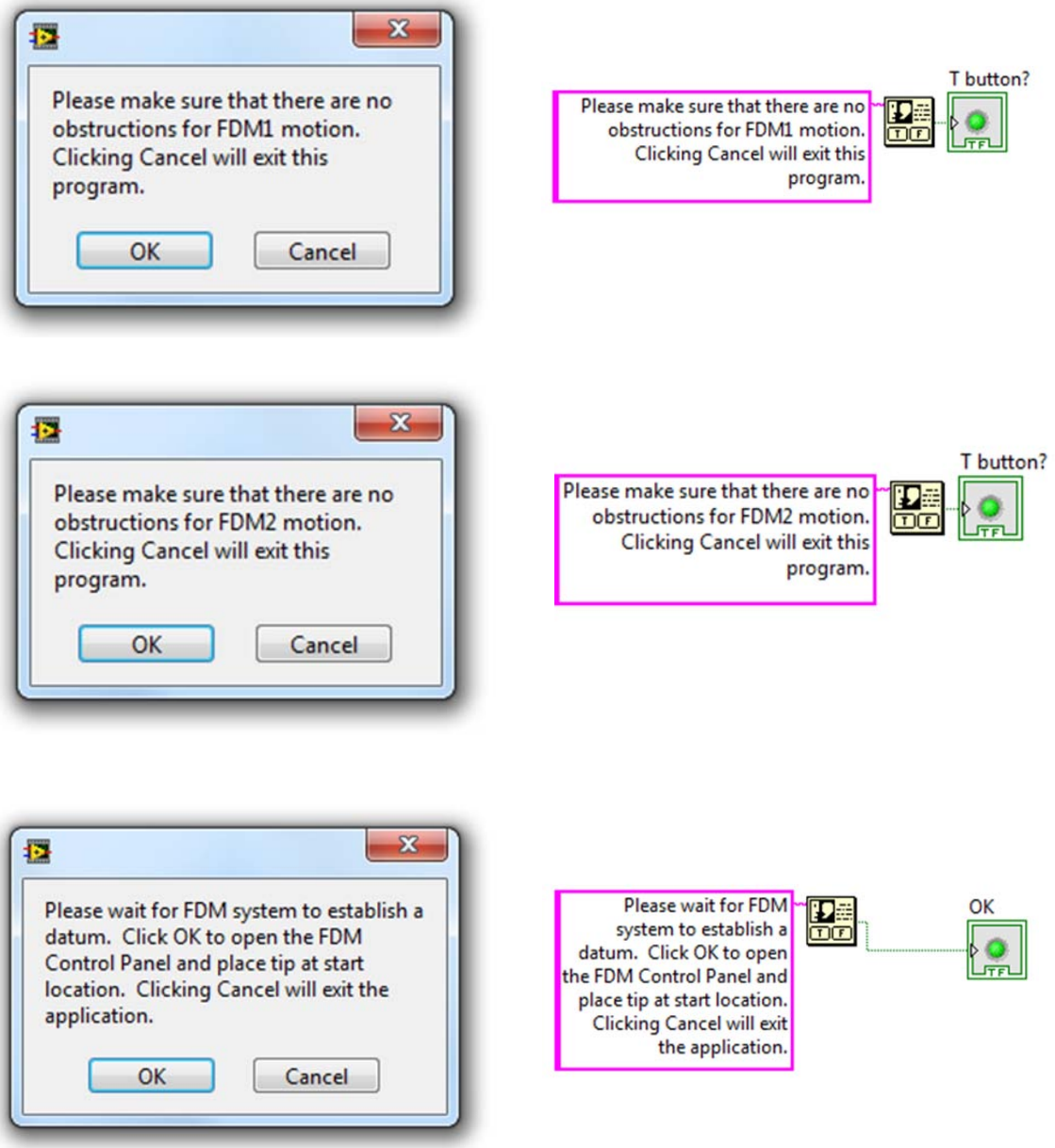

Figure C25. Front panels and block diagrams for ”FDM1 clear.vi” (top), “FDM2 clear.vi” (middle), and “start location.vi” (bottom).

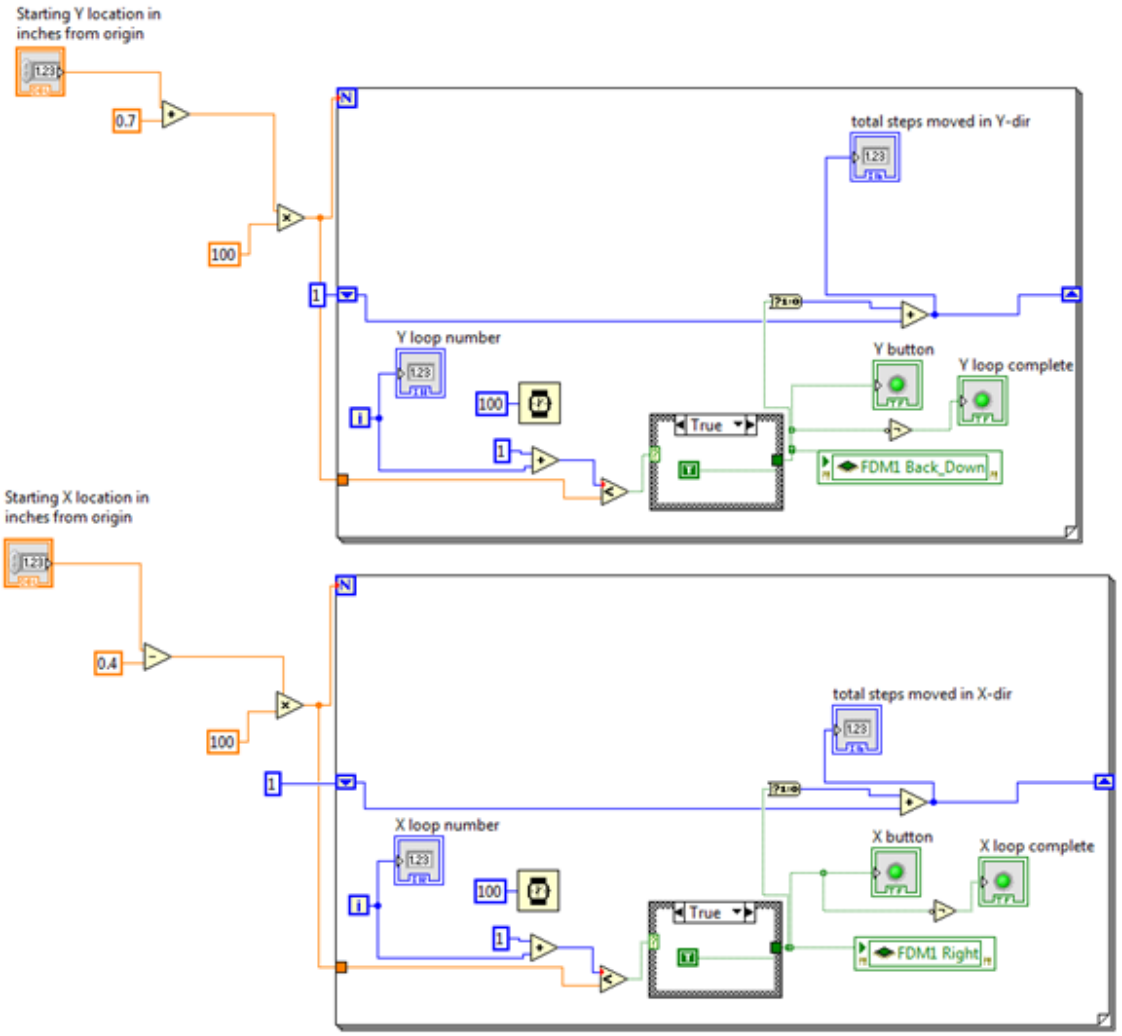

Figure C26. Block diagram for “start build location.vi.” showing true case

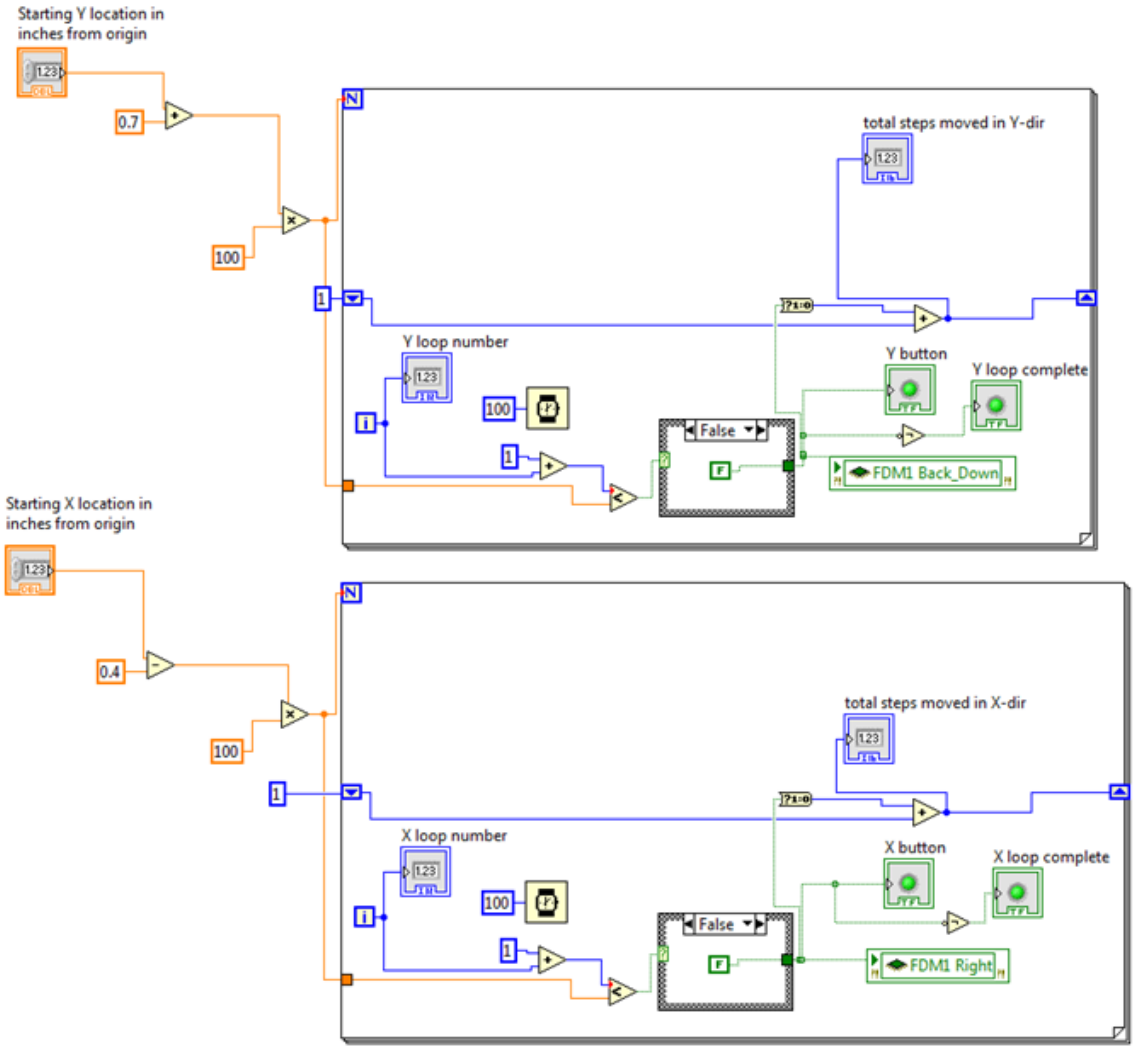

Figure C27. Block diagram for “start build location.vi.” showing false case

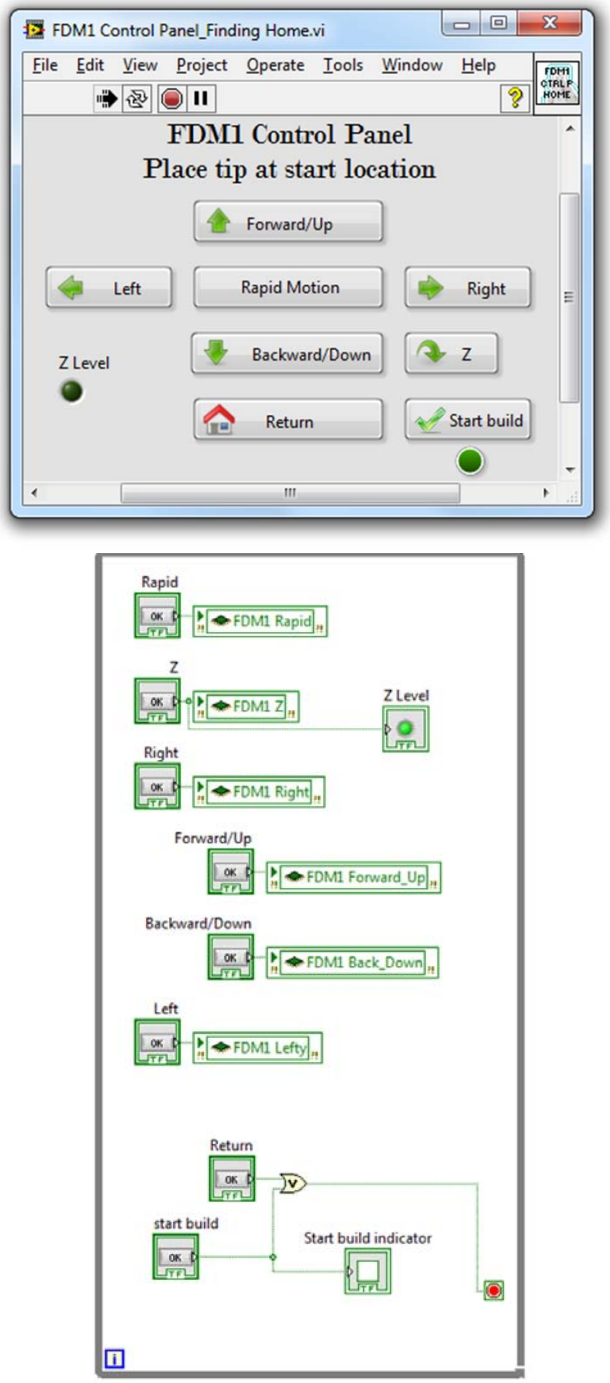

Figure C28. Front panel and block diagram for "FDM1 Control Panel_Finding Home.vi."

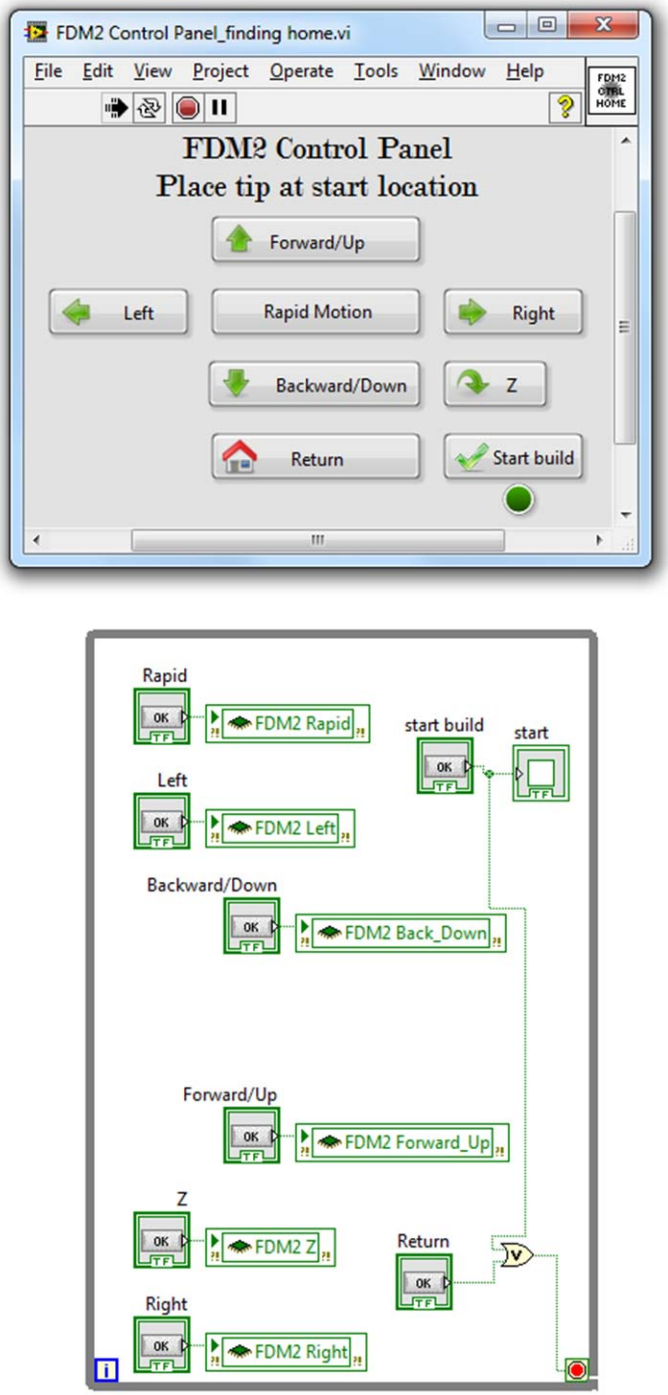

Figure C29. Front panel and block diagram for "FDM2 Control Panel_finding home.vi."

APPENDIX D

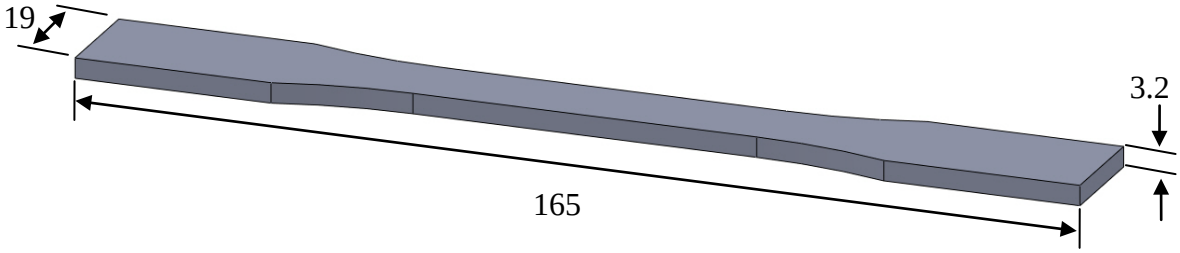

Figure D1. ASTM D638 Type I specimen (all units in millimeters)

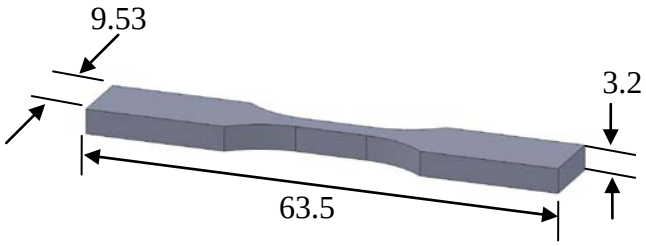

Figure D2. ASTM D638 Type V specimen (all units in millimeters)

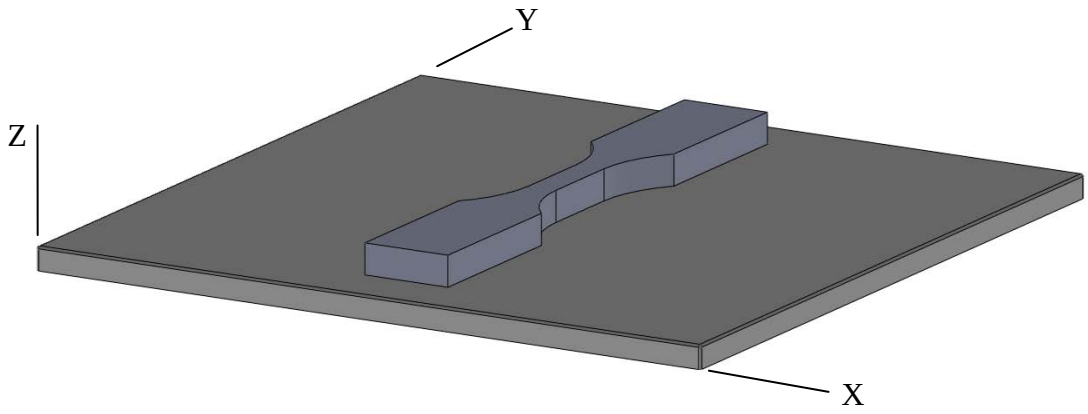

Figure D3. Tensile test specimen build in the YXZ orientation

APPENDIX E

Table E1. Run order for UV/O_3 experiments

Exposure time-replicate	Random fabrication order	Random testing order
0-TS1	1.0-TS2	1.0-TS5
0-TS2	2.0-TS1	0-TS5
0-TS3	1.0-TS5	1.5-TS1
0-TS4	3.0-TS4	3.0-TS5
0-TS5	1.5-TS1	1.0-TS3
0.5-TS1	3.0-TS1	1.0-TS4
0.5-TS2	0.5-TS5	0.5-TS4
0.5-TS3	0-TS3	0.5-TS3
0.5-TS4	0-TS4	0.5-TS5
0.5-TS5	3.0-TS3	2.0-TS5
1.0-TS1	0-TS1	1.5-TS5
1.0-TS2	1.5-TS5	3.0-TS1
1.0-TS3	2.0-TS2	0-TS4
1.0-TS4	1.5-TS4	3.0-TS3
1.0-TS5	1.0-TS4	1.0-TS1
1.5-TS1	3.0-TS5	0-TS3
1.5-TS2	1.5-TS2	3.0-TS2
1.5-TS3	0-TS5	0.5-TS2
1.5-TS4	0.5-TS2	3.0-TS4
1.5-TS5	2.0-TS5	2.0-TS4
2.0-TS1	1.0-TS3	2.0-TS2
2.0-TS2	0.5-TS1	2.0-TS1
2.0-TS3	1.5-TS3	0.5-TS1
2.0-TS4	1.0-TS1	1.5-TS3
2.0-TS5	0.5-TS3	1.5-TS4
3.0-TS1	2.0-TS3	0-TS1
3.0-TS2	2.0-TS4	0-TS2
3.0-TS3	3.0-TS2	1.0-TS2
3.0-TS4	0.5-TS4	1.5-TS2
3.0-TS5	0-TS2	2.0-TS3

Vita

David Espalin Jr was born on January 12, 1978 and is the son of Mrs. Luz E. Espalin and Mr. David Espalin (1951-1979). David obtained a high school diploma in May of 1996 from Santa Teresa High School located in New Mexico. He obtained a Bachelor of Science Degree in Mechanical Engineering with *cum laude* distinction from the University of Texas at El Paso in May of 2010. As an undergraduate student, David received the Best Paper Award at the 2009 International Solid Freeform Fabrication Symposium for his work entitled "Fused deposition modeling of patient-specific polymethylmethacrylate implants", which was also published in the Rapid Prototyping Journal. That same year he also received an honorable mention at the 2009 National Science Foundation LSAMP Conference. While pursuing a graduate degree, David regularly helped college students with classes, tutored high school students on the weekends, hosted training sessions related to lab equipment and software, peer-reviewed technical papers as well as wrote technical papers and proposals. In 2012, he was part of a group that received the Best Business Plan Award at the 2012 Camino Real Venture Competition.

Permanent address: 313 Poplar Ct.
Sunland Park, NM, 88063

This thesis was typed by David Espalin, Jr.